UQAT
UNIVERSITÉ DU QUÉBEC
EN ABITIBI-TÉMISCAMINGUE

Integration of distributed generation along with energy storage system to reduce the high penetration impacts of renewable energy sources into the power grid

By

Md Jahidur Rahman

Under the direction of Professor Tahar Tafticht,
and the co-direction of Professor Mamadou Lamine Doumbia

Thesis presented at the University of Quebec at Abitibi-Témiscamingue for the purpose of obtaining the degree of Doctor of Philosophy (Ph.D.) in engineering – concentration in Electrical Engineering offered as an extension under an agreement with the Université du Québec à Chicoutimi

Defended on 15 February 2024

Jury :

Mr. Nahi Kandil, Ph.D., Université du Québec en Abitibi-Témiscamingue, President of the Jury

Mr. Alben Cardenas, Ph.D., Université du Québec à Trois-Rivières, External Member

Mr. Tahar Tafticht, Ph.D., Université du Québec en Abitibi-Témiscamingue, Supervisor

Mr. Mamadou Lamine Doumbia, Ph.D., Université du Québec à Trois-Rivières, Co-supervisor

Québec, Canada

UNIVERSITÉ DU QUÉBEC
EN ABITIBI-TÉMISCAMINGUE

Intégration de la génération décentralisée associée à un système de stockage d'énergie pour réduire les impacts de la pénétration élevée des sources d'énergie renouvelable dans le réseau électrique

Par

Md Jahidur Rahman

Sous la direction du Professeur Tahar Tafticht,
et la codirection du Professeur Mamadou Lamine Doumbia

Thèse présentée à l'Université du Québec à Abitibi-Témiscamingue en vue de l'obtention du grade de Philosophie Doctorat (Ph.D.) en ingénierie – concentration ingénierie électrique offert en extension en vertu d'un protocole d'entente avec l'Université du Québec à Chicoutimi

Soutenue le 15 Février 2023

Jury :

M. Nahi Kandil, Ph.D., Université du Québec en Abitibi-Témiscamingue, Président du Jury

M. Alben Cardenas, Ph.D., Université du Québec à Trois-Rivières, Membre externe

M. Tahar Tafticht, Ph.D., Université du Québec en Abitibi-Témiscamingue, Directeur

M. Mamadou Lamine Doumbia, Ph.D., Université du Québec à Trois-Rivières, Co-directeur

Québec, Canada

ACKNOWLEDGMENTS

I begin by expressing my deepest gratitude to the Almighty ALLAH (SWT) for granting me the strength, courage, and patience to navigate through the journey of completing this thesis. ALLAH'S divine guidance has been the cornerstone of my perseverance.

Following this, I extend my heartfelt thanks to all those who have contributed to the successful completion of my research project. I am immensely grateful to my Research Director, Professor Tahar Tafticht, whose unwavering support, encouragement, and insightful guidance have been invaluable throughout this endeavor. His mentorship has not only shaped my academic pursuits but has also enriched me socially and philosophically.

I am indebted to my Co-supervisor, Professor Mamadou Lamine Doumbia, for his continuous assistance, guidance, and unwavering support throughout the research process. His expertise has been instrumental in shaping the trajectory of my work.

Furthermore, I extend my appreciation to Professor Nahi Kandil, President of the Jury, and Professor Alben Cardenas for their meticulous evaluation of my thesis and for providing invaluable suggestions and advice.

Lastly, I would like to express my profound gratitude to my elder brother, Dr. Mohammad Habibur Rahman, whose unwavering support and guidance have been a source of strength since my childhood. I would like to express my deepest gratitude to my mother, Hasina Akter, whose unwavering love, encouragement, and support have been the cornerstone of my academic journey. Her sacrifices, guidance, and belief in me have fueled my determination to pursue this Ph.D. degree. I also extend my heartfelt thanks to my beloved wife, Fatima Tuj Jhohora (Sarna), whose unwavering support throughout these four years of research and writing has been indispensable. Her love and encouragement have been the driving force behind my accomplishments, for which I am eternally grateful.

INTEGRATION OF DISTRIBUTED GENERATION ALONG WITH ENERGY STORAGE SYSTEM TO REDUCE THE HIGH PENETRATION IMPACTS OF RENEWABLE ENERGY SOURCES INTO THE POWER GRID

Md Jahidur RAHMAN

ABSTRACT

Being the fluctuation behavior of Renewable Energy Sources (RESs), generation, balance, and demand are not easy tasks to control because it is not desirable to have constant power generation from RESs due to natural prospects. As a result, the dynamic stability of power flow and control of frequency is becoming more challenging due to the high penetration impacts of RESs. Control strategies of converter/inverter with filter are also required to maintain the proper power supply in the entire microgrid where energy storage device plays crucial roles. The objective of this study is to explore critical aspects of distributed generation (DG), renewable energy integration, and energy storage systems, focusing on enhancing power network efficiency while minimizing power losses and environmental air pollution. This doctoral thesis acknowledges the environmental and economic benefits of distributed generation (DG) while highlighting the inherent challenges in managing fluctuating renewable energy sources (RESs). A control algorithm for a high-penetration hybrid diesel-wind-based energy storage system is designed to maintain dynamic stability in power flow and control network frequency. The key findings include the effective reduction of transient time in wind power flow and frequency fluctuations through the use of an integral-derivative (I-D) controller. On the other hand, it recognizes the challenges posed by the intermittent nature of renewable energy sources (RESs) and their impact on dynamic stability and frequency control. This thesis introduced a control algorithm employed with a Fuzzy Logic (FL) controller for a wind-based energy storage system using the power-sharing method. By comparing this approach to the traditional Proportional Integral Derivative (PID) controller, the study demonstrated substantial improvements in reducing transient time in wind power flow and frequency fluctuations. A storage system (battery) plays a crucial role in maintaining network stability while minimizing energy losses. As a part of this thesis, a comprehensive survey of various DC-DC converters is done to determine the most suitable energy storage device for smart grid applications. The main objective is to identify this application's most appropriate energy storage device. The advantages of this technology are high efficiency and reliability, which can connect various energy sources and reduce conduction losses in the power converters. The study analyzed the efficiency and reliability of different converters and evaluated their performance in charging and discharging conditions of a battery. The operating ranges of boost-buck, buck-boost, and buck-boost (-Vout) converters are analyzed to optimize the energy storage system. This doctoral thesis also presents a comprehensive analysis of a simulation scheme that leverages a solar system composed of photovoltaic (PV) panels integrated with the electrical grid, various loads, and an energy storage device. The research begins by investigating the modeling of PV panel cells and their operational characteristics. Subsequently, an adaptive notch filter synthesis is developed to mitigate input current fluctuations. The research further explores the efficiency and control mechanisms of power converters and inverters, facilitating the seamless

integration of the energy storage system with the electrical grid. Multiple simulations are conducted, employing nonlinear control techniques to evaluate the performance of the system with different configurations, including a simple inverter, a multi-variable filter, a notch filter, and a filter-less setup. The research aims to achieve effective regulation of the DC bus within the proposed grid. The key advantage of these nonlinear controllers is their ability to compensate for reactive power and harmonic currents, resulting in a disturbance-free power network and a reduction in the Total Harmonic Distortion (THD) rate of the inverters, ultimately enhancing the overall efficiency of the power grid. This thesis contributes valuable insights into optimizing the performance of wind and solar systems along with energy storage device and their integration with the grid through advanced control and filtering techniques, with significant implications for improving the stability and reliability of renewable energy sources in the power grid.

Keywords: renewable energy sources, distributed generation, dynamic stability, power flow control, frequency control, energy storage systems, network efficiency, power losses, air pollution, integral-derivative controller, fuzzy logic controller, PID controller, DC-DC converters, smart grid, efficiency reliability, photovoltaic panels, notch filter, nonlinear controller, total harmonic distortion

INTÉGRATION DE LA GÉNÉRATION DÉCENTRALISÉE ASSOCIÉE À UN SYSTÈME DE STOCKAGE D'ÉNERGIE POUR RÉDUIRE LES IMPACTS DE LA PÉNÉTRATION ÉLEVÉE DES SOURCES D'ÉNERGIE RENOUVELABLE DANS LE RÉSEAU ÉLECTRIQUE

Md Jahidur RAHMAN

RÉSUMÉ

Compte tenu du comportement aléatoire et fluctuant des sources d'énergie renouvelable (SER), l'équilibre entre la génération et la demande ne sont pas faciles à contrôler. Par conséquent, la stabilité dynamique du flux d'énergie et le contrôle de la fréquence deviennent de plus en plus difficiles en raison des impacts de la pénétration élevée des SER dans les micro-réseau électrique. Des stratégies de contrôle des convertisseurs/onduleurs avec filtre sont nécessaires pour maintenir l'alimentation électrique appropriée dans l'ensemble du micro-réseau. L'objectif de notre travail est d'explorer les aspects critiques de la génération distribuée (GD), de l'intégration des énergies renouvelables et des systèmes de stockage de l'énergie, en mettant l'accent sur l'amélioration de l'efficacité du réseau électrique tout en minimisant la pollution atmosphérique. Cette thèse reconnaît les avantages environnementaux et économiques de la GD tout en soulignant les défis inhérents à la gestion des sources d'énergie renouvelable fluctuantes. Un algorithme de contrôle pour un système de stockage d'énergie hybride diesel-éolien à forte pénétration est conçu pour maintenir la stabilité dynamique du flux d'énergie et le contrôle de la fréquence du réseau. Les principaux résultats comprennent la réduction efficace du temps de transition dans le flux d'énergie éolienne et des fluctuations de fréquence. D'autre part, cette étude répond aux défis posés par la nature intermittente des SER et leur impact sur la stabilité dynamique et le contrôle de la fréquence. Nous avons introduit un algorithme de contrôle utilisant la logique floue pour un système de stockage d'énergie éolienne en utilisant la méthode de partage de puissance. En comparant cette approche au contrôleur conventionnel, l'algorithme proposé a démontré des améliorations substantielles dans la réduction du temps de transition dans le flux d'énergie éolienne et des fluctuations de fréquence. Dans le cadre de cette thèse, une étude complète de divers convertisseurs statiques est réalisée afin de déterminer le dispositif de stockage d'énergie le plus approprié pour les applications de réseaux intelligents. Ce système de stockage joue un rôle essentiel dans le maintien de la stabilité du réseau tout en minimisant les pertes d'énergie. L'objectif est d'identifier le dispositif de stockage d'énergie le plus adapté à cette application. Les avantages de cette technologie sont d'une grande efficacité et fiabilité, qui peuvent connecter diverses sources d'énergie et réduire les pertes de conduction dans les convertisseurs de puissance. On a analysé l'efficacité et la fiabilité de différents convertisseurs et évalué leur performance dans des conditions de charge et de décharge du système de stockage. Les plages de fonctionnement des convertisseurs élévateur-abaisseur, abaisseur-élévateur et abaisseur-élévateur (-Vout) ont été analysées pour optimiser le système de stockage d'énergie. Cette thèse présente également une analyse complète d'un schéma de simulation qui exploite un système solaire composé de panneaux photovoltaïques intégrés au réseau électrique, à diverses charges, et à un dispositif de stockage d'énergie. Après la modélisation des panneaux photovoltaïques et de leurs caractéristiques opérationnelles, un

filtre adaptatif est développé pour atténuer les fluctuations du courant d'entrée. On a exploré en outre l'efficacité et les mécanismes de contrôle des convertisseurs de puissance et des onduleurs, facilitant ainsi l'intégration du système de stockage d'énergie avec le réseau électrique. Plusieurs techniques de contrôle non linéaires sont utilisées pour évaluer les performances du système avec différentes configurations, y compris un onduleur simple, un filtre multi-variable, un filtre passe bande et une configuration sans filtre. Cette recherche nous a permis de proposer une régulation efficace du bus DC au sein du réseau électrique. L'avantage clé de ces régulateurs non linéaires est leur capacité à compenser la puissance réactive et les courants harmoniques, ce qui se traduit par un réseau électrique sans perturbations et une réduction du taux de distorsion harmonique totale (DHT) des onduleurs, améliorant finalement l'efficacité globale du réseau électrique. Cette thèse apporte des connaissances précieuses pour optimiser les performances des systèmes éoliens et solaires ainsi que du dispositif de stockage d'énergie, et leur intégration au réseau grâce à des techniques de contrôle et de filtrage avancées, avec des implications significatives pour l'amélioration de la stabilité et de la fiabilité des sources d'énergie renouvelable dans le réseau électrique.

Mots-clés: sources d'énergie renouvelable, génération distribuée, stabilité dynamique, contrôle du flux d'énergie, contrôle de la fréquence, systèmes de stockage d'énergie, efficacité du réseau, pertes d'énergie, régulateur logique floue, régulateur PID, convertisseurs DC-DC, réseau intelligent, efficacité, fiabilité, panneaux photovoltaïques, filtre encoche, contrôleur non linéaire, distorsion harmonique totale.

TABLE OF CONTENTS

Page

CHAPTER 1 INTRODUCTION 1
1.1 Research problem 4
1.2 Literature review 6
1.2.1 Distributed generation system 6
1.2.2 Energy storage system 7
1.2.3 Control techniques used in power grid 9
1.3 Research objectives 12
1.4 Research methodology 13
1.5 Research originality and contribution 14
1.6 List of publications 15

CHAPTER 2 POWER STABILITY AND FREQUENCY CONTROL TECHNIQUES OF DG FOR A HIGH PENETRATION WIND-BASED ENERGY STORAGE SYSTEM USING INTEGRAL–DERIVATIVE CONTROLLER 17
2.1 Introduction 18
2.2 Modeling of power sources 20
2.2.1 Synchronous condenser 20
2.2.2 Wind turbine 20
2.2.3 Secondary/DL system 21
2.2.4 Battery-based energy storage system 21
2.3 Network control algorithms for WDHPS 22
2.3.1 Frequency control technique in WDHPS 23
2.3.2 Control of BESS 26
2.4 Connecting a wind turbine to the power grid with storage system 26
2.5 Simulation and result 27
2.6 Conclusion 33
2.7 References 34

CHAPTER 3 DYNAMIC STABILITY OF WIND POWER FLOW AND NETWORK FREQUENCY FOR A HIGH PENETRATION WIND-BASED ENERGY STORAGE SYSTEM USING FUZZY LOGIC CONTROLLER 37
3.1 Introduction 38
3.2 Modeling of distributed generation grid 42
3.2.1 Wind turbine 42
3.2.2 Secondary/Dump load system 42
3.2.3 Battery-based energy storage system 43
3.2.4 Synchronous condenser 44
3.3 Control algorithms for WDHPS 45
3.3.1 Control technique of frequency in the WDHPS network 46
3.3.2 The BESS control strategies 48
3.4 Control techniques applied to the network 48
3.4.1 Fuzzy logic control technique 49
3.4.2 Operational principle of MF and their rules 50

3.5 Connection of wind turbine with SL and BESS to the power network 53
3.6 Simulation and result 53
3.6.1 Power produced by wind turbine (PT) is > overall load demand (PL). in this situation, the BESS (PS) will be charged..... 54
3.6.2 Power produced by wind turbine (PT) is < overall load demand (PL). in this situation, the BESS (PS) will be discharged..... 56
3.7 Discussion 58
3.8 Conclusion 59
3.9 References 59

CHAPTER 4 OPTIMAL INVERTER CONTROL STRATEGIES FOR A PV POWER GENERATION WITH BATTERY STORAGE SYSTEM IN MICROGRID.....63
4.1 Introduction.....64
4.2 Modeling of a solar photovoltaic cell 69
4.3 Photovoltaic system sonnected to the power grid.....71
4.3.1 Nonlinear control technique of an inverter 73
4.3.1.1 Modeling the ‘abc’ plane transformation..... 74
4.3.1.2 Modeling the filter ‘abc/dq’ plane transformation..... 75
4.3.2 Nonlinear control with adaptive notch filter..... 78
4.3.3 Nonlinear control with multi-variable filter..... 80
4.3.4 Nonlinear control without filter 82
4.4 Simulation results.....83
4.4.1 Using a simple nonlinear controller..... 83
4.4.1.1 Assembled with loads, solar radiation, and without a battery system 83
4.4.1.2 Assembled with load, solar radiation, and variation of the battery charge..... 85
4.4.1.3 Assembled with solar radiation, battery charge, and variation of the load..... 87
4.4.1.4 Assembled with battery charge, load, and with variation of the solar radiation..... 88
4.4.2 Using nonlinear controller with multi-variable filter..... 89
4.4.2.1 Assembled with loads, solar radiation, and without a battery system 89
4.4.2.2 Assembled with load, solar radiation, and variation of the battery charge..... 91
4.4.2.3 Assembled with solar radiation, battery charge, and variation of the load..... 92
4.4.2.4 Assembled with battery charge, load, and with variation of the solar radiation..... 93
4.4.3 Using nonlinear controller with notch filter..... 94
4.4.3.1 Assembled with loads, solar radiation, and without a battery system 94

4.4.3.2 Assembled with load, solar radiation, and variation of the battery charge 95
4.4.3.3 Assembled with solar radiation, battery charge, and variation of the load 97
4.4.3.4 Assembled with battery charge, load, and with variation of the solar radiation 99
4.4.4 Using nonlinear controller without filter 99
4.4.4.1 Assembled with loads, solar radiation, and without a battery system 99
4.4.4.2 Assembled with load, solar radiation, and variation of the battery charge 100
4.4.4.3 Assembled with solar radiation, battery charge, and variation of the load 101
4.4.4.4 Assembled with battery charge, load, and with variation of the solar radiation 102
4.5 Comparison of nonlinear controllers with various filters 103
4.6 Conclusion 105
4.7 References 107

CHAPTER 5 POWER CONVERTERS ANALYZED IN ENERGY STORAGE SYSTEMS TO ENHANCE THE PERFORMANCE OF THE SMART GRID APPLICATION 111
5.1 Introduction 112
5.2 Study of converters used in energy storage systems 116
5.3 Operational technique of different dc converters 116
5.3.1 Operational equations of the boost-buck converter 116
5.3.2 Operational equations of the buck-boost converter 121
5.3.3 Operational equations of the buck-boost converter with negative output voltage 122
5.4 Simulation results 123
5.4.1 Simulation results using the boost-buck converter 123
5.4.2 Simulation results using the buck-boost converter 124
5.4.3 Simulation results using the buck-boost converter with negative output voltage 124
5.5 Resultant functional voltage of the converters 125
5.6 Conclusion 126
5.7 References 126

CONCLUSIONS 131

RECOMMANDATIONS 133

BIBLIOGRAPHIE 139

LIST OF TABLES

Page

Table 2.1 Data for tested system 21

Table 3.1 Parameters for tested WDHPS network. 45

Table 3.2 Fuzzy logic operation with “If-Then” rules. 52

Table 3.3 Fuzzy rule-based operation.....53

Table 4.1 Simulation data of the proposed grid. 83

Table 4.2 Ranking of controllers according to their performance.....104

Table 5.1 Summary of converters usable in an energy storage system.....125

LIST OF FIGURES

Page

Figure 2.1 Block diagram of power converter with BESS 22

Figure 2.2 Charging and discharging stages of battery in WDHPS using power sharing method 23

Figure 2.3 Frequency control scheme of the WDHPS system 25

Figure 2.4 ower-sharing strategy between the BESS and DL 25

Figure 2.5 Operational diagram of frequency control using an I–D controller 27

Figure 2.6 (a) Power produced by the wind turbine. (b) Reactive power supply from the synchronous condenser where battery is charged 28

Figure 2.7 (a) Power consumed by consumer load. (b) Power supplied from BESS and (c) power consumed by DL where battery is charged.....28

Figure 2.8 (a) Network frequency conditions and (b) speed generated by ASM generator where BESS is charged 29

Figure 2.9 (a) Voltage at load bus and (b) current at DL where BESS is charged. 30

Figure 2.10 (a) BESS SOC condition, (b) BESS current condition, and (c) BESS voltage condition where BESS is charged 30

Figure 2.11 (a) Power produced by the wind turbine and (b) reactive power supply from the synchronous condenser where BESS is discharged 31

Figure 2.12 (a) Power consumed by consumer load. (b) Power supplied from BESS and (c) power consumed by DL where BESS is discharged.....31

Figure 2.13 (a) Network frequency conditions and (b) speed generated by ASM generator where BESS is discharged.....32

Figure 2.14 (a) Voltage at load bus and (b) current at DL where BESS is discharged 33

Figure 2.15 Fig. 15. (a) BESS SOC condition, (b) BESS current condition, and (c) BESS voltage condition where BESS is discharged.....33

Figure 3.1 Operational characteristics of the wind turbine.....42

Figure 3.2 (a) Eight-bit three-phase GTO switches. (b) Operational block diagram of three-phase resistive loads.....43

Figure 3.3 (a) Block diagram of a power converter with BESS. (b) Control scheme of current-controlled inverter.....44

Figure 3.4 The control scheme of a synchronous condenser.....44

Figure 3.5 The control algorithm for the proposed WDHPS network.....45

Figure 3.6 (a) Frequency control scheme of the WDHPS system. (b) Power-sharing strategy between the BESS and SL.....47

Figure 3.7 (a) Frequency control scheme using PID controller. (b) Frequency control scheme using fuzzy logic controller.....48

Figure 3.8 Operational diagram fuzzy logic controller.....50

Figure 3.9 (a) Membership function, Input variable 1. (b) Membership function, Input variable 2.....51

Figure 3.10 Output variables of membership function.....51

Figure 3.11 (a) The power produced by the wind turbine. (b) Reactive power supply from the synchronous condenser. (c) Power consumed by consumer load. (d) Power supplied from the BESS. (e) Power consumed by SL, when the battery is charged.....54

Figure 3.12 (a) Network frequency conditions. (b) Speed generated by ASM generator. (c) Voltage at load bus. (d) The current at SL, when the BESS is charged. 55

Figure 3.13 (a) BESS SOC condition, (b) BESS current condition and, (c) BESS voltage condition, where the BESS is charged. 56

Figure 3.14 (a) The power produced by the wind turbine. (b) Reactive power supply from the synchronous condenser. (c) Power consumed by consumer load. (d) Power supplied from BESS. (e) Power consumed by SL, when the battery is discharged.....57

Figure 3.15 (a) Network frequency conditions. (b) Speed generated by ASM generator. (c) Voltage at load bus. (d) Current at SL, where the BESS is discharged.....58

Figure 3.16 (a) The BESS SOC condition, (b) BESS current condition and, (c) BESS voltage condition, where the BESS is discharged.....58

Figure 4.1 I-V and P-V curves of PV modules with temperature variation 70

Figure 4.2 I-V and P-V curves of PV modules with the variation of sun radiation 70

Figure 4.3 Generic circuit diagram of a boost converter 71

Figure 4.4 The control scheme of a boost converter....73

Figure 4.5 Proposed diagram of PV connected grid. 73

Figure 4.6 Bode diagram of the filter for different cutoff frequencie....77

Figure 4.7 Block diagram of nonlinear control....78

Figure 4.8 The operational block diagram of the adaptive notch filte....79

Figure 4.9 Final diagram of the modified adaptive notch Filter....80

Figure 4.10 Bode diagram representation of different values of K 81

Figure 4.11 THD of the grid for different values of K 81

Figure 4.12 Diagram of the nonlinear controller without an inverter filter....83

Figure 4.13 Dynamic response of the grid with solar radiation of G = 800 W/m2 84

Figure 4.14 Power flow in the grid with solar radiation. Power flow in the grid with solar radiation G=8....84

Figure 4.15 Harmonic spectrum of the grids and load current with solar radiation of G = 800 W/m....85

Figure 4.16 Dynamic state response with battery charge variation....86

Figure 4.17 Power flow with battery charge variation 86

Figure 4.18 Battery state of charge....87

Figure 4.19 Dynamic response with load variation 87

Figure 4.20 Power flow with load variation 88

Figure 4.21 Dynamic response with the variation of solar radiation....88

Figure 4.22 Power flow with a variation of solar radiation 89

Figure 4.23 Dynamic response with solar radiation of G = 800 W/m2 using a multi-variable filter 89

Figure 4.24 Power flow with the variation of solar radiation G=800W/m2 using multi-variable filter 90

Figure 4.25 Harmonic spectrum of the grid and load current using a multi-variable filter..90

Figure 4.26 Dynamic response with battery charge variation using a multi-variable filter .91

Figure 4.27 Power flow with battery charge variation using a multi-variable filter 91

Figure 4.28 Battery state of charge using multi-variable.....92

Figure 4.29 Dynamic response with load variation using a multi-variable filter 92

Figure 4.30 Power flow with load variation using a multi-variable filter 93

Figure 4.31 Dynamic response with a variation of solar radiation using a multi-variable filter 93

Figure 4.32 Power flow with a variation of solar radiation using a multi-variable filter 94

Figure 4.33 Dynamic response with solar radiation of G = 800 W/m2 using a notch filter.94

Figure 4.34 Power flow with solar radiation G = 800 W/m2 using a notch filter 95

Figure 4.35 Harmonic spectrum of the grid and load current using a notch filter.....95

Figure 4.36 Dynamic state response with battery charge variation using a notch filter.....96

Figure 4.37 Power flow with battery charge variation using a notch filter 96

Figure 4.38 Battery state of charge using a notch filter.....96

Figure 4.39 Dynamic response with load variation using a notch filter 97

Figure 4.40 Power flow with load variation using a notch filter 97

Figure 4.41 Dynamic response with a variation of solar radiation using a notch filter.....98

Figure 4.42 Power flow with a variation of solar radiation using a notch filter.....98

Figure 4.43 Dynamic response with solar radiation of G = 800 W/m2 without a filter.....99

Figure 4.44 Power flow with solar radiation of G = 800 W/m2 without a filter 99

Figure 4.45 Harmonic spectrum of the grid and load current without a filter.....100

Figure 4.46 Dynamic State response with battery charge variation without a filter. 100

Figure 4.47 Dynamic state response with battery charge variation without a filter 101

Figure 4.48 Battery state of charge using without a filter. 101

Figure 4.49 Dynamic response with load variation without a filter 102

Figure 4.50 Power flow with load variation without a filter 102

Figure 4.51 Dynamic responses with a variation of solar radiation without a filter..... 103

Figure 4.52 Power flow with variation of solar radiation without a filter 103

Figure 4.53 DC bus regulation with various controllers..... 104

Figure 5.1 Equivalent circuit diagram of a battery with bidirectional boost-buck converter 117

Figure 5.2 Diagram of the boost-buck converter when the switch is blocked..... 118

Figure 5.3 The control scheme of the boost-buck converter 121

Figure 5.4 Circuit diagram of the buck-boost converter Circuit diagram of the buck-boost converter 121

Figure 5.5 The control scheme of the buck-boost converter 122

Figure 5.6 Circuit diagram of the buck-boost converter with negative output voltage 122

Figure 5.7 Battery states of charge with boost-buck converter for (a) 250 V, (b) 350 V (c) 500 V, and (d) 650 V 123

Figure 5.8 Battery states of charge with buck-boost converter for (a) 250 V, (b) 350 V (c) 500 V, and (d) 650 V 124

Figure 5.9 Battery states of charge with modified buck-boost converter for (a) 250 V, (b) 350 V (c) 500 V, and (d) 650 V..... 125

LIST OF ABBREVIATIONS, ACRONYMS

DG	Distributed Generation
RES	Renewable Energy Source
MPC	Predictive Control
MCC	Magnetic Coupling Converters
ECC	Electrically Coupled Converters
SC	Supercapacitors
HESS	Hybrid energy storage system
VOC	voltage oriented control
LFC	Load frequency control
ED	Economic dispatch
PID	Proportional Integral Derivative
K_p	Proportional Gain
K_d	Derivative Gain
K_i	Integral Gain
WDHS	Wind Diesel Hybrid System
IGBT	Insulated-Gate Bipolar Transistor
AGC	Automatic Generation Control
BESS	Battery-based Energy Storage System
ESS	Energy Storage System
DL	Dump Load
SL	Secondary Load

SM	Synchronous Machine
ASM	Asynchronous Machine
PWM	Pulse Width Modulator
CCI	Current Controlled Inverter
PPL	Positive Power Limit
PLL	Phase Locked Loop
STATCOM	Static Synchronous Compensator
SVC	Static Var Compensator
BES	Battery Energy Storage
SOC	State of Charge
FC	Fuel Cell
AC	Alternative Current
DC	Direct Current
PSO	Particle swarm optimization
GA	Genetic Algorithm
SOA	Seeker Optimization Approach
VSC	Voltage Source Converter
HVDC	High Voltage Direct Current
GTO	Gate turn-off thyristor switches
MF	Membership Function
GMPPT	Global Maximum Power Point Tracking
MPPT	Maximum Power Point Tracking
MPP	Maximum Power Point

MICAPAS	Mitigation Control Against Partial Shading Effects
MIC	Module Integrated Converter
THD	Total Harmonic Distortion
P&O	Perturb and Observe

LIST OF SYMBOLS AND UNITS OF MEASUREMENT

P_m	Mechanical power delivered by the wind turbine	kW
ω	Velocity of the synchronous machine shaft	rad/s
p	Poles number of the synchronous machine	Without unit
V_{nom}	Wind velocity	m/s
P_{nom}	Wind Power	kW
P_S	BESS supplied power	kW
P_T	Wind turbine generated power	kW
P_L	Load consumed power	kW
SL	Secondary load consumption	kW
DL	Dump load consumption	kW
P_{ref}	Reference power	kW
$\Delta\omega$	Frequency error signal	Hz
$\Delta(\Delta\omega)$	Change of frequency error signal	Hz
$\mathring{u}$ (t)	Output of the fuzzy logic	Without unit
h_i	Output membership value of i-th rule	Without unit
μ_i	Output membership function of the i-th rule	Without unit
P_m	Mechanical power input of the synchronous machine	kW
N_P	Number of cells in parallel	Without unit
N_S	Number of cells in series	Without unit
I_{pv}	Current for a photovoltaic cell;	A or pu
I_{sc}	Short-circuit current of a cell	A or pu

I_0	Diode reverse bias current	A or pu
V_{pv}	Voltage for a photovoltaic cell	V or pu
V_T	Thermal voltage of a cell	V or pu
R_p	Resistance losses by recombination of the carriers	Ohm (Ω
R_s	Resistance losses by joule effects in the semiconductor	Ohm (Ω)
T	Cell's operating temperature	Kelvin
T_r	Reference temperature	Kelvin
E_{G0}	Silicon's bandwidth	eV
β	Ideality factor	Without unit
I_{os}	Reverse saturation current of the cell	A
I_{or}	Saturation current of the cell	A
q	Charge of electrons	C
G	Solar radiation	kWh/m^2
d	Duty cycle of the converter	Without unit
cos φ	power factor	Without unit
$I\tilde{d}/\ I\tilde{q}$	Errors of the currents	A
Id^*/Iq^*	References of the currents	A
$\widetilde{V_{DC}}$	voltage error of DC bus	V
V_{DC}^*	voltage reference of DC bus	V
e(t)	Error signal	Without unit
$x_{\alpha\beta}$	Input signal of the multi-variable filter	Without unit
$\hat{x_{\alpha\beta}}$	Output signal of the multi-variable filter	Without unit
I_{PV}	Solar Panel Current	A

V_{PV}	Solar Panel Voltage	V
P_{PV}	Solar Panel Power	kW
L	Bidirectional converter inductance,	mH
C	Bidirectional converter capacitance	F
V_0	Nominal voltage of the battery	V
I_0	Nominal current of the battery	A
K	Bias voltage of the battery	V
A	Exponential voltage of the battery	V
B	Exponential capacity of the battery	Ah
R_i	Number of resistors of the battery	Ohm (Ω)
Q	Total capacity of the battery	Ah
R	Fixed resistor of the battery	Ohm (Ω)
β	Orientation angle of the blades 'pitch angle' wind	deg
V_{wind}	Wind velocity	m/s
ρ	Density of air	Kg/m3
T_m	Mechanical torque	pu
P_m	Mechanical power generated by the wind turbine	kW or pu
P_s	Stator electrical power by the wind turbine	kW or pu
P_r	Rotor electric power	kW or pu
f	Grid frequency	Hz or pu
U_i	Voltage at i bus	V or pu
$P_{D\text{-}NOM}$	Rated power dissipation of DL loads of WHDS	kW or pu

XXX

P_T	Power generated by the wind turbine WHDS	kW or pu
$P_{T\text{-}NOM}$	Rated power of wind turbine WHDS	kW or pu
P_S	Power consumption / generated by the BESS WHDS	kW or pu
$P_{S\text{-}NOM}$	Rated power of the BESS WHDS	kW or pu
P_L	Active power consumed by the WHDS	kW or pu
$P_{L\text{-}NOM}$	Nominal load power of WHDS	kW or pu

CHAPTER 1

INTRODUCTION

The global energy landscape is undergoing a profound transformation driven by the need for sustainability, resilience, and energy security. Distributed Generation (DG), characterized by decentralized, smaller-scale power generation at or near the point of use, is at the forefront of this transformation. This thesis explores the synergies between DG systems powered by wind and photovoltaic (PV), and energy storage as a transformative force for future power systems [1, 2]. The modern power system is standing at the crossroads of transformation. It faces the dual challenge of accommodating the world's growing energy demands while urgently reducing its environmental footprint. In this critical juncture, the integration of Distributed Generation (DG) systems, primarily harnessing renewable energy sources like wind and PV technologies, in tandem with energy storage systems, emerges as a powerful solution to address these pressing concerns [3-5]. This thesis also sets the stage for an exploration of how DG systems, fueled by wind and PV, coupled with energy storage, hold the potential to reshape the future of the power system. The conventional energy landscape, dominated by centralized power generation from fossil fuels, has long been scrutinized for its environmental impact and vulnerability to supply disruptions. DG systems offer a paradigm shift by enabling localized, decentralized energy production, often leveraging clean and sustainable sources. Wind turbines tap into the kinetic energy of the wind, while PV panels convert sunlight into electricity, embodying the essence of clean energy. However, their inherent intermittency poses challenges in terms of grid integration and consistent power supply. Energy storage systems, comprising a range of technologies from lithium-ion batteries to pumped hydro storage, play a pivotal role in mitigating the variability of renewable sources. They store surplus energy during periods of high generation and release it when needed, ensuring grid stability and facilitating the seamless incorporation of renewable energy sources [6]. Beyond acting as energy buffers, energy storage systems enhance grid resilience, improve power quality, and provide ancillary services, making them indispensable components in the transition to a more sustainable and reliable power system. This

exploration seeks to delve deeper into the potential of distributed generation systems powered by wind and PV, coupled with energy storage, to shape the future of the power system. It aims to examine the technical aspects, economic feasibility, and environmental implications of this transformative combination, providing insights into how it can contribute to a cleaner, more resilient, and sustainable energy landscape.

The objective of this thesis is to explore critical aspects of distributed generation (DG), renewable energy integration, and energy storage systems, focusing on enhancing power network efficiency while minimizing power losses and environmental air pollution. A control algorithm for a high-penetration hybrid diesel-wind-based energy storage system is designed to maintain dynamic stability in power flow and control network frequency. The key findings include the effective reduction of transient time in wind power flow and frequency fluctuations through the use of an integral-derivative (I-D) controller [1]. On the other hand, it recognizes the challenges posed by the intermittent nature of renewable energy sources (RESs) and their impact on dynamic stability and frequency control. A control algorithm was introduced which is employed with a Fuzzy Logic (FL) controller for a wind-based energy storage system using the power-sharing method [2]. By comparing this approach to the traditional Proportional Integral Derivative (PID) controller, the study demonstrated substantial improvements in reducing transient time in wind power flow and frequency fluctuations. The storage system (battery) plays a crucial role in maintaining network stability while minimizing energy losses. As a part of this thesis, a comprehensive survey of various DC-DC converters is done to determine the most suitable energy storage device for smart grid applications. The main objective is to identify this application's most appropriate energy storage device. The advantages of this technology are high efficiency and reliability, which can connect various energy sources and reduce conduction losses in the power converters [3]. The study analyzed the efficiency and reliability of different converters and evaluated their performance in charging and discharging conditions of a battery. The operating ranges of boost-buck, buck-boost, and buck-boost (-Vout) converters are analyzed to optimize the energy storage system. A comprehensive analysis of a simulation scheme that leverages a solar system composed of photovoltaic (PV) panels integrated with the electrical grid, various loads, and an energy storage device. The research investigated the modeling of

PV panel cells and their operational characteristics. Subsequently, an adaptive notch filter synthesis is developed to mitigate input current fluctuations. The research further explores the efficiency and control mechanisms of power converters and inverters, facilitating the seamless integration of the energy storage system with the electrical grid [4].

The organization of this thesis is given as follows: Chapter 1 describes the research problem, gives the literature review, states the objectives, gives the methodology, and finally claims the originality and contributions of the work. Since this document is a papers-based thesis, consequently, Chapters 2, 3, 4, and 5 present the main results of the work in the form of published papers. The main contributions of this thesis are summarized as follows:

Chapter 2 presents the environmental and economic benefits of distributed generation (DG) while highlighting the inherent challenges in managing fluctuating renewable energy sources (RESs). The research proposes a control algorithm for a high-penetration hybrid diesel-wind-based energy storage system, specifically designed to maintain dynamic stability in power flow and control network frequency. The key findings include the effective reduction of transient time in wind power flow and frequency fluctuations through the use of an integral-derivative (I-D) controller. Additionally, a storage system (battery) is employed to store excess wind energy efficiently, reducing wastage and supplying surplus wind power during high-load demand periods.

Chapter 3 presents the challenges posed by the intermittent nature of renewable energy sources (RESs) and their impact on dynamic stability and frequency control. It introduces a control algorithm employing Fuzzy Logic (FL) for a wind-based energy storage system. By comparing this approach to the traditional Proportional Integral Derivative (PID) controller, the study demonstrates substantial improvements in reducing transient time in wind power flow and frequency fluctuations. A storage system (battery) plays a crucial role in maintaining network stability while minimizing energy losses.

Chapter 4 presents an experimental validation of the control technique of power supply in microgrids, particularly those incorporating photovoltaic (PV) panels and energy storage. The study explores various nonlinear control techniques to address the challenges of managing power converters/inverters, compensating for reactive power, and mitigating

harmonic currents. The study includes simulations, modeling PV panels, designing adaptive notch filters, and assessing the efficiency of power converters.

Chapter 5 investigates the comprehensive survey of various DC-DC converters to determine the most suitable energy storage device for smart grid applications. The study examines the efficiency and reliability of different converters and evaluates their performance in charging batteries. Operating ranges of boost-buck, buck-boost, and buck-boost ($-V_{out}$) converters are analyzed to optimize energy storage. The comparison of the DC converters is analyzed to know the functional voltage for the energy storage system.

1.1 Research problems

Research in the domain of distributed generation (DG) systems, characterized by the integration of renewable energy sources such as wind and photovoltaic (PV), in conjunction with energy storage systems within the power system, confronts a spectrum of multifaceted challenges. One prominent area of inquiry revolves around optimizing the sizing and configuration of these integrated systems to strike an intricate balance between energy generation efficiency, energy storage capacity, and cost-effectiveness. This involves determining the ideal proportion of wind and PV sources and the appropriate scale and technology for energy storage to ensure maximal system performance under varying conditions [7-9]. Managing the intermittent and variable nature of renewable energy resources is another pivotal research problem. Researchers strive to develop advanced forecasting techniques and energy management strategies that can accurately predict the availability of wind and solar resources, enabling grid operators to proactively adjust generation and consumption, thus ensuring a reliable and consistent power supply. Moreover, effective grid integration is critical for the seamless adoption of these DG systems with energy storage, and research is imperative in this domain [10]. This includes investigations into grid stability and voltage regulation, grid management tools and protocols, and the development of bidirectional communication systems to maintain a reliable connection between the distributed generators and the grid. Energy management and control systems also represent a significant research focus. Developing sophisticated control algorithms that can efficiently balance energy generation, storage, and consumption in real-time while

adapting to dynamic load profiles and variable resource availability is crucial. Furthermore, research endeavors extend to the economic viability of these integrated systems. This encompasses cost-benefit analyses, financial models, and assessments of potential financial incentives or policies to encourage wider adoption, considering long-term economic sustainability. Environmental sustainability constitutes a critical facet of research, with life-cycle assessments and studies on emissions reductions playing a pivotal role. Researchers assess the net environmental impact of DG systems integrated with energy storage to understand their overall sustainability [11-13]. Additionally, the resilience and reliability of these systems, particularly in adverse scenarios like grid outages or natural disasters, is an essential area of study, which involves evaluating the capacity of these systems to provide backup power and grid support during emergencies. Regulatory and policy challenges represent another set of problems. Researchers investigate the impact of existing regulations and policies, as well as propose new frameworks to overcome regulatory hurdles or facilitate the adoption of DG and energy storage technologies. Hybrid systems, which combine multiple renewable energy sources, are also a subject of inquiry. This comprehensive body of research problems collectively contributes to the advancement of cleaner, more reliable, and sustainable energy systems for the future, helping to address the critical challenges faced by the power sector [14, 15].

Being the fluctuation behavior of Renewable Energy Sources (RESs), generation, balance, and demand are not easy tasks to control because it is not desirable to have constant power generation from RESs due to natural prospects. The high penetration of wind/PV energy in the power network causes frequency disturbance. Also, excess energy needs to be dumped when there is low load demand. Switching the storage system (battery) during the time of operation can break the dynamic stability of wind power flow and create fluctuation in the frequency. As a result, the dynamic stability of power flow and control strategies of Energy storage systems (ESS) has become more challenging due to the high penetration impacts of RESs [1, 2].

1.2 Literature review

Most of the research work on this type of power system has been focused on the following three points: The distributed generation system, energy storage system, and control techniques used in the power grid.

1.2.1 Distributed generation system

The distribution systems typically operate at medium voltage levels, bridging the gap between the high-voltage transmission systems and the end consumers. However, due to the relatively low voltage and the resultant need for high currents, power losses along the distribution lines tend to be higher compared to the more efficient transmission systems [16]. These losses contribute to increased energy costs and have a detrimental impact on the voltage profiles across the distribution system. Notably, the active power losses not only compromise system efficiency but also have adverse effects on voltage profiles, underscoring the significance of minimizing these losses in distribution system design and planning [17,18].

The integration of distributed power generation facilities into distribution systems has emerged as a transformative solution. Such integration brings about improvements in system efficiency, voltage stability, and overall reliability. Notably, with distributed generation (DG) in place, voltage profiles are significantly enhanced, reducing the reliance on equipment for stability improvements. Moreover, the deployment of DGs results in lower power losses and reduced emissions, significantly bolstering system reliability [19, 20]. However, the strategic placement, sizing, and connection of DGs within the distribution system is a complex challenge. Suboptimal placement can lead to increased system losses, underscoring the importance of careful consideration [21]. Moreover, the over-sizing of DG units can exacerbate losses within the system [22]. Consequently, determining the appropriate size and connection points for DGs has become a nonlinear optimization problem.

This problem necessitates the simultaneous solution of multiple objective functions, including improving the voltage profile, minimizing power losses, reducing emissions, alleviating line loads, enhancing system reliability, and adhering to voltage limits on buses, all while constraining the capacity of the DG units [23–30]. The advent of DGs has

revolutionized distribution system design and planning by not only meeting active power demands but also significantly reducing line losses. Furthermore, the introduction of DGs has substantially decreased losses traditionally associated with long transmission lines, peak power demand, and excess heat generation during centralized electricity generation [31]. In addition, DGs have a remarkable impact on boosting voltages across all distribution system buses [32, 33].

To harness the full potential of DG in distribution systems, optimization strategies have evolved. Analytical methods, suitable for less complex systems, have been used to determine the optimal locations and capacities of DGs with the primary objective of loss reduction [34–39]. In recent years, heuristic algorithm-based approaches have gained prominence, offering more sophisticated ways to determine DG connection points and sizes in distribution systems [40]. These approaches accommodate a variety of objective functions, including the minimization of active power losses, enhancement of voltage profiles, and improvements in voltage stability across all buses within the system [41–44].

1.2.2 Energy storage system

Ensuring the sustainability of contemporary and future power grids hinges on the adoption of a net-zero strategy, coupled with the real-time storage of surplus energy generation [45]. The efficient coordination of Energy Storage Systems (ESSs) plays a pivotal role in enhancing power reliability and resilience, particularly in the deployment of Renewable Energy Sources (RESs) [46]. Among the most widely adopted ESSs are Battery Energy Storage Systems (BESS) and supercapacitors (SC). Consequently, the concept of a Hybrid Energy Storage System (HESS), integrating BESS and SC, emerges as a means to ensure system reliability and elevate BESS and network performance [47]. Nonetheless, HESS grapples with a myriad of challenges, notably pertaining to durability, power density, life cycle, battery utilization, temperature management, manufacturing cost, and charging duration while prolonging battery lifespan [48, 49].

Efforts to reduce reliance on petroleum and coal focus on curbing energy consumption through energy-saving measures and enhancing energy efficiency in residential, commercial, and industrial settings [50]. Acknowledging the fundamental role of Energy Storage Systems

(ESS) in renewable energy (RE) implementation, the influence of ESS on storage capacity and supply capabilities is underscored [51]. HESS, a fundamental instrument for maximizing the potential of RESs, combines with a battery state-of-health model to explore the impact of parameter estimation on battery longevity [52]. The integration of SC into HESS is an innovative development to enhance system efficiency and extend HESS lifespan. Although SCs exhibit low energy density alongside high power density and longevity, they remain in the domain of ongoing development [53].

The HESS operation results in balanced supply and demand, improved power reliability, reduced stress from RES fluctuations, and the provision of auxiliary services such as frequency and voltage management within microgrid operations, among other benefits [54]. HESS configurations have evolved as a strategic response to the limitations of individual ESS technologies. Their effectiveness is derived from the coupling of two or more energy storage technologies, addressing issues such as short lifespan, high costs, low energy and power density, and dynamic response associated with single ESS technologies [55, 56].

Given the susceptibility of Renewable Energy Sources (RES) to unpredictable weather variations, complementary resources are required to ensure their effectiveness. ESSs are pivotal in this regard, offering the flexibility needed to support RES integration. However, a single ESS can only partially fulfill the multifaceted demands of a given application, necessitating the deployment of hybrid storage systems to enhance ESSs for renewable energies [57]. The development of RES is instrumental in addressing energy crises and environmental pollution [58]. The variable and unpredictable nature of RES necessitates the use of ESS to mitigate the impacts of RE integration into the grid [59, 60].

In contrast to past standards, current guidelines for RES and ESS capacity planning in electrical systems have evolved. In the past, grid-tied RES capacity was restricted, and RES characteristics were not integrated into ESS planning. Several ESS innovations are currently being explored to mitigate the variability and uncertainty of large-scale RES integration into the grid [61]. To ensure future economic feasibility, RES, ESS, and RE generation capacity must be simultaneously optimized for power stations to operate efficiently [62]. Traditional planning methods often segregated ESS and RE generation capacity, with ESS capacity

typically dictated by demand. This led to conservative estimates of ESS capacity, increasing RES curtailment. Recent academic attention has turned to the planning of ESS and RE capacity, offering distributed optimization frameworks to optimize the capacity of hybrid ESS and RES generation systems. However, most of these models focus on maximizing RES and energy storage capacity individually [63, 64].

Numerous research endeavors have been devoted to planning and operating isolated grids for various types of ESS [65, 66]. However, these models are often not suited for interconnected systems due to the infrequent consideration of transmission power line constraints. Furthermore, these models typically prioritize the minimization of system costs in power system capacity planning. Simultaneously planning for ESS and RES generation introduces additional decision variables and larger model dimensions, rendering the problem more challenging to address [67, 68]. Researchers have attempted to mitigate the impact of RE restrictions in various regional systems, adopting a bi-level model to overcome multi-objective optimization challenges and achieve solutions more efficiently [69-71]. However, selecting an appropriate probability density function for RE production that accurately reflects its complex properties remains challenging. Current research often relies on the average-day approach or the Monte Carlo method for stochastic simulation, with some studies using statistical analysis to estimate average PV generating output based on typical weather data [72, 73]. Stochastic, multistage, and co-planning models have also been proposed to address the challenges of transmission expansion with ESS [74, 75].

However, these approaches have limitations, such as the inability to capture the annual output properties of RE power or to expose temporal features of RE energy. Additionally, the current RE modeling challenge struggles to gather a variety of yearly RE sequences in the area [76].

1.2.3 Control techniques used in power grid

In the domain of distributed generation control systems, several predominant approaches are discernible, including active and reactive power control, the interconnection of generation units, island detection, and notably, the control of the inner loops of DC-AC inverters. Distributed generation units typically interface with the electrical supply network via three-

phase inverters, with a primary focus on power control strategies tailored to these inverters. Several studies exploring power flow control strategies can be found in [77, 78]. Additionally, [79-81] delves into the intricacies of reactive power control. Interconnecting different generation units is another crucial aspect of distributed generation systems, primarily aimed at mitigating voltage signal distortions to ensure system stability. This aspect is explored in works such as [82, 83]. A particularly intriguing facet involves interconnecting hybrid systems, which integrate generation units of varying natures. These studies also emphasize energy dispatch, often employing predictive techniques (forecasting) to determine the required power supply at specific intervals. Reference [84] presents a focus on coordinating the injection of power from distributed generators by introducing a method for voltage control in distribution networks based on the voltage sensitivity matrix. This matrix plays a pivotal role in synchronizing the complex power injection from distributed generators by assessing the influence of each generator on the nodes within the distribution network. In situations where a distribution system operates in islanding mode, electrically isolating itself from the larger generation system yet maintaining the power supply for a specified duration, several applications centered on the detection and control of this phenomenon can be found in [85-87].

In the domain of PID (Proportional, Integral, and Derivative) control applications, various aspects are explored, including the control of diverse generation units, the management of the interconnections between these units, and the regulation of the internal loops within the inverter. This approach is applied to a range of power generation plants, encompassing hydraulic turbines [88], thermal systems [89], wind turbines [90], photovoltaic systems [91], and more. In the context of interconnecting distributed generation systems, a series of works, such as those detailed in [92-94], can be observed. These works often employ optimization algorithms to fine-tune control parameters. Concerning inverters, [95] presents a comprehensive controller design, while [96] introduces an interface design tailored to the integration of solar photovoltaic generation systems. [97] This study presents an enhanced approach to Voltage Oriented Control (VOC) for regulating an inverter connected to a three-phase network, with the inverter serving as a central component of the Distributed

Generation System. To attain optimal performance of the DG unit within the network, the study utilizes an iterative optimization method to fine-tune the PID controller parameters.

In the context of robust control applications within distributed generation systems, two primary areas of focus have been identified: the interconnection of control units and the regulation of energy conversion components, particularly inverters. Robust control applications aimed at interconnecting generation units are detailed in works such as [98], where voltage control is a key consideration, as well as in [99] for frequency control, and [100] addressing conditions of imbalance. Notably, designs based on H∞ are presented in [101, 102]. Regarding robust control applications that emphasize the control loops of inverters, [103] introduce a robust predictive scheme characterized by intrinsic synchronism for direct power control. [104] presents a robust control design tailored for distributed generation in microgrids, focusing on the direct control of voltage. The Lyapunov method is applied in [105] to ensure the stable operation of distributed generation systems based on multilevel converters. Furthermore, [106] illustrates the design of a sliding mode regulator optimized for maximum power delivery, while [107] offers insights into a hybrid robust control strategy tailored for single-phase DC-AC inverters with input voltage variations.

[108, 109] introduce predictive control systems designed for Load Frequency Control (LFC) with the primary objective of achieving permanent regulation of frequency errors following load changes in each region. Furthermore, these systems aim to ensure that the power flow within each area remains within the specified parameters. In contrast, [110] delves into energy management within local microgrids, emphasizing the utilization of predictive control strategies. On a different note, [111] presents a stochastic predictive control framework tailored for energy dispatch within a wind farm. Meanwhile, [112] focuses on the incorporation of Economic Dispatch (ED) principles for microgrid operation and introduces a predictive control methodology. This distributed control system enables communication between different distributed generation systems, facilitating an iterative optimization process. The study utilizes microgrid simulations with various energy sources to evaluate performance in comparison to a centralized control strategy.

In studies focusing on the interconnection of distributed generation units, [113] introduces the design of a fuzzy system for load frequency control within a multi-area generation system. Moreover, [114-116] investigates the interconnection of generation units of various types, such as fuel cells and battery banks. Additional strategies involving fuzzy control for interconnecting hybrid systems are presented in [117, 118]. These works stand out for their implementation of evolutionary algorithms to optimize control systems. Furthermore, [119] outlines the design of a robust fuzzy controller intended for an isolated generator linked to an infinite dam to predict load-related changes. [120] presents a control system for interconnecting distributed generation resources with electrical networks through power electronic converters. The proposed approach entails a fuzzy adaptive control system based on the Lyapunov stability theory for the converter's power loop. The primary objective of this control scheme is to ensure accurate tracking of the reference current, resulting in a suitable dynamic response.

As for control strategies primarily centered on inverter control loops, [121, 122] showcase the utilization of neuro-fuzzy systems within various components of the energy conversion system. In the domain of alternative applications, [123] outlines the development of a fuzzy controller tailored for a micro-turbine within a distributed generation system. [124] focuses on the control of a fuel cell, specifically emphasizing voltage regulation. [125] introduces the design of a fuzzy controller configured for an induction generator equipped with a dual set of stator coils.

1.3 Research objective

The main task consists of developing a new strategy that allows us to operate the multisource system optimally and distribute the energy between the connected loads according to their demand with higher efficiency. Referring to these matters of fact, several themes of objectives have been established as follows:

- Investigate the literature in the area of high penetration DG-based power networks to identify the causes of wind power instability, energy losses, partial sharding of PV, and fluctuation behavior of frequency;

- Investigate the literature on power converters to choose the most suitable for the energy storage system;
- Develop a control strategy to regulate the active and reactive power flows in an autonomous microgrid;
- Design a control scheme for a battery-based energy storage system to regulate the network frequency as well as maintain the load demand according to the wind power generation;
- Analyze the control scheme to share the wind and battery power (priority-based) in the network using a logical algorithm;
- Develop the Fuzzy logic rules and membership functions to reduce the transient time of wind power flow and the fluctuation behavior of frequency in the network;
- Integrate the different renewable energy sources (i.e. PV, hydro, wind) in the network to analyze the dynamic stability of power and frequency fluctuation in the network.

1.4 Research Methodology

The following steps are taken to develop the methodology of this thesis work :

- Modeling of DG Network: Concept, structure, and modeling of a PV and wind-diesel hybrid power system network.
- Modeling of the different components of the microgrid: Modeling of secondary/ dump load to absorb the minimum excess power from the wind turbine. Determine the main load consumer according to the production and design of the power converters, etc.
- Design a Battery Control System: Development of a control strategy for a battery-based energy storage system to maintain the overall power network in unpredictable situations.
- Design Frequency Regulate Algorithm: Design a robust control techniques scheme with different conditions to regulate the network frequency.
- Develop Fuzzy Logic Rules: Development of Fuzzy logic rules and membership functions according to the PWM signal of the network.
- Validation of control strategies and techniques: Implementation of power management strategies and control techniques in a real-time environment in order to validate them. Compensation of the harmonic currents and the reactive power generated RESs to obtain a disturbance-free grid.

1.5 Research originality and contribution

The contributions of research work in my thesis compared to the prior research are listed below:

- Reduced the transient time of wind power flow and the fluctuation behavior of frequency using a PID controller and a Fuzzy logical controller;
- Compared the robustness of the Fuzzy logical controller over the PID controller to reduce the fluctuation behavior of frequency in the network;
- Regulated the network frequency using a storage system;
- Designed a control scheme to share the power between the networks using a logical algorithm;
- Reserved the surplus wind power using a storage system and maintained a high load demand by supplying them to the network;
- Studying the technique of DC converters to reduce the operational response time in the battery system;
- Designed the control scheme for different switched-mode converters to help the batteries store/supply a desired amount of energy at maximum speed;
- Analyzed the operating ranges of Buck, Boost, SEPIC, Boost-Buck, and Buck-Boost converters to enhance the efficiency of battery and renewable energy sources;
- Compared the DC converters to know the functional voltage for the energy storage system.
- Extracted PV energy using the boost converter to track the maximum power point (MPPT).
- Designed DC/AC converters to maintain the unbalanced nonlinear load of the PV-based battery storage system.
- Reduced the Total Harmonic Distortion (TDH) of the inverters to enhance the efficiency of the power grid.

1.6 List of publications

This section presents only the published peer-reviewed journal papers to support this doctorate thesis:

1. **M.J. Rahman**, T. Tafticht, and M.L. Doumbia. Power Converters Analyzed in Energy Storage Systems to Enhance the Performance of Smart Grid Applications. *International Journal of Power Electronics and Drive Systems*. Vol. 15, No. 2, June **2024**, pp. 913~924 ISSN: 2088-8694, doi: 10.11591/ijpeds.v15.i2.pp913-924.

2 **Rahman, M.J**.; Tafticht, T.; Doumbia, M.L.; Messaïf, I. Optimal Inverter Control Strategies for a PV Power Generation with Battery Storage System in Microgrid. *Energies* **2023**, *16(10)*, 4228. https://doi.org/10.3390/en16104228.

3 **M. J. Rahman,** T. Tafticht and M. L. Doumbia, "Power Stability and Frequency Control Techniques of DG for a High Penetration Wind-Based Energy Storage System Using Integral–Derivative Controller," in *IEEE Canadian Journal of Electrical and Computer Engineering*, vol. 45, no. 3, pp. 232-241, Summer **2022**, doi: 10.1109/ICJECE.2021.3103524.

4 **Rahman, M.J.;** Tafticht, T.; Doumbia, M.L.; Mutombo, N.M.-A. Dynamic Stability of Wind Power Flow and Network Frequency for a High Penetration Wind-Based Energy Storage System Using Fuzzy Logic Controller. *Energies* **2021**, *14*, 4111. https://doi.org/10.3390/en14144111.

CHAPTER 2

POWER STABILITY AND FREQUENCY CONTROL TECHNIQUES OF DG FOR A HIGH PENETRATION WIND-BASED ENERGY STORAGE SYSTEM USING INTEGRAL–DERIVATIVE CONTROLLER

Md Jahidur Rahman[1], Tahar Tafticht[1], Mamadou Lamine Doumbia[2]

[1] Department of Engineering, Université du Québec en Abitibi-Témiscamingue, Rouyn-Noranda, QC J9X 5E4, Canada
[2] Department of Electrical and Computer Engineering, Université du Québec à Trois-Rivières, Trois-Rivières, QC G8Z 4M3, Canada

Paper published in *IEEE Canadian Journal of Electrical and Computer Engineering*, December 2021

Abstract

Distributed generation (DG) has environmental as well as economic benefits and develops new concepts to make the power network more effective and minimize pollution in the environment. Being the fluctuation behavior of renewable energy sources (RESs), generation, balance, and demand is not an easy task to control because it is not desirable to have a constant power generation from RESs due to natural prospects. As a result, the dynamic stability of power flow and control of frequency is becoming more challenging due to the high penetration impacts of RESs. In this article, we have proposed a control algorithm with two scenarios for a high-penetration/hybrid diesel wind-based energy storage system to maintain the dynamic stability of power flow and control the frequency in the overall power system. The results show that using an integral–derivative (I–D) controller, the transient time of wind power flow and the fluctuation rate of frequency are reduced significantly compared to the prior research publication. To regulate the network frequency, a storage system (battery) is used to store the excess energy without throwing it to the secondary/dump load (DL) and minimize the wastage of power produced by the wind turbine. The battery supplied the excess wind power when there is a high load demand.

Index Terms— Distributed generation (DG), frequency control, integral–derivative (I–D) controller, power stability, storage system, wind energy.

2.1 Introduction

In recent years, the percentage of renewable energies on power grids has increased significantly. Climate protection and environmental fossil resources of electric power systems need acceptable technical and economic solutions to increase the rate of power generation from non-fossil types of energy. Furthermore, the globalization of electricity sectors, which was initiated a few years ago, also allows the improvement of new technologies of electricity production. Some small-scale productions of renewable energy sources (RESs) cannot be equipped with the transmission lines of electricity [1], [2]. The connection is made straight to the distribution side of the network and now it is defined as a distributed generation (DG). The new prospect started with this type of production makes it challenging which is considered the top area study in the field of the power system. DG is mainly connected with the same transmission network which is maintained from the central station. Therefore, different technical problems arise associated with protection, reliability, harmonics, energy storage, and control systems [1]–[5]. Under these conditions, many scientists have taken attempts to find and investigate the main constraints that might happen throughout the connection made between the power grid and DG. As a consequence of that, they have established new mechanisms to analyze the nature of the variables involved in the new power network such as power stability, current, voltage, and frequency fluctuations [4], [6]. To improve these variables, many researchers have made efforts to develop the power network control schemes in their conceiver research. Most of the controllers are integrated with proportional, integral, and derivative (PID)-based control techniques; artificial intelligence (AI) control techniques; genetic algorithm-based control techniques; fuzzy logic techniques; classical control techniques; genetic algorithm-based techniques; neural network and particle swarm-based control techniques; and linear quadratic regulator (LQR) control techniques [3], [7], [8]. To investigate these types of control strategies on DG-based power systems, several works of literature have been reviewed here to gather the information and

investigate the dynamic stability of power flow and fluctuation behavior of frequency caused by high penetration impacts of RES.

In [9], a unique rule is proposed to separate the two areas into two systems (sender and receiver). Another two subsystems are counted independently by alternatively iterating to get the result of power flow. Blaabjerg et al. [10], Ahshan et al. [11], and Kermani et al. [12] proposed to develop the distributed power flow management for a multiarea power network by using the asynchronous iterative method, where the power share and the output of automatic generation control (AGC) generators are adjusted independently by the key iterative process. A variable droop technique is proposed to regulate the primary frequency with unloaded wind turbines [10], [13], [14]. They have developed a control method of the active power flow using the inconstant velocity of wind turbines to cooperate in the primary frequency regulator. A reserve capacity of energy production is proposed to reduce the frequency fluctuation in the network [15]–[17]. To minimize the time-domain function, a bacteria foraging optimization (BFO) algorithm is proposed to verify the data for an optimal [11], [18], [19]. A control technique and novel converter for a flywheel energy storage system (FESS) are proposed to improve the regulation of grid frequency and balance the power flow in a smart grid network [9], [20], [21]. The fluctuation of power flow due to the change in wind speed always leads to a frequency fluctuation in the power systems. As a result, they have proposed an energy storage system to fix this problem whose objective is to preserve energy when there is surplus production of energy and supply the energy in some emergency situations when there is a lack of energy in the power network [4], [16], [18].

By analyzing the above works of literature, we found that they have to dump all the surplus energy to the secondary/dump load (DL) to maintain the desired level of frequency in a DG-based power generation system. This is one of the main drawbacks of a future power plant. Taking that into consideration, we have proposed a technical rule for a storage system to store the surplus power from the wind turbine and supply it to the grid when we have a high load demand with respect to power generation. The stability of wind power flow depends upon the natural situation. Therefore, to improve the wind power flow and reduce the frequency fluctuation of the network, we have proposed and developed a new control strategy to minimize the transient time of wind power flow and the fluctuation behavior of

frequency in the grid by increasing the high penetration of DG using an integral–derivative (I–D) controller. This article is an extended version of our conference paper (IEEE Electrical Power and Energy Conference (EPEC) 2020) [3]. The contributions of this article compared to the prior research of publication are listed as follows :

1. Reduction of transient time of wind power flow and fluctuation behavior of frequency using an I–D controller.
2. Regulation of the network frequency using a storage system.
3. Designing of control scheme to share the power between the networks using a logical algorithm.
4. Reserving the surplus wind power using a storage system and maintaining a high load demand by supplying it into the network.

The rest of this article has been illustrated as follows. Section 2.2 describes the model of power sources. Section 2.3 provides the formulation of the grid control algorithms for a wind-diesel hybrid power system (WDHPS). Section 2.4 represents a test model connected by a WDHPS to a power network using a battery-based storage system. Section 2.5 presents the simulation results and performance evaluations of the proposed method, and in the end, Section 2.6 concludes this article.

2.2 Modeling of power sources

2.2.1 Synchronous condenser

The synchronous condenser (nominal rated power of 300 kVA) generates the voltage signal to regulate the network voltage when the diesel engine is shut down. The voltage regulator of the synchronous condenser will regulate the excitation of the condenser in order to supply the reactive power at a nominal voltage level at different buses. Here, the primary task of the synchronous condenser is to supply the reactive power in the DG network [22], [23].

2.2.2 Wind turbine

The wind DG is equipped with an asynchronous machine (ASM), rated power of 480 kVA with an inertia of 2 s. The wind DG helps to produce a Pwind, wind power to regulate the

velocity of rotation of the ASM shaft to determine its mechanical torque. Here, the DG is treated to be a constant velocity of the power generator. Thus, it does not have control over its pitch angle [24], [25].

Table 2.1 Data for tested system [3]

Sources	Symbols/Parameters
Network	480 V, 300 kVA Synchronous Generator
Turbine	480 V, 275 kVA Asynchronous Generator; Wind velocity, Vnom= 10 m/s; Wind Power, Pnom= 200 kW; Pitch angle 0^0
Synchronous Condenser Bus	SC
Wind Turbine Bus	WT
Secondary/Dump Load Bus	DL, vary 0 to 446.25 kW by step of 1.75 kW
Load Bus	L, load (main) 100kW, load (Extra) 50 kW, 30 kW, and 45kW
Storage System	SS, 240V, 390 Ah, SOC 50%
Transformer	150 kVA, 120 kV/ 480 V

2.2.3 Secondary/DL system

The DL helps to control the system frequency by absorbing the excess wind energy corresponding to the consumer demand. It consists of three-phase eight sets of resistors and is associated in series with the gate turn-off thyristor switches. The nominal power of all sets of resistors maintains a binary (8-bit) advancement in order to absorb the wind power by DL. The load can be varied (0–446.25 kW) by steps of 1.75 kW. The DL is only designed to control the fluctuation of frequency in the power grid by consuming the power produced by the wind turbine that the battery cannot be charged [3], [26], [27].

2.2.4 Battery-based energy storage system

The battery-based energy storage system (BESS) is composed of a battery bank. The power (PS-NAME = 150 kW) of a bidirectional IGBT bridge transistor is regulated in the current mode. The role of the IGBT transistor is to convert the DC sources to the AC sources in the BESS interface connecting with an isolated power network. The BESS rated capacity is 390

Ah with a voltage of 240 V, which is allowed to charge and discharge the BESS corresponding to the load demand. The control scheme of the current controlled inverter (CCI) is shown in Figure 2.1. The control technique of CCI is carried out in a structure of rotating dq-coordination. A phase-locked loop (PLL) is used to follow the waveform of grid voltage that provides the reference for the coordinate of dq-abc and abc-dq transformation. The output of the CCI current is calculated and transformed in the rotating frame as well as the currents (both active and reactive) regulated in four quadrants to generate the pulsewidth modulation (PWM) signal using an I–D controller. An LC filter is connected in CCI to minimize the current ripples [20].

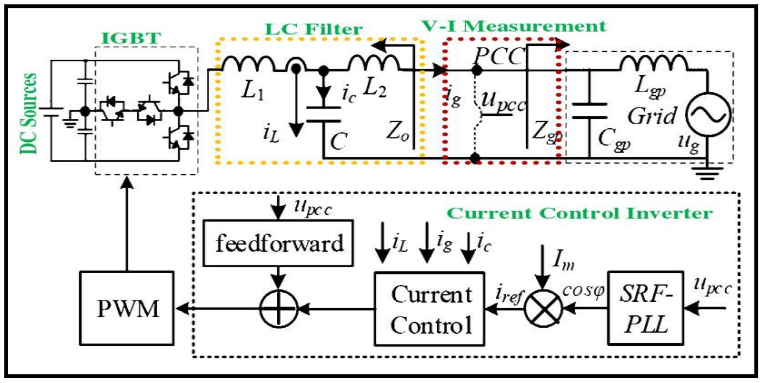

Figure 2.1 Block diagram of power converter with BESS

2.3 Modeling of power sources

The principle of dynamic stability of wind power flow and the control technique of frequency in the WDHPS network is presented by a logical algorithm shown in Figure 2.2 [3]. To secure the performance of WDHPS, the system needs an effective control scheme by using the optimum operating mode to avoid any interruption that occurs during the wind power flow as well as in the frequency of the network. Therefore, two types of control schemes should be considered: one is to ensure the dynamic stability of the power network and reduce the frequency fluctuations while another is to fulfill the energy demand with BESS logical algorithm [28].

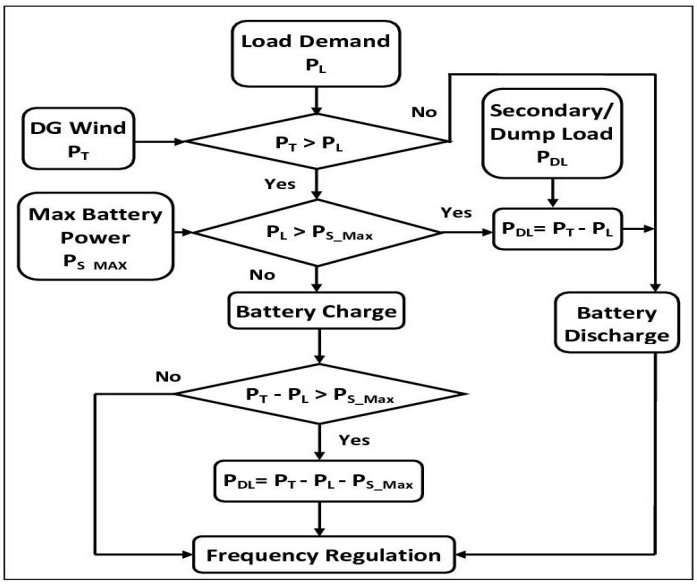

Figure 2.2 Charging and discharging stages of battery in WDHPS using power-sharing method [3].

2.3.1 Frequency Control Technique in WDHPS

To regulate the network frequency, an instantaneous level of active power must be generated and consumed by the loads. To maintain the desired level of wind power flow, the network of the DL absorbs the active power that BESS cannot store due to its capacity limitations [1], [3], [29]. In this situation, $P_T > P_L$ where $P_S > 0$. Where P_S: BESS supplied power; P_T: wind turbine generated power; P_L: load consumed power. The BESS supplies the energy to the WDHPS: in this situation, $P_T < P_L$ where $P_S < 0$.

Here, all the surplus wind energy is absorbed by the secondary/DL, $0 < P_D$, it can be written as :

$$P_T - P_L - P_D - P_S = J\,\omega\,\frac{d\omega}{dt} \qquad 2.1$$

Here, P_D denotes the power absorbed by the secondary/DL and J is the inertia of system.

$$\omega = 2\,\pi f / p \qquad 2.2$$

where, ω is the velocity (rad/s) of the synchronous machine shaft; p is the poles number of the synchronous machine. The losses in equation 2.1 are not considered in this case. Thus, P_S

$< P_{S\_nom}$ and $P_D < P_{D\_nom}$ (converter nominal value). To keep a steady-state velocity of ASM, we can write:

$$\frac{d\omega}{dt} = 0 \tag{2.3}$$

The control strategy of the BESS and DL systems should be coordinated with each other. The DL should consume the surplus wind power that the BESS cannot store. Therefore, equation 2.1 can be written as :

$$P_T - P_L = P_D + P_S \tag{2.4}$$

$$P_{ref} = P_{S\_ref} + P_{D\_\mathrm{ref}} \tag{2.5}$$

$$P_{D\_ref} = 0 \text{ when } P_{ref} < P_{S\_nom} \tag{2.6}$$

Equation 2.5 becomes $P_{D\_ref} = P_{ref,,}$ if the BESS reaches its maximum capacity (P_{S_ref}). The DL helps to absorb the wind power if P_{ref} is more than the BESS nominal power. The P_{S_max} varies with 0 and P_{S_nom}, by using a positive power limit (PPL) signal. The power share between the BESS and DL is confirmed by the priority of power consumption using a logical algorithm (i.e., DL only consumed the surplus power that the BESS cannot store) [3], [29].

However,

$$P_{S\_ref} = P_{ref} \text{ when } Pref \leq 0 \tag{2.7}$$

$$P_{S\_ref} = P_{S\_max} \text{ when } P_{ref} > 0 \tag{2.8}$$

In the DL,

$$P_{D\_ref} = P_{ref} - P_{S\text{-}max} \text{ when } P_{ref} > 0 \tag{2.9}$$

$$P_{D\_ref} = 0 \text{ when } P_{ref} \leq 0 \tag{2.10}$$

The BESS and DL should recognize the P_{ref} (reference power) simultaneously and maintain the accuracy at the time of operation. Thus, three types of control techniques can be implemented [1] [2] [8]. Using the DL only when the BESS is completely charged, $P_{s\text{-}max} < P_T - P_{L,}\ P_S = 0_{;}$ by using the BESS only ($0 = P_D$) if $|P_T - P_L| \leq P_{S\_nom}$; by using both BESS and DL, if ($P_{ref} > 0$) $P_T - P_L > 0$.

Generally, a Supervisory Control and Data Acquisition (SCADA) system is used to monitor and control each part of the system. The SCADA system interacts with each part of the entire system. The SCADA system allows each part of the system to be informed about the active

power of other parts. The use of the Modbus communication protocol allows for the exchange of the data necessary for the system's proper functioning. Communication channels can be either wired or wireless. The basic communication methods used are power-line carrier, broadband over power line, leased telephone line, global system for mobile (GSM) communication, LAN/ WAN / Internet (TCP/IP), wireless radio communication, optic fiber, WiFi802.11b, WiMAX 802.16 and IEEE 802.15.4 [30]. The principle of the frequency control scheme for a WDHPS system and the method of power-sharing between the BESS and DL are represented in Figures 3 and 4 respectively. [4] [29]. Here, the three-phase Phase Locked Loop (PLL) collects the error of frequency which is the divergence of the reference frequency (60 Hz) and the actual network frequency, and supplies the P_{ref} to confirm the power-sharing priority between the BESS and DL using a logical algorithm. The power in the BESS node remains at its nominal value under normal situations [3] [7].

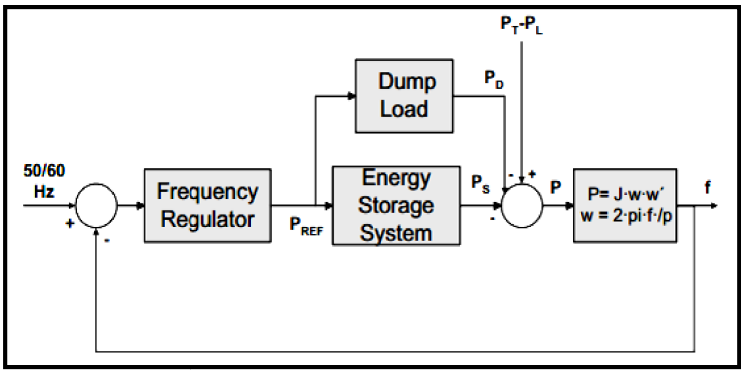

Figure 2.3 Frequency control scheme of the WDHPS system [1] [3] [29].

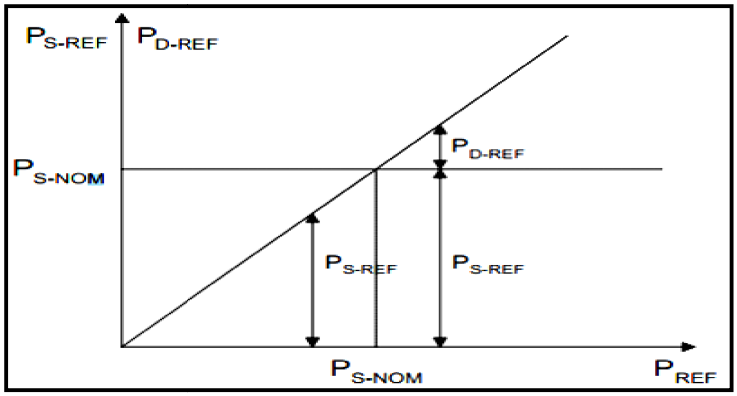

Figure 2.4 Power sharing strategy between the BESS and DL [1] [3] [29].

2.3.2 Control of BESS

The BESS performs the two strategies of control mode [1] [8].

As a mode of an inverter, the BESS supplies power to the network, where $Ps < 0$. As a result, the BESS discharges as well as the current pass through the network to provide the required power to fulfill the load demand. In this situation, the velocity of the wind turbine is defined. Therefore, the power produced by the wind turbine is not enough to provide the power to the load consumer.

As a mode of a rectifier, the BESS consumes the surplus power from the network, where $Ps > 0$. Hence, the BESS charges bypass the current from the network. In this situation, the velocity of the wind turbine is very high. The power produced by the wind turbine cannot be consumed by the load consumer. Therefore, the surplus power is consumed by the BESS and supplies the power in an emergency situation.

2.4 Connecting a wind turbine to the power grid with storage system

In this paper, we have analyzed the dynamic stability of the wind power flow and the behavior of the frequency fluctuation using a BESS in the power network. In this case study, an example has been considered for a High Penetration, No Storage of Wind-Diesel system (HPNSWD) [1] [3] [14]. This model was developed by Hydro-Quebec for an isolated region to reduce the installation and maintenance cost of the power generation system. The maximum power produced by the wind turbine relies on the feasible wind resources as well as the fuel cost [6]. A wind turbine asynchronous generator rated at 480 V, 275 kVA, a synchronous condenser generator rated at 480 V, 300 kVA, a BESS rated at 240 V, 390Ah, a secondary/dump load (varying between 0 to 446.25 kW), and consumer load rated up to 230 kW is used in this case study. According to the cases, we have considered two scenarios of operation of the power network to ensure the dynamic stability of the power flow and control of the frequency fluctuation [1] [3].

Scenario 1: Power Produced by Wind Turbine (P_T) is > Overall Load Demand (P_L). In this situation, BESS (P_S) will be charged;

Scenario 2: Power Produced by Wind Turbine (P_T) is < Overall Load Demand (P_L). In this situation, BESS (P_S) will be discharged.

Figure 2.5 shows an I-D controller has been optimized to observe the dynamic stability of power flow and the behavior of the frequency fluctuation in the network. The I-D controller is a control technique where the proportional part of a PID controller is not taken into account (i.e. it's set to zero). By using an I-D controller, the nonlinearity behavior of a wind-based BESS power network can be easily well-controlled. A three-phase PLL is used for amplification of the network frequency. The network voltage is supplied as an input of the PLL. To generate a frequency error, a reference frequency (60 Hz) is created to compare with the network frequency. After that, the frequency error is integrated to obtain a phase error. In the end, the phase error is implemented using an l-D controller to initiate an output PWM signal to receive the desired level of load power in the network.

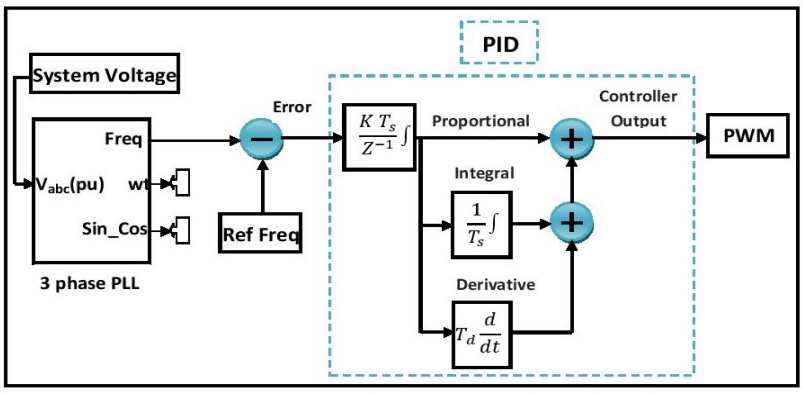

Figure 2.5 Operational diagram of frequency control using an I-D controller [3].

2.5 Simulation and result

2.5.1 Power produced by wind turbine (PT) is > overall load demand (PL). In this situation, BESS (PS) will be charged

To produce an adequate level of power, the wind velocity at 10 m/s should be kept in the turbine to supply the power to the consumer. Here, the diesel generator is idled. The synchronous machine runs as a synchronous condenser when the input of the synchronous machine's mechanical power (Pm) is set to zero. When the wind turbine operates at the velocity of 10 m/s, we obtain an output power of 206 kW. The wind turbine produces 200 kW due to the losses in ASM. To analyze the dynamic stability of wind power flow, we have

used an I-D controller. Figure 2.6 (a) shows, the transient time of wind power flow is significantly reduced and the wind power fluctuation rate at 2.5 s due to the excess load, 50 kW is improved from 256 kW to 246 kW using the I-D controller. The synchronous condenser supplies reactive power at a rate of 15 kVA to maintain an acceptable level of voltage to the power network. Figure 2.6 (b) shows the transient time of reactive power flow produced by the synchronous condenser was also reduced using an I-D controller.

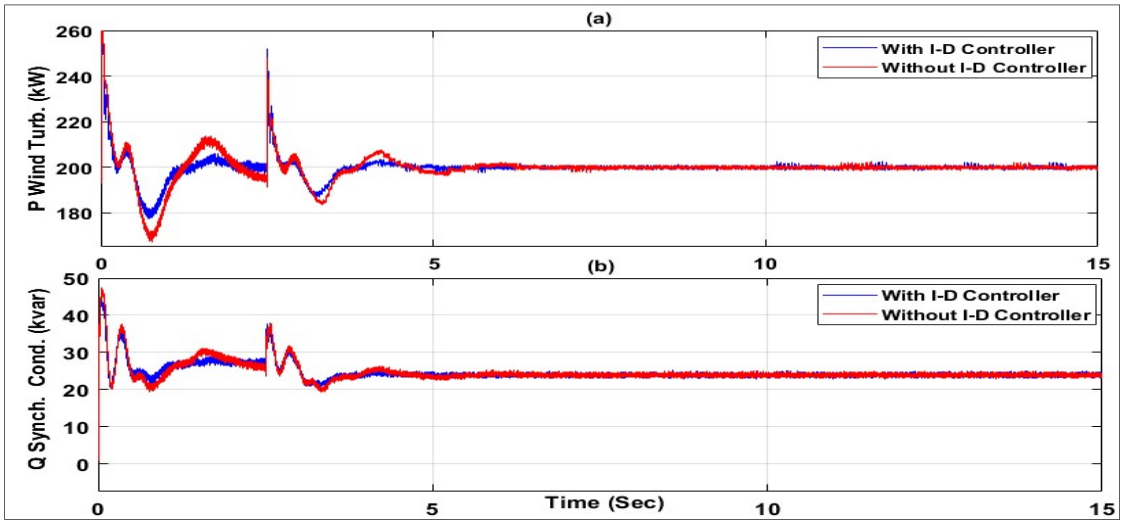

Figure 2.6 (a) Power produced by the wind turbine and, (b) Reactive power supply from the synchronous condenser, where battery is charged.

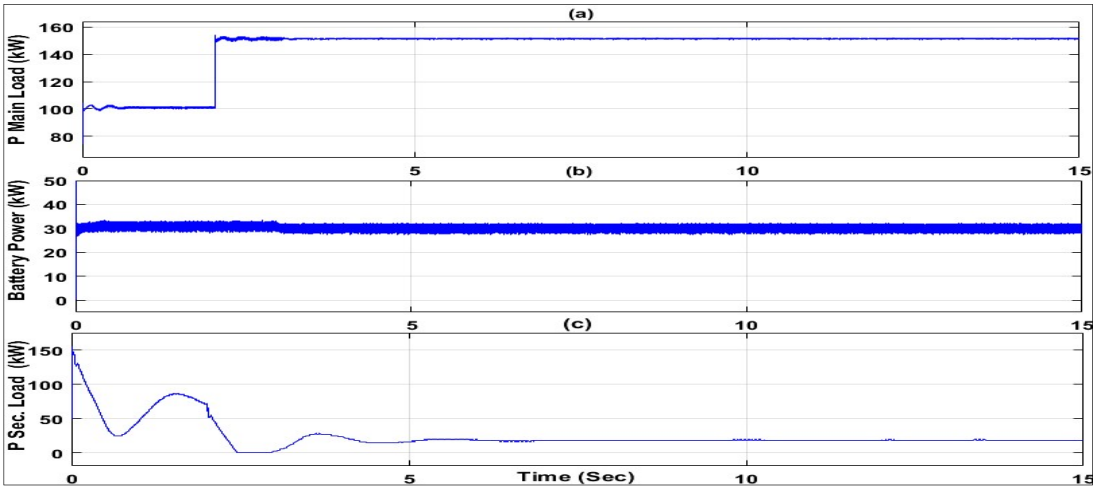

Figure 2.7 (a) Power consumed by consumer load (b) Power supplied from BESS and, (c) Power consumed by DL, where battery is charged.

Figure 2.7 (a) shows, the main consumer load is 100 kW. An excess load, of 50 kW has been connected at 2.5 s to observe the power stability and fluctuation of frequency in the network. Here, the total load of the network is now 150 kW. Which is less than wind power production with respect to the load demand. As a result, the BESS was charged (rate of 30 kW), shown in Figure 2.7 (b) at 3 s without throwing all the power to the DL. Figure 2.7 (c) shows, DL is only absorbed 20 kW that the battery cannot store to regulate the frequency in 60 Hz.

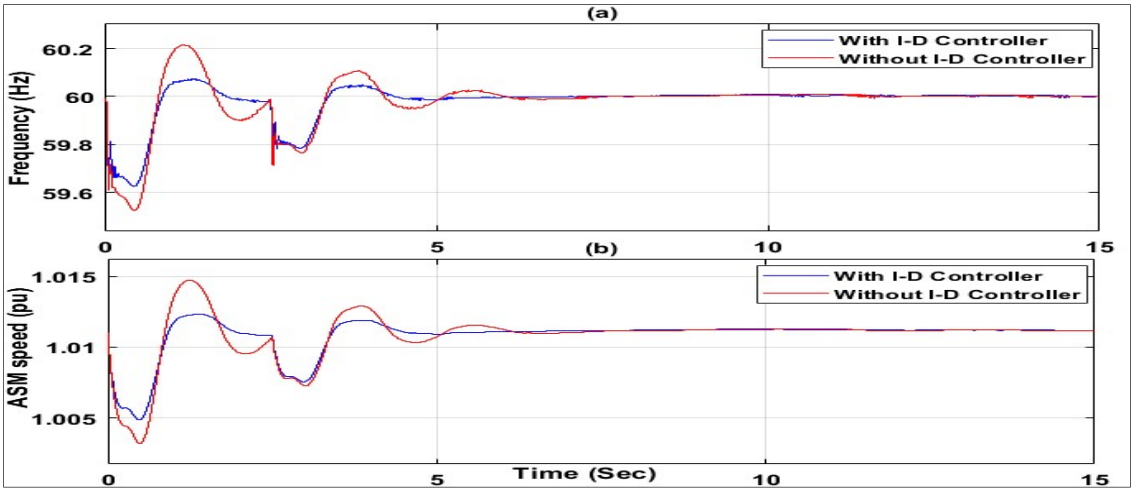

Figure 2.8 (a) Network frequency conditions and, (b) Speed generated by ASM generator, where BESS is charged.

Figure 2.8 (a) shows, the transient time of network frequency is significantly reduced and the frequency fluctuation rate at 2.5 s due to the excess load, 50kW is improved from 59.68 Hz to 59.77 Hz using an I-D controller. The velocity of the ASM is reached at 1.01 pu and runs in a generator mode. The transient time of ASM velocity is also reduced using an I-D controller shown in Figure 2.8 (b). Figure 2.9 (a) shows, the system voltage stays at 1 pu. For more observations, data was taken from 11 s -13 s. The current of DL is decreased at 2.5 s due to an excess load, 50 kW. The DL is also decreased at 3 s due to the BESS (rate of 30 kW) charging situation, shown in Figure 2.9 (b). Figure 2.10 (a) presents the BESS (50%) State of Charge (SOC), where the BESS is charged from 49.7% to 49.9%. The BESS current situation is shown in Figure 2.10 (b). The BESS current was zero before 3 s, but after 3s, the BESS received -200 A current to charge by itself and consumed 30 kW energy from the network. The voltage of BESS is increased at 3s and stays at 262 V during simulation, shown in Figure 2.10 (c).

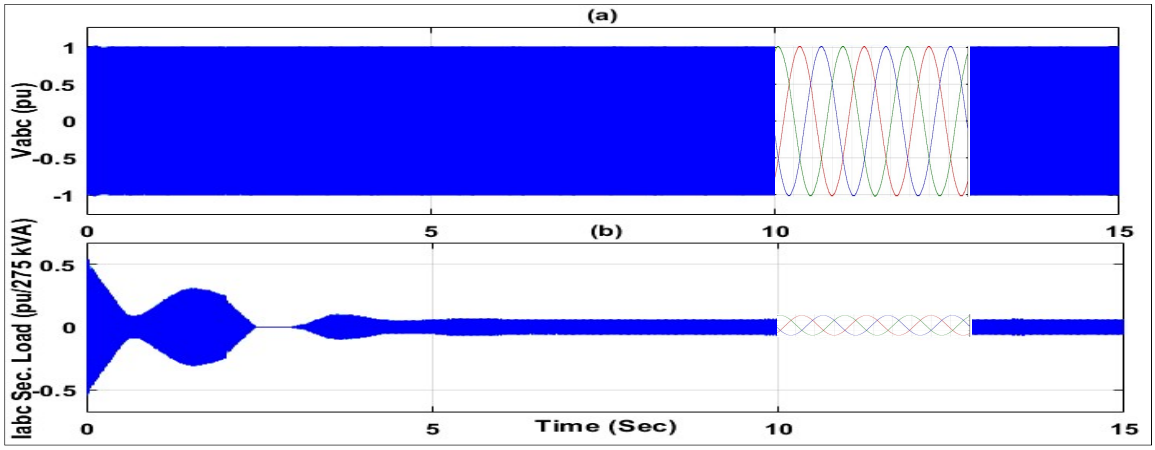

Figure 2.9 (a) Voltage at load bus and, (b) Current at DL, where BESS is charged.

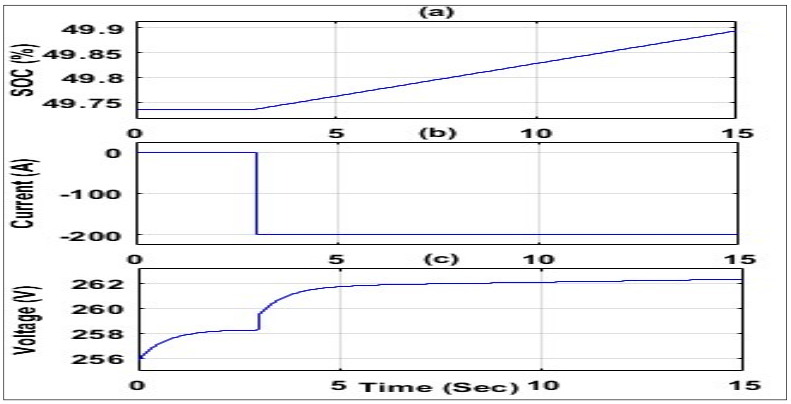

Figure 2.10 (a) BESS SOC condition, (b) BESS current condition and,
(c) BESS voltage condition, where BESS is charged.

2.5.2 Power produced by wind turbine (P_T) is < overall load demand (P_L). In this situation, BESS (P_S) will be discharged

To produce an adequate level of power, the wind velocity should be kept at 10 m/s in the turbine to supply the power to the consumer. Here, the diesel generator is idled. The synchronous machine runs as a synchronous condenser when the input of the synchronous machine's mechanical power (Pm) is set to zero. When the wind turbine operates at the velocity of 10 m/s, we obtain an output power of 206 kW. The wind turbine produces 200 kW due to the losses in ASM. To analyze the dynamic stability of wind power flow, we have used an I-D controller. Figure 2.11 (a) shows, the transient time of wind power flow is significantly reduced and the wind power fluctuation rate at 0.5 s, 3 s, and 7.5 s due to the

excess load, 50 kW, 30 kW, and 45 kW are improved from 256 kW to 248 kW, 232 kW to 227 kW and 257.5 kW to 243.5 kW respectively using an I-D controller. The synchronous condenser supplies reactive power at a rate of 15 kVA to maintain an acceptable level of voltage to the power network. Figure 2.11 (b) shows the transient time of reactive power flow produced by the synchronous condenser was also reduced using an I-D controller.

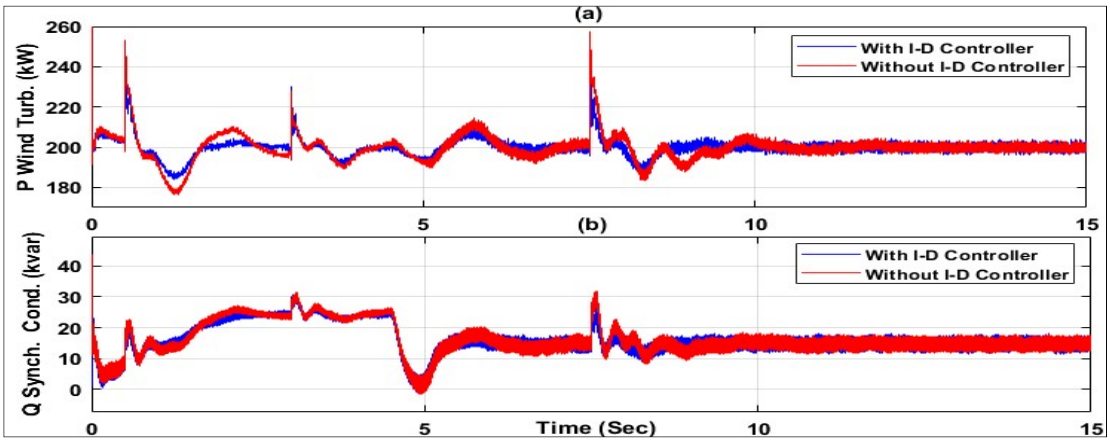

Figure 2.11 (a) Power produced by the wind turbine and, (b) Reactive power supply from the synchronous condenser, where BESS is discharged.

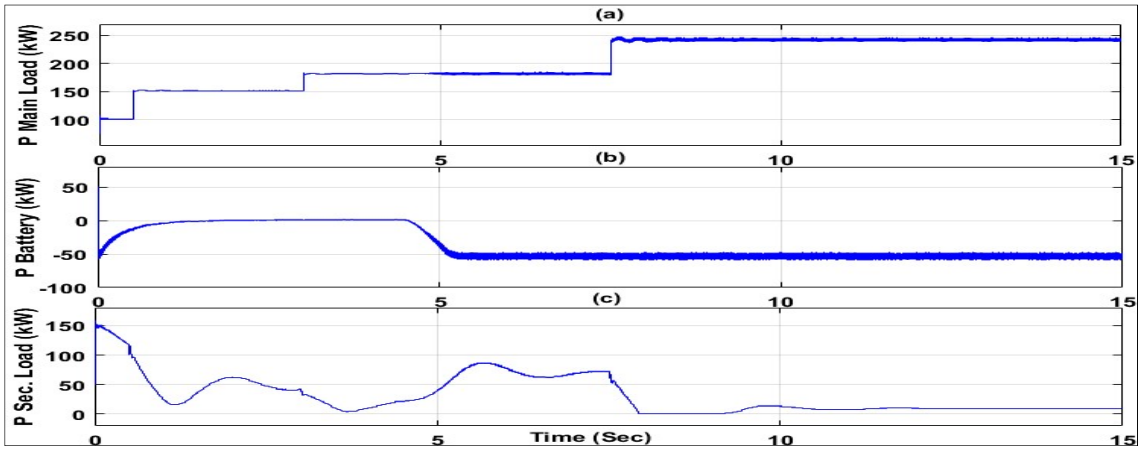

Figure 2.12 (a) Power consumed by consumer load (b) Power supplied from BESS and, (c) Power consumed by DL, where BESS is discharged.

Figure 2.12 (a) shows, the main consumer load is 100 kW. An excess load, 50 kW, 30 kW, and 45 kW is connected at 0.5 s, 3 s, and 7.5 s respectively to analyze the wind power stability and fluctuation of frequency in the network. Here, the total load of the network is now 230 kW. Which is more than the total load demand with respect to wind power

generation. Therefore, the BESS was discharged (rate of 50 kW) at 4.5 s is shown in figure 2.12 (b) to maintain the high load demand in the network. Figure 2.12 (c) shows, DL is only absorbed 20 kW that the battery cannot store to regulate the frequency in 60 Hz.

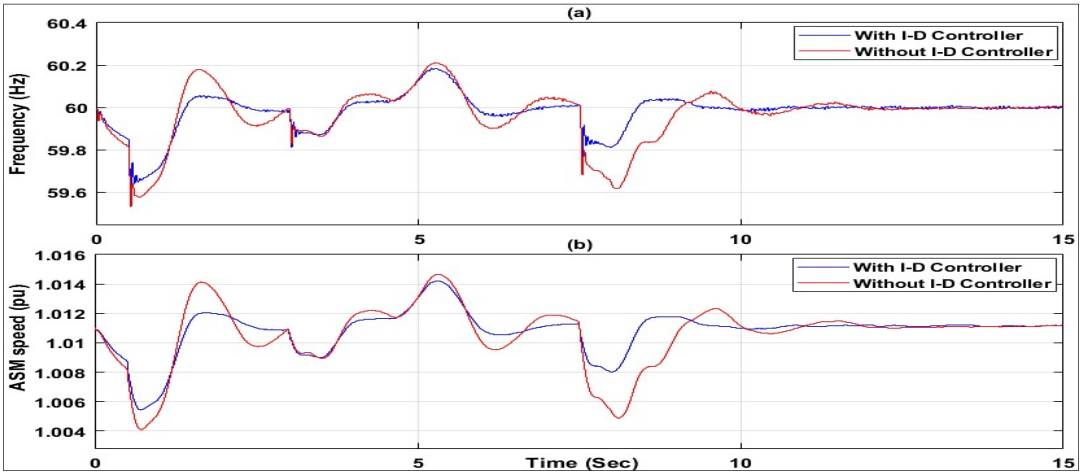

Figure. 2.13. (a) Network frequency conditions and, (b) Speed generated by ASM generator, where BESS is discharged.

Figure 2.13 (a) shows, the transient time of network frequency is significantly reduced and the frequency fluctuation rate due to the excess load, 50 kW, 30 kW and, 45 kW at 0.5 s, 3 s, and 7.5 s are improved from 59.53 kW to 59.58 kW, 59.78 kW to 59.85 kW, and 59.68 kW to 59.76 kW respectively using an I-D controller. The velocity of the ASM is reached at 1.01 pu and runs in generator mode. The transient time of ASM velocity is also reduced using an I-D controller shown in Figure 2.13 (b). Figure 2.14 (a) shows, the system voltage stays at 1 pu. For more observations, the data was taken from 11 s - 13 s. Figure 2.14 (b) shows, the current of DL is decreased due to the excess load, 50 kW, 30 kW, and 45 kW at 0.5 s, 3 s, and 7.5 s respectively. The DL is also decreased at 4.5 s due to the BESS (rate of 50 kW) discharging situation. Figure 2.15 (a) represents the BESS (50%) State of Charge (SOC), where the BESS is discharged from 49.73% to 49.60%. The BESS current situation is shown in Figure 2.15 (b). The BESS current was zero before 4.5 s, but after 4.5 s, the BESS received 200 A to discharge by itself and supplied 50 kW energy to maintain the load demand in the network. The voltage of BESS was decreased at 4.5 s and stayed at 254 V during the simulation shown in Figure 2.15 (c).

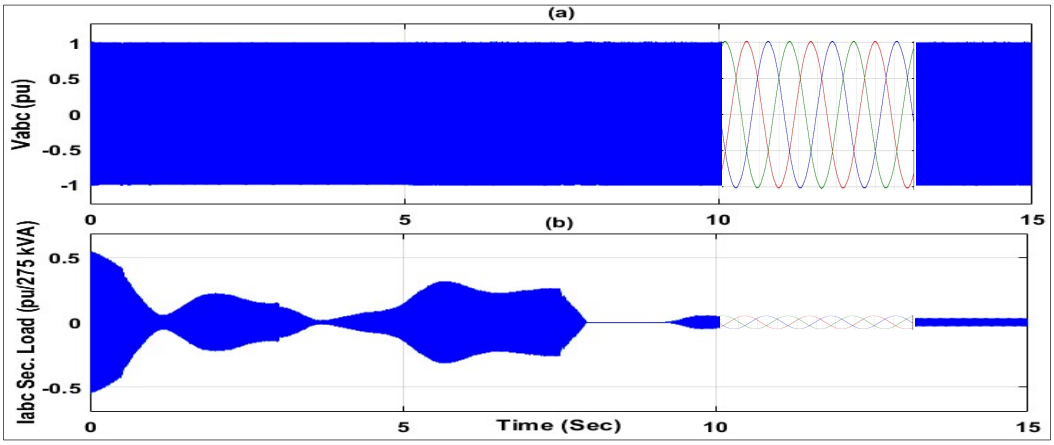

Figure 2.14 (a) Voltage at load bus and, (b) Current at DL, where BESS is discharged.

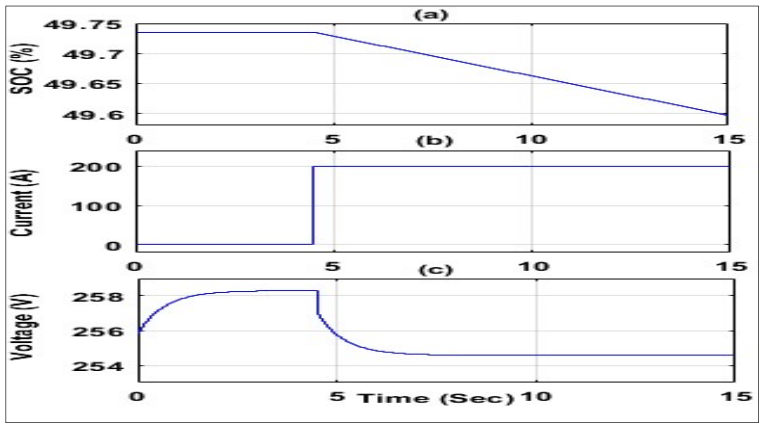

Figure 2.15 (a) BESS SOC condition, (b) BESS current condition and, (c) BESS voltage condition, where BESS is discharged.

From the above simulation, the result shows, using the I-D-based PID controller the variation of wind power flow and the fluctuation of frequency were reduced significantly compared to the previous research. It's also observed that, without throwing a large amount of power in a secondary/dump load to maintain the acceptable level of frequency, a storage system (battery) was used to charge when the power from a wind turbine is higher than the total load demand and discharged when the power from a wind turbine is less than total load demand.

2.6 Conclusion

In this paper, the technologies associated with wind-based DG, the frequency fluctuation behavior along with wind turbines were identified and simulated. The wind power stability

and the frequency control technique were analyzed elaborately. Power-sharing methods between the BEES and DL are presented with a high penetration-based DG using a logical algorithm. In addition, it is also observed that without throwing a large amount of power in a secondary/DL, a storage system can be used to store the energy and supply when there is a high load demand with respect to the power generation by the wind turbine. The response of the BESS usually depends on the technology used and its dynamics which can cause a wide variation in the power network (i.e. power flow, voltage and, frequency). The simulation shows, the load variation at different times to analyze the dynamic stability of wind power flow and the fluctuation behavior of frequency with I-D-based PID controller.

2.7 References

1. Rahman, M.J., "Frequency control in the presence of renewable energy sources in the power network. 2017." M.S. thesis, Dept. Elect. Eng., Electron. Montreal, École de Technologie Supérieure, Montreal, QC, Canada, 2017.
2. R. Lingamuthu and R. Mariappan, Power flow control of grid connected hybrid renewable energy system using hybrid controller with pumped storage. *International Journal of Hydrogen Energy*, 2019. 44(7): p. 3790-3802.
3. M. J. Rahman, T. Tafticht, and M. L. Doumbia, "Frequency control for a high penetration wind-based energy storage system in the power network," in Proc. *IEEE Electr. Power Energy Conf. (EPEC)*, Nov. 2020, pp. 1–6.
4. S. Impram, S. Varbak Nese, and B. Oral, "Challenges of renewable energy penetration on power system flexibility: A survey," *Energy Strategy Rev.,* vol. 31, Sep. 2020, Art. no. 100539.
5. Y.-S. Kim, E.-S. Kim, and S.-I. Moon, "Frequency and voltage control strategy of standalone microgrids with high penetration of intermittent renewable generation systems," *IEEE Trans. Power Syst*., vol. 31, no. 1, pp. 718–728, Jan. 2016.
6. E. I. Vrettos and S. A. Papathanassiou, "Operating policy and optimal sizing of a high penetration RES-BESS system for small isolated grids," *IEEE Trans. Energy Convers.,* vol. 26, no. 3, pp. 744–756, Sep. 2011.
7. M. H. Nazari, M. Ilic, and J. P. Lopes, "Dynamic stability and control design of modern electric energy systems with large penetration of distributed generators," in *Proc. IREP Symp. Bulk Power Syst. Dyn. Control VIII (IREP)*, Aug. 2010, pp. 1–7.
8. S. de la Rue du Can, G. Leventis, A. Phadke, and A. Gopal, "Design of incentive programs for accelerating penetration of energy-efficient appliances," *Energy Policy*, vol. 72, pp. 56–66, Sep. 2014.

9. D. Zhao et al., “Construction of an example system for AC/DC hybrid power grid with high-proportion renewable energy,” *J. Eng*., vol. 2019, no. 16, pp. 1117–1121, Mar. 2019.
10. F. Blaabjerg, Y. Yang, D. Yang, and X. Wang, “Distributed powergeneration systems and protection,” *Proc. IEEE*, vol. 105, no. 7, pp. 1311–1331, Jul. 2017.
11. R. Ahshan, S. A. Saleh, and A. Al-Badi, “Performance analysis of a Dq power flow-based energy storage control system for microgrid applications,” *IEEE Access*, vol. 8, pp. 178706–178721, 2020.
12. H. R. Kermani, M. V. Dahraie, and H. R. Najafi, “Frequency control of a microgrid including renewable resources with energy management of electric vehicles,” in *Proc. Iranian Conf. Renew. Energy Distrib. Gener. (ICREDG),* Apr. 2016, pp. 114–118.
13. C. Zhao, U. Topcu, N. Li, and S. Low, “Design and stability of loadside primary frequency control in power systems,” *IEEE Trans. Autom. Control,* vol. 59, no. 5, pp. 1177–1189, May 2014.
14. L. Mott, *Commercial Wind-Diesel Project*, St. Paul Island, St. Paul, Alaska, 1999.
15. N. E. Y. Kouba, M. Menaa, M. Hasni, and M. Boudour, “Load frequency control in multi-area power system based on fuzzy logic-PID controller,” in *Proc. IEEE Int. Conf. Smart Energy Grid Eng. (SEGE)*, Aug. 2015, pp. 1–6.
16. J. Syamala and I. Naidu, “Load frequency control of multi-area power systems using PI, PID, and fuzzy logic controlling techniques,” *Int. J. Innov. Res. Sci., Eng. Technol., vol. 3, pp. 1285–1288, 2014.*
17. K. V. Vidyanandan and N. Senroy, “Primary frequency regulation by deloaded wind turbines using variable droop,” *IEEE Trans. Power Syst.*, vol. 28, no. 2, pp. 837–846, May 2013.
18. M. A. Zamee, D. Mitra, and S. Y. Tahhan, “Load frequency control of interconnected hydro-thermal power system using conventional PI and fuzzy logic controller,” I*nt. J. Energy Power Eng.,* vol. 2, no. 5, pp. 191–196, 2013.
19. Z. A. Obaid, L. M. Cipcigan, L. Abrahim, and M. T. Muhssin, “Frequency control of future power systems: Reviewing and evaluating challenges and new control methods,” *J. Mod. Power Syst. Clean Energy*, vol. 7, no. 1, pp. 9–25, 2019.
20. E. S. Ali and S. M. Abd-Elazim, “BFOA based design of PID controller for two area load frequency control with nonlinearities,” *Int. J. Electr. Power Energy Syst.*, vol. 51, pp. 224–231, Oct. 2013.
21. M. Darabian, A. Jalilvand, and M. Azari, “Power system stability enhancement in the presence of renewable energy resources and HVDC lines based on predictive control strategy,” *Int. J. Elect. Power Energy Syst*., vol. 80, pp. 363–373, Sep. 2016.
22. H. S. Salama, M. M. Aly, M. Abdel-Akher, and I. Vokony, “Frequency and voltage control of microgrid with high WECS penetration during wind gusts using superconducting magnetic energy storage,” *Electr. Eng.*, vol. 101, no. 3, pp. 771–786, Sep. 2019.

23. K. N. Bangash, M. E. A. Farrag, and A. H. Osman, “Investigation of energy storage batteries in stability enforcement of low inertia active distribution network,” *Technol. Econ. Smart Grids Sustain. Energy*, vol. 4, no. 1, pp. 1–12, Dec. 2019.

24. H. Amano, Y. Ohshiro, T. Kawakami, and T. Inoue, “Utilization of battery energy storage system for load frequency control toward largescale renewable energy penetration,” in *Proc. 3rd IEEE PES Innov. Smart Grid Technol. Eur. (ISGT Eur.),* Oct. 2012, pp. 1–7.

25. Z. Zhao and L. Wu, “Impacts of high penetration wind generation and demand response on LMPs in day-ahead market,” *IEEE Trans. Smart Grid*, vol. 5, no. 1, pp. 220–229, Jan. 2014.

26. Z. Wang et al., “Research on the active power coordination control system for wind/photovoltaic/energy storage,” in *Proc. IEEE Conf. Energy Internet Energy Syst. Integr. (EI)*, Nov. 2017, pp. 1–5.

27. G. Magdy, E. A. Mohamed, G. Shabib, A. A. Elbaset, and Y. Mitani, “Microgrid dynamic security considering high penetration of renewable energy,” *Protection Control Modern Power Syst.,* vol. 3, no. 1, pp. 1–11, Dec. 2018.

28. Z. Conka, M. Kolcun, and G. Morva, “Impact of renewable energy sources on power system stability,” *Power Electr. Eng.*, vol. 32, pp. 25–28, Nov. 2014.

29. R. Sebastián and J. Quesada, “Distributed control system for frequency control in a isolated wind system,” *Renew. Energy,* vol. 31, no. 3, pp. 285–305, Mar. 2006.

30. P. Chavan and R. J. Devi, “Survey of communication system for DG’s and microgrid in electrical power grid,” *Int. Res. J. Eng. Technol*., vol. 3, no. 7, pp. 1155–1164, 2016.

CHAPTER 3

DYNAMIC STABILITY OF WIND POWER FLOW AND NETWORK FREQUENCY FOR A HIGH PENETRATION WIND-BASED ENERGY STORAGE SYSTEM USING FUZZY LOGIC CONTROLLER

Md Jahidur Rahman [1], Tahar Tafticht [1], Mamadou Lamine Doumbia [2] and Ntumba Marc-Alain Mutombo [3]

[1] Department of Engineering, Université du Québec en Abitibi-Témiscamingue, Rouyn-Noranda, QC J9X 5E4, Canada
[2] Department of Electrical and Computer Engineering, Université du Québec à Trois-Rivières, Trois-Rivières, QC G8Z 4M3, Canada
[3] Department of Electrical Engineering, Mangosuthu University of Technology, Durban 4031, South Africa

Paper published in *Energies,* July 2021

Abstract

Major changes in the technologies of power generation and distribution systems have been introduced in recent years due to concern over rapid climate change. Therefore, disturbances in the large-scale generation, transmission, and distribution of energy are expected to occur in the near future. This is due to the difficulty in controlling the transmission and distribution of energy produced from renewable energy sources (RESs), caused by the instability of these sources and the intermittent nature of their energy. As a result, maintaining the dynamic stability of wind power flow and control of the network frequency is becoming more challenging due to the high penetration impacts of RESs. In this paper, a control algorithm using the power-sharing method is proposed for a wind-based energy storage system to maintain the dynamic stability of wind power flow and control of frequency in the power network. To maintain the network stability, a storage system (battery) was installed to store the excess wind power without throwing it into the Secondary/Dump Load (SL) and minimize losses in power generated by the wind turbine. The results show, the transient time of wind power flow and the fluctuation rate of frequency are reduced significantly using a

Fuzzy Logic (FL) controller compared to the Proportional Integral Derivative (PID) controller.

Keywords: wind energy; power stability; storage system; secondary/dump load; frequency control; PID controller; fuzzy logic controller

3.1 Introduction

In recent years, the percentage of renewable energies on power grids has increased significantly. This rise was prompted by policies aimed at combating climate change and securing a sustainable energy supply. The Intergovernmental Panel on Climate Change (IPCC) reported that: "the production of greenhouse gases, such as nitrous oxide (N_2O), carbon dioxide (CO_2) and methane (CH_4) are responsible for global warming due to the evolution of fossil fuels" [1]. The replacement of fossil energy sources by renewable energy sources (RESs) such as wind, solar, biomass, hydroelectricity, etc., and their integration into low and high-voltage electrical networks is currently the subject of research in several countries such as the United States, Canada, Germany, and China.

Concerns about climate change caused by the usage of fossil fuels have made renewable energy one of the most popular research topics [2]. Around 23.7 percent of the world's power is produced by RESs. This implies that renewable energy accounts for a quarter of global power generation, with photovoltaic (PV) and wind turbine (WT) systems accounting for 77% of new renewable energy installations [2]. The main focus in renewable energy is on microgrids, which are hybrid renewable energy systems that are the subject of intense investigation. A microgrid is a system that produces clean, sustainable, steady, and dependable electricity by combining renewable resources with one or more conventional power sources [3]. They can be connected to the grid or run independently [2]. Due to the requirement for a control system to efficiently manage the operation of intermittent renewable resources, an energy management system is generally included inside a microgrid [4]. This is mainly achieved by including an energy storage system to increase the effectiveness and stability of the microgrid. Recently, several studies have implemented a fuzzy logic controller to employ Energy Management Systems (EMS) on Microgrids. Due to its ability to handle many tasks effectively and forecast wind speed, solar radiation, load

usage, and even the grid's health, fuzzy logic is an effective microgrid control, particularly when several functions are performed on the microgrid [2]. It can regulate many operations in the microgrid, including load shedding, energy cost reductions, and CO_2 emissions [5].

Several studies in the literature used the Fuzzy Logic Energy Management System (FLEMS) to regulate the level of charge of battery energy storage in microgrids of various topologies in order to extend their lifetime and provide smooth operation [2]. The lifespan of the battery for a microgrid constituted of PV, WT, and Battery Energy Storage (BES), and supplying different sorts of loads, can be increased by maintaining the State of Charge (SOC) of the batteries using FLEMS [6, 7]. Considerable achievement in battery lifespan can also be made by estimating the Fuel Cell (FC) electrolyzer and battery power based on the batteries' SOC and the FC's hydrogen tank level using FLEMS for a standalone microgrid equipped with PV, WT, battery storage, and an FC [8, 9]. A FLEMS can also be used to maximize hydrogen production and optimize power flow and generation in a microgrid composed of PV, FC, and BESS controlled by FLEMS [10]. Furthermore, the grid power profile can be smoothed in a grid-connected AC microgrid while maintaining the SOC of the BESS with the lowest possible fuzzy logic rules using an FLMS [11].

Maintaining the SOC of battery storage is one of the key issues of building the EMS of microgrids of various topologies, as we can see from past research. According to the research, there are several benefits to using intelligence methods to optimize the FLEMS of various microgrid topologies [2]. FLEMS optimization allows for more accurate control, resulting in more efficient operation, reduced backup system costs, and a more balanced operation between generation and consumption [2]. Several studies have been published that have improved the FLEMS of microgrids. Many optimization approaches for microgrids FLEMS have been utilized. Particle swarm optimization (PSO) [12, 13, 14], genetic algorithm (GA) optimization technique [15], seeker optimization approach (SOA) [16], and ABC optimization technique [17, 18] are all examples of this.

One of the most popular forms of renewable energy today is wind energy [19, 20]. However, the stochastic nature of this energy makes it difficult to integrate it into the power grid, especially when it comes to large-scale integration into Voltage Source Converter-based

High Voltage Direct Current (VSC-HVDC) power grids. In addition, perfect synchronization is required to improve power quality as well as the frequency for keeping the network stable and robust. The globalization of the electricity sector, which was initiated a few years back, allows the improvement of new technologies of power generation. Some small-scale productions of RESs may not be equipped with transmission lines of electricity [21, 22]. The connection of RESs is made straight to the distribution side of the grid and the microgrid is defined as a Distributed Generation (DG). The new prospect with this type of energy production makes it challenging, which is considered the top area of study in power system generation.

DG is mainly connected with the same transmission network which is maintained from the central station. Therefore, different technical problems arise associated with protection, reliability, harmonics, energy storage, and control systems [21, 22, 23, 24]. Due to changes in the environmental parameters, it is difficult to have continuous power generation from RESs. The fluctuating nature of power generated from these systems, wind in particular [25], makes it difficult to control, balance, and demand their energy. As a result, the dynamic stability of network frequency is becoming more challenging due to the high penetration impacts of RESs. Under these conditions, many scientists have made attempts to find and investigate the main constraints that might happen throughout the connection between the power grid and DG. The impacts of one non-renewable and two renewable types of DG on voltage profiles and power losses on a distribution network were examined [26]. The conclusion was different types of DG differently influence the distribution network, and their precise location and size are vital in reducing power losses and improving voltage stability. Consequently, new mechanisms to analyze the nature of the variables involved in the new power network such as power stability, current, voltage, and frequency fluctuations have been established [21, 22, 23, 27, 28]. To improve these variables, many researchers made efforts to develop power network control schemes in their pioneer research. Most of the controllers are based on classical control techniques such as Proportional Integral Derivative (PID), and Artificial Intelligence Control Techniques such as Genetic Algorithms, Fuzzy Logic, Neural Networks, Particle Swarm, and Linear Quadratic Regulator Control Techniques [29, 30]. To investigate these types of control strategies on DG-based power systems, literature was carried out to

gather information and investigate the dynamic stability of power flow and fluctuation behavior of frequency caused by the high penetration of RESs into the grid. To keep the acceptable frequency level in a DG-based power generation system, the excess power produced by the RESs compared to the total load demand needs to be thrown in the Secondary/Dump Load (SL). This has been found to be one of the main drawbacks of a future power plant system [31, 32, 33]. In this paper, a technical rule to store excess energy from the wind turbine and supply it to the grid in case of power shortage is proposed. The stability of wind power flow depends upon the natural situation. Therefore, to improve the wind power flow and reduce the frequency fluctuation of the network, a new control strategy has been developed and proposed to minimize the transient time of wind power flow as well as the fluctuation behavior of frequency in the grid. This is achieved by increasing the high penetration of DG using PID and fuzzy logical controllers.

The contributions of this paper are summarized as follows:

- Designing a control scheme to share the power between the networks using a logical algorithm;
- Regulation of the network frequency using a storage system;
- Reduction of the transient time of wind power flow and the fluctuation behavior of frequency using a fuzzy logical controller;
- Storing the surplus wind power and maintaining a high load demand by supplying it into the network;
- Comparing the robustness of the fuzzy logic controller over the PID controller to reduce the fluctuation behavior of frequency in the network.

The rest of the paper is organized as follows: Section 3.2 describes the modeling of the distributed generation grid. Section 3.3 provides the control algorithm formulation for a Wind–Diesel Hybrid Power System (WDHPS). Section 3.4 highlights the control techniques applied to the network. Section 3.5 presents the tested scheme connected with a WDHPS to a power network using a battery-based storage system. Simulation results and performance evaluations of the proposed method are presented in Section 3.6, and Section 3.7 concludes the paper.

3.2 Modeling of distributed generation grid

3.2.1 Wind turbine

The wind turbine is equipped with an Asynchronous Machine (ASM), rated power of 480 kVA with an inertia of 2 s. The wind DG helps to produce a wind power P_{wind} to regulate the velocity of rotation of the ASM shaft to determine its mechanical torque. Here, the DG operated at a constant velocity (10 m/s) of the wind power generator. Thus, it does not admit to control over its pitch angle [20]. As a function of turbine speed and wind speed, a 2-D lookup chart is used to measure the output of the turbine torque (Tm). The characteristics of the wind turbine are presented in Figure 3.1.

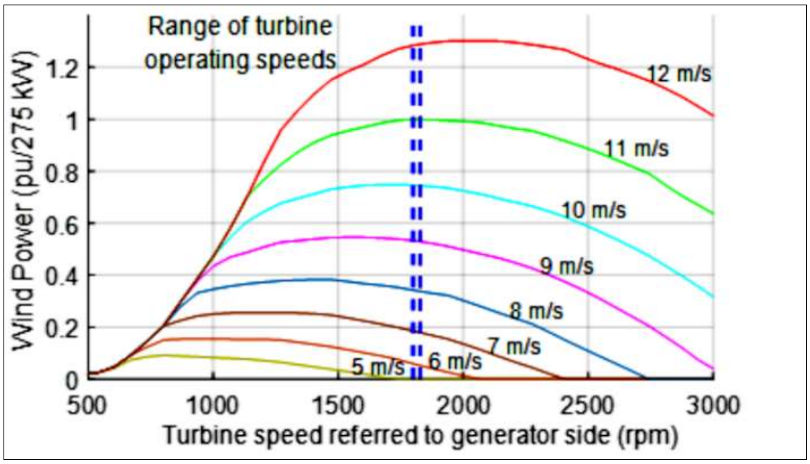

Figure 3.1 Operational characteristics of the wind turbine.

3.2.2 Secondary/Dump Load System

The Secondary Load (SL) helps to control the system frequency by absorbing the excess wind energy corresponding to the consumer demand. It consists of three-phase eight sets of resistors grouped in series with Gate turn-off thyristor switches (GTO), shown in Figure 3.2a. The nominal power of all sets of resistors, shown in Figure 3.2b, maintains binary (8-bit) advancement to absorb the wind power by the SL. The resistive loads can be varied from 0 to 446.25 kW by steps of 1.75 kW. The SL is only designed to control the fluctuation of frequency in the power grid by consuming the power produced by the wind turbine that the battery cannot store [23, 27]. GTOs are simulated by ideal switches.

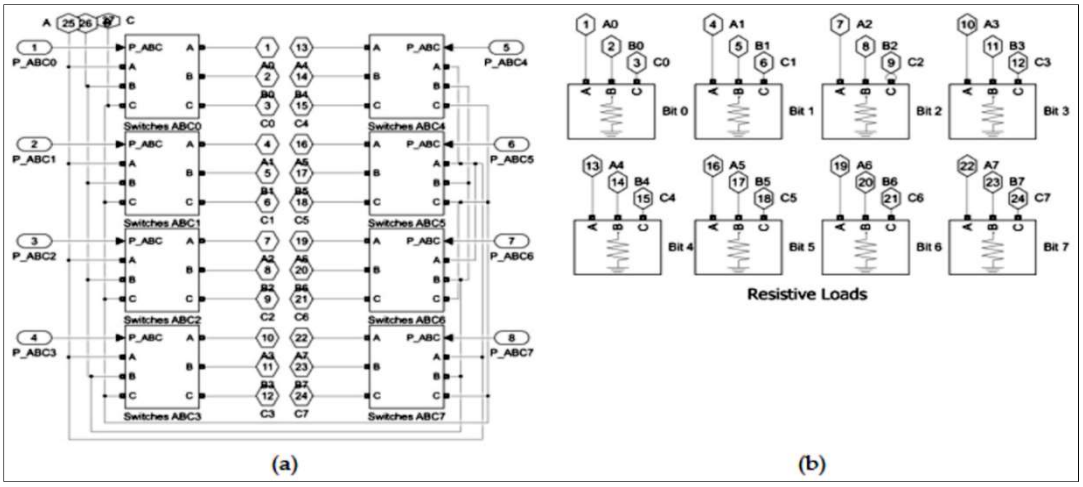

Figure 3.2 (a) 8-bit three-phase GTO switches (b) Operational block diagram of three-phase resistive loads.

3.2.3 Battery-based energy storage system

A Battery-based Energy Storage System (BESS) with a power converter is shown in Figure 3.3a. The BESS is composed of a battery bank. The power ($P_{S\text{-}NAME}$ = 150 kW) of a bridge bidirectional Insulated Gate Bipolar Transistor (IGBT) is regulated in the current mode. The role of the IGBT is to convert the DC sources to the AC sources in the BESS interface connecting with an isolated power network. The BESS-rated capacity is 390 Ah with a voltage of 240 V, which can charge and discharge the BESS corresponding to the load demand of the power network. The control scheme of the Current Controlled Inverter (CCI) is shown in Figure 3.3b. The control technique of CCI is carried out in a structure of rotating dq-coordination. A Phase-Locked Loop (PLL) is used to follow the waveform of grid voltage that provides the reference for the coordinate of dq-abc and abc-dq transformation. The output of the CCI current is calculated and transformed in the rotating frame as well as the currents (both active and reactive) regulated in four quadrants using a Proportional Integral (PI) controller. According to the rating of the proportional gain Kp = 1, the integral gain Ki = 200, and sample time 50 μs, the response time of the CCI is less than 1 min/s. Therefore, the control of frequency becomes very fast in the power grid [35]. An LC filter is connected in the CCI to minimize the current ripples. A step-down transformer rated 120 kV/480 V, 150 kVA is used to connect the BESS with an isolated network.

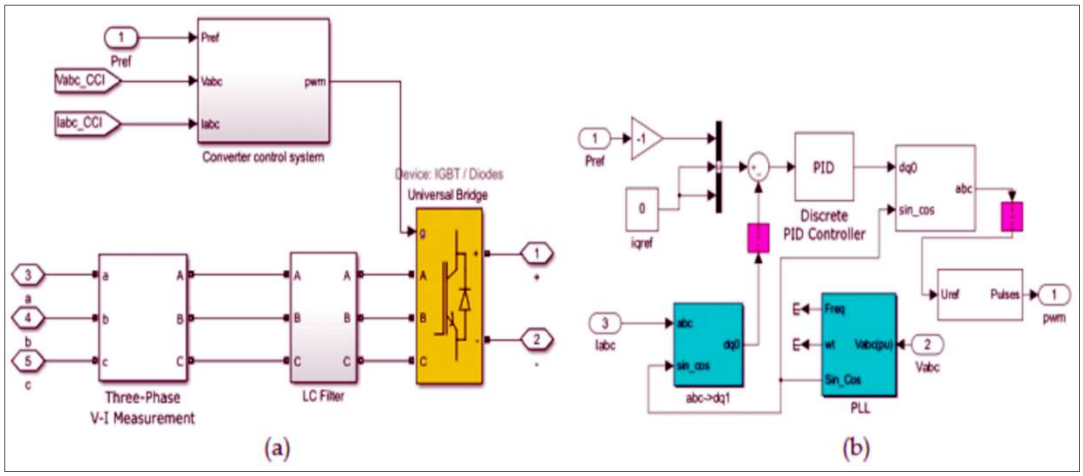

Figure 3.3 (a) Block diagram of a power converter with BESS.
(b) Control scheme of a current-controlled inverter.

3.2.4 Synchronous condenser

A synchronous condenser (nominal rated power of 300 kVA) generates the voltage signal to regulate the network voltage when the diesel engine is shut down. The voltage regulator of the synchronous condenser regulating the excitation of the condenser to supply the reactive power at a nominal voltage level at different buses is shown in Figure 3.4. Here, the primary task of the synchronous condenser is to supply the reactive power in the DG network [36, 37].

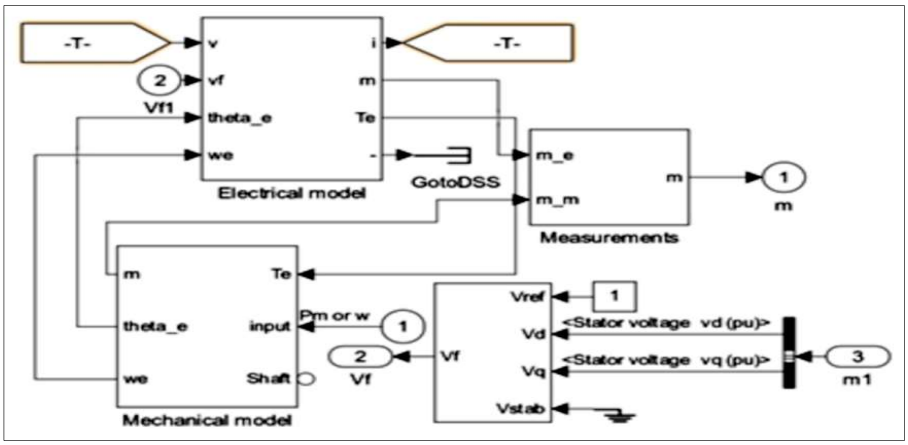

Figure 3.4 The control scheme of a synchronous condenser.

Parameters of the WDHPS network with BESS systems are presented in Table 3.1.

Table 3.1 Parameters for tested WDHPS network

Sources	Symbols/Parameters
Network	480 V, 300 kVA Synchronous Generator
Turbine	480 V, 275 kVA Asynchronous Generator; Wind velocity, Vnom= 10 m/s; Wind Power, Pnom= 200 kW; Pitch angle 0^0
Load Bus	L, load (main) 100 kW, load (Extra) 50 kW, 30 kW, and 45 kW
Secondary/Dump Load Bus	SL, vary 0 to 446.25 kW by step of 1.75 kW
Synchronous Condenser Bus	SC
Wind Turbine Bus	WT
Storage System	SS, 240V, 390 Ah, SOC 50%
Transformer	150 kVA, 120 kV/ 480 V

3.3 Control algorithms for WDHPS

The principle of dynamic stability of wind power flow and the control technique of frequency in the WDHPS network is presented by a logical algorithm shown in Figure 3.5.

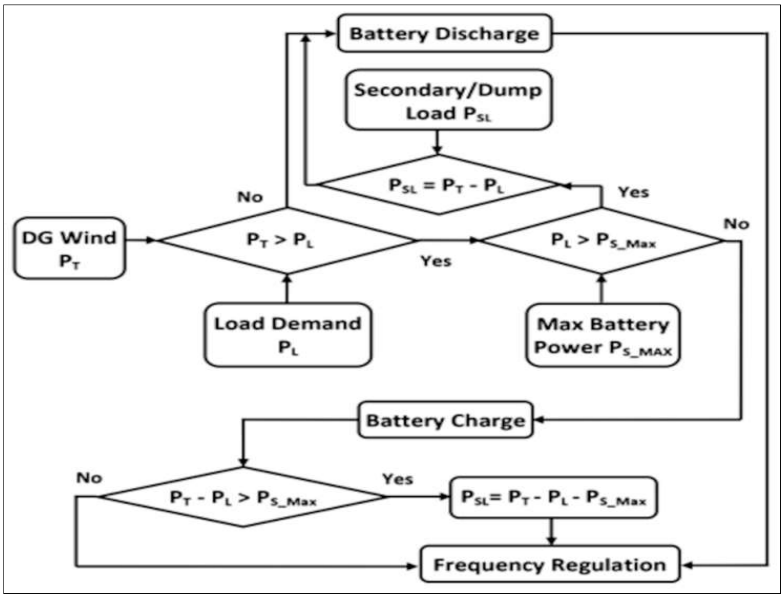

Figure 3.5 The control algorithm for the proposed WDHPS network.

To secure the performance of WDHPS, the system needs an effective control scheme by using the optimum operating mode to avoid any interruption that occurs during the wind

power flow as well as in the frequency of the network. Therefore, two types of control schemes should be considered: one is to ensure the dynamic stability of the power network and reduce the frequency fluctuations while another is to fulfill the energy demand with BESS logical algorithm.

3.3.1 Control technique of frequency in WDHPS network

To regulate the network frequency, an instantaneous level of active power must be generated and consumed by the loads. To maintain the desired level of wind power flow in the network, the SL absorbs the active power that the BESS cannot store due to its capacity limitations [27, 29, 38-40]. In this situation, $P_T > P_L$, when $P_S > 0$. Where P_S: BESS supplied power; P_T: Wind turbine generated power; P_L: Load consumed power. In case the BESS supplies the energy to the WDHPS, $P_T < P_L$ when $P_S < 0$. Here, all the surplus wind energy is absorbed by the SL, $0 < P_{SL}$. It can be written:

$$P_T - P_L - P_{SL} - P_S = J\omega \frac{d\omega}{dt} \quad 3.1$$

Where P_{SL} denoted the power absorbed by the SL and J is the inertia of the system,

$$\omega = 2\pi f/p \quad 3.2$$

Where ω is the velocity (rad /s) of the synchronous machine shaft; p is the pole number of the synchronous machine. The losses in Equation 3.1 are not being considered in this case. Thus, $P_S < P_{S\_nom}$ and $P_{SL} < P_{SL\_nom}$ (converter nominal value). To keep a steady-state velocity of ASM, we can write:

$$\frac{d\omega}{dt} = 0 \quad 3.3$$

The control strategy of the BESS and SL systems should be coordinated with each other. The SL should consume the surplus wind power that the BESS cannot store. Therefore, Equation 3.1 can be written:

$$P_T - P_L = P_{SL} + P_S \quad 3.4$$

$$P_{ref} = P_{S\_ref} + P_{SL\_ref} \quad 3.5$$

$$P_{SL\_ref} = 0 \ when \ P_{ref} < P_{S\_nom} \quad 3.6$$

Equation 3.5 becomes $P_{SL\text{-}ref} = P_{ref,}$ if the BESS reaches its maximum capacity (P_{S_ref}). The SL helps to absorb the wind power if P_{ref} is more than the BESS nominal power. The $P_{S\text{-}max}$

varies between 0 and P_{S_nom}, by using a Positive Power Limit (PPL) signal. The power shared between the BESS and the SL is determined by the priority of power consumption using a logical algorithm. (i.e., SL only consumed the surplus power that the BESS cannot store).

However:

$$P_{S\_ref} = P_{ref} \ when \ \ P_{ref} \leq 0 \quad 3.7$$

$$P_{S\_ref} = P_{S\_max} \ when \ \ P_{ref} > 0 \quad 3.8$$

In SL:

$$P_{SL\_ref} = P_{ref} - P_{S\_max} \ when \ \ P_{ref} > 0 \quad 3.9$$

$$P_{SL\_ref} = 0 \ when \ P_{ref} \quad 3.10$$

The BESS and SL should recognize the P_{ref} (reference power) simultaneously and maintain accuracy at the time of operation. Thus, three types of control techniques can be implemented [19, 23, 27]. Using the SL only when BESS is completely charged, $P_{S\text{-}max} < P_T - P_L$, $P_S = 0$; using the BESS only ($0 = P_{SL}$) if $|P_T - P_L| \leq P_{S\_nom}$; and using both BESS and SL, if ($P_{ref} > 0$) $P_T - P_L > 0$.

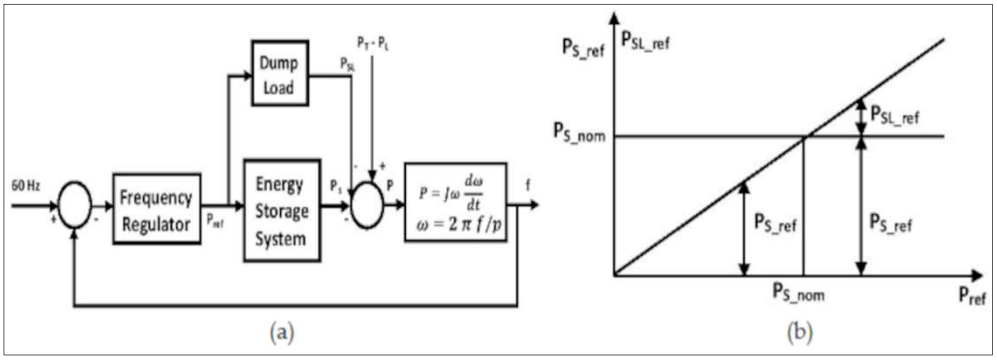

Figure 3.6 (a) Frequency control scheme of the WDHPS system. (b) Power-sharing strategy between the BESS and SL.

The principle of the frequency control scheme for a WDHPS system and the method of power sharing between the BESS and SL are represented in the following Figure 3.6 a, b, respectively. Here, the three-phase Phase Locked Loop (PLL) collects the error of frequency (which is the difference between the reference frequency of 60 Hz and the actual network frequency); and supplies the P_{ref} to confirm the power-sharing priority between the BESS and

SL [38]. This is done by using a logical algorithm. At this stage, the power in the BESS node remains at its nominal value under normal situations.

3.3.2 The BESS control strategies

The BESS follows two strategies of control mode [21, 22, 41].

As an inverter, the BESS supplies power to the network, $Ps < 0$. As a result, the BESS discharges to provide the required power to fulfill the load demand as the current passes through the network. Thereby, the velocity of the wind turbine is defined. Consequently, the power produced by the wind turbine is not enough to cover consumer load demand.

As a rectifier, the BESS consumes the surplus power from the network, $Ps > 0$. Hence, the BESS charges bypass the current from the network. In this situation, the velocity of the wind turbine is very high. The power produced by the wind turbine is more than the total load demand. Therefore, the surplus power is stored by the BESS and supplied in case of sudden or peak demand.

3.4 Control techniques applied to the network

In these scenarios, a fuzzy logic controller and a PID controller are used and compared to each other to analyze the wind power flow and frequency stability in the network. Figure 3.7 a, b shows the operational block diagram of the PID controller and fuzzy logic controller, respectively.

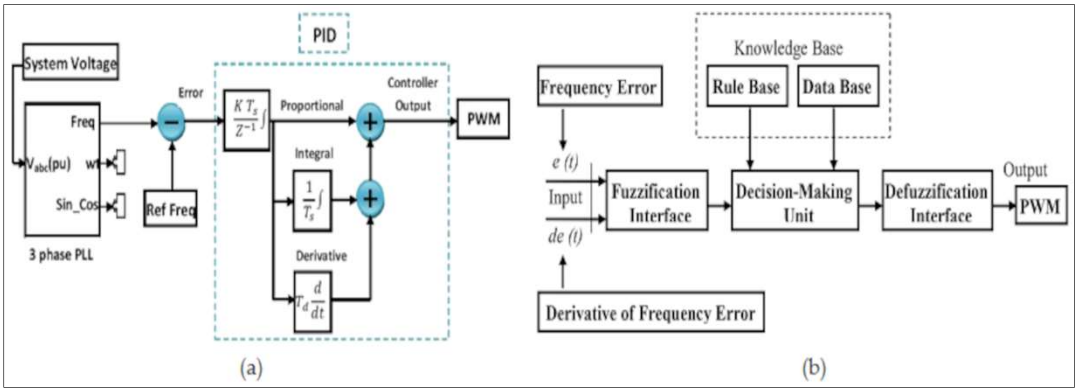

Figure 3.7 (a) Frequency control scheme using PID controller.
(b) Frequency control scheme using fuzzy logic controller.

A three-phase PLL is used to amplify the network frequency. The network voltage is supplied as an input of the PLL. To generate a frequency error, a reference frequency of 60 Hz is considered and compared to the network frequency. The obtained frequency error is integrated to generate a phase error. In the end, the phase error is implemented using the PID controller to initiate an output signal to receive the desired level of load power. According to the characteristics of the network, the proportional gain, Kp = 255, integral gain Ki = 0, and the derivative gain Kd = 55 of the PID controller with a sample time Ts = 200 μs has been tuned to maintain the dynamic stability of the frequency in the power grid [35]. For the fuzzy logic controller, the frequency error (input 1) is merged with the derivative of frequency error (input 2) and sent to the fuzzification interface where the defuzzification (output) is previously determined according to the characteristics of the PWM signal.

3.4.1 Fuzzy logic control technique

Fuzzy Logic is a logical algorithm that allows the true condition to be between 0 and 1. In these situations, the Fuzzy Logic controller can be defined as a degree of truth. It mainly involves four operational units: (a) Fuzzification-interface, (b) Rule matrix-interface, (c) Fuzzy engine-interference, and (d) Defuzzification-interface as shown Figure 3.8. Fuzzification-interface especially associates with the input's parameters. To decide the pre-defined Membership Function (MF), input parameters are fuzzified. The MF can be designed with different structures like sinusoidal, triangular, exponential, and trapezoidal. It is defined by selecting the position of input on the x-axis and the quantity of class variables input on the y-axis. The MF should have to keep the quantity of class variables in the range between 0 and 1. The rule matrix interface unit is used to determine the sets of fuzzy rules and the operation of the conditional functions. The rules of fuzzy logic are described as follows:

$$\text{If } x = A \text{ and } y = B, \text{ then } z = C$$

Where both A and B are sets of conditions to be fulfilled, and C is a set of results to be analyzed. Defuzzification-interface transforms the fuzzy values into crisp values. Several operational techniques of defuzzification-interface can be performed (weight average, bisector mean, centroid, and max-membership) [42, 43].

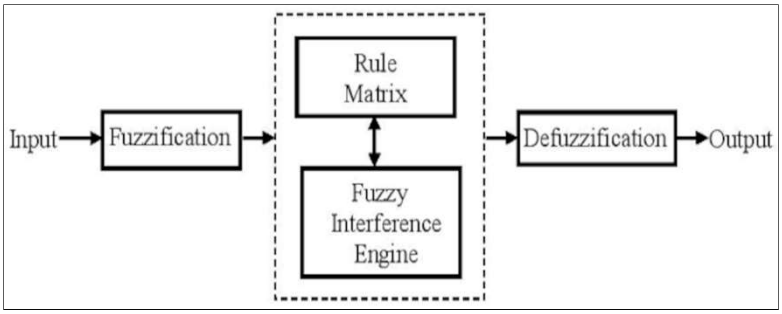

Figure 3.8 Operational diagram fuzzy logic controller.

3.4.2 Operational principle of MF and their rules

Stage 1: At the beginning of the operation, the input and output of the fuzzy logic controller as well as the dimensions of its variables must be determined. According to the matrix rule, the input signal must be in the 'IF' segment and the output signal must be in the 'THEN' segment.

Stage 2: The MF and the fuzzy sets must be defined. Then, the degree of fuzzy MF must connect with all input variables where the output signal is previously identified.

Stage 3: Here, the fuzzy-interference engine must be described. Then, the rules of the fuzzy logic should be converted to the control rules and regulate the controller with respect to the rules.

Stage 4: At the end, the defuzzification interface processes the rules and transforms the output values of fuzzy logic to crisp values.

For this case study, the fuzzifier converts two input signals. The first signal is the frequency error ($\Delta\omega$) and the other one is the signal of the derivative of the frequency error which can be defined as the rate of change of the frequency error signal $\Delta(\Delta\omega)$. As an output signal, the defuzzification decodes the PWM signal. In this fuzzy logic controller, the frequency error signal is applied as input 1. The dimension of this input variable is in the range +1 to −1 which has three MFs. The domain of MFs is split up into three linguistic areas designated by 'Positive Error' (0 1 1), 'Zero Error' (−1 0 1), and 'Negative Error' (−1 −1 0). The structure of the three MFs corresponds with a triangular-based MF. Figure 3.9a shows the MFs of the three linguistic variables. The rate of change of the frequency error signal $\Delta(\Delta\omega)$ is applied as input 2. The dimension of this input variable is in the range +1 to −1 which has three MFs.

The domain of MFs is split up into three linguistic areas designated by ‘Positive Error’ (0 1 1), ‘Zero Error’ (−1 0 1), and ‘Negative Error’ (−1 −1 0). The structure of the three MFs corresponds with a triangular-based MF and they overlay each other. Figure 3.9b shows the MFs of three linguistic variables.

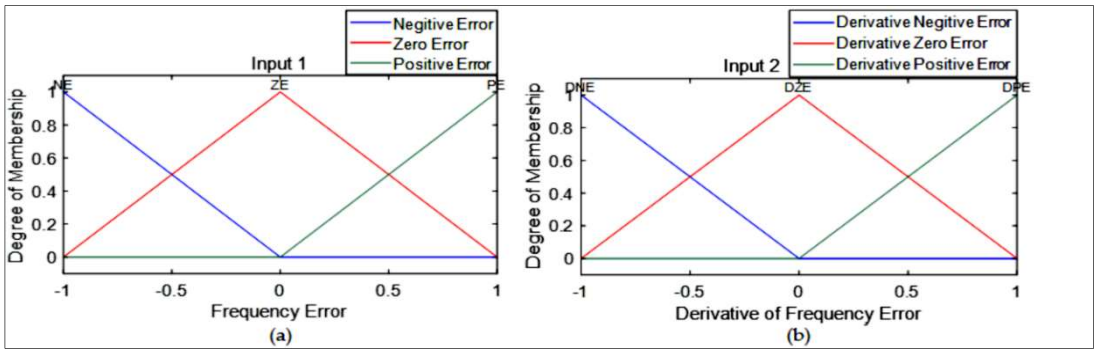

Figure 3.9 (a) Membership function, Input variable 1.
(b) Membership function, Input variable 2.

The output fuzzy logic consists of five MFs which are based on the PWM signal. The dimension of this output variable is in the range −1 to +1. The domain of the output MF is split up to five linguistic areas designated by ‘Positive Large’ (1 1 1), ‘Positive Small’ (0.5 0.5 0.5), ‘Zero’ (0 0 0), ‘Negative Small’ (−0.5 −0.5 −0.5), and ‘Negative Large’ (−1 −1 −1). The structure of all MFs corresponds with a triangular-shaped MF. Figure 3.10 shows the MFs of the three linguistic variables.

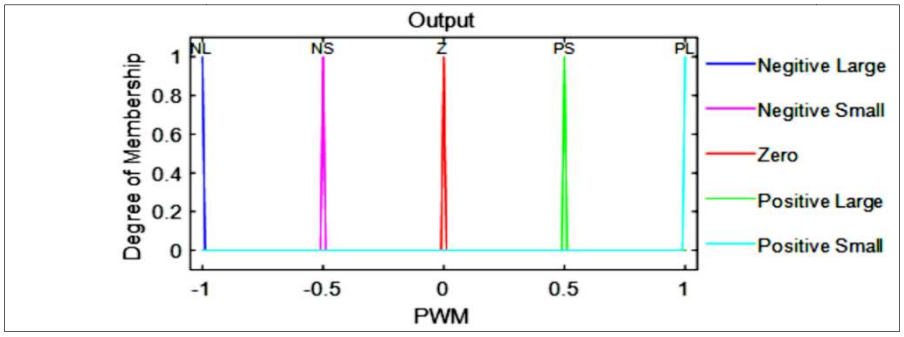

Figure 3.10 Output variables of membership function.

The major components of the fuzzy logic controller are the mechanism inference and the rules. Generally, the fuzzy logic rules are classified in a set of linguistic algorithms. Each rule is triggered with varying judgment to support the MF’s inputs as well as output. To operate

the entire system, a set of nine IF-THEN rules are shown in Table 3.2. A triangular-based MF is used for each fuzzy set.

Table 3.2 Fuzzy logic operation with If-Then rules.

Number	Fuzzy Logic Rules
1	If Frequency Error is Negative Error and Derivative of Frequency Error is Negative Derivative Error, Then PWM is Negative Large
2	If Frequency Error is Negative Error and Derivative of Frequency Error is Zero Derivative Error, Then PWM is Negative Small
3	If Frequency Negative Error and Derivative of Frequency Error is Positive Derivative Error, Then PWM is Zero
4	If Frequency Error is Zero Error and Derivative of Frequency Error is Negative Derivative Error, Then PWM is Negative Small
5	If Frequency Error is Zero Error and Derivative of Frequency Error is Zero Derivative Error, Then PWM is Zero
6	If Frequency Error is Zero Error and Derivative of Frequency Error is Positive Derivative Error, Then PWM is Positive Small
7	If Frequency Error is Positive Error and Derivative of Frequency Error is Negative Derivative Error, Then PWM is Zero
8	If Frequency Error is Positive Error and Derivative of Frequency Error is Zero Derivative Error, Then PWM is Positive Small
9	If Frequency Error is Positive Error and Derivative of Frequency Error is Positive Derivative Error, Then PWM is Positive Large

To set up the fuzzy rule-based system, the Zadeh logical 'and' is used and it is defined as:

$$\mu X \text{ and } \mu Y = \min \{\mu X, \mu Y\} \qquad 3.11$$

Where, μX, μY are the input membership functions of the Fuzzy sets of X and Y, respectively. The operational rules-base of the fuzzy logic controller is presented in Table 3.3. A centroid defuzzifier interface is used to convert the fuzzy sets into real numbers. The output $\mathring{u}\ (t)$ of the fuzzy logic controller is as follows:

$$\mathring{u}(t) = \frac{\sum h_i \mu_i}{\sum \mu_i} \qquad 3.12$$

Where, h_i is the output member value of *i*-th rule and μ_i is the value of the output membership function of the *i*-th rule. To obtain the final required PWM duty cycle, Equation 3.12 should be integrated.

Table 3.3 Fuzzy rule-based operation.

Frequency Error →	NE	ZE	PS
Derivative of Frequency Error ↓			
DNE	NL	NS	ZE
DZE	NS	ZE	PS
DPE	ZE	PS	PL

3.5 Connection of wind turbine with SL and BESS to the power network

In this paper, the analysis of the dynamic stability of wind power flow and the behavior of frequency fluctuation using a BESS in the power network is performed. In this case study, an example is considered for a High Penetration, No Storage Wind–Diesel system (HPNSWD) [23, 27, 44]. This model was developed by Hydro Quebec for an isolated region to reduce the installation and maintenance cost of the power generation system. The maximum power produced by the wind turbine relies on the feasible wind resources as well as fuel cost [42]. A wind turbine asynchronous generator rated at 480 V, 275 kVA, a synchronous condenser generator rated at 480 V, 300 kVA, a BESS rated at 240 V, 390 Ah, a SL (varying between 0 to 446.25 kW), and consumer load rated up to 230 kW are used in this case study. According to the studied case, two scenarios of operation of the power network to ensure the dynamic stability of the power flow and control of the frequency fluctuation are considered [21, 22].

Scenario 1: Power produced by a wind turbine (PT) is > overall load demand (PL). In this situation, the BESS (PS) will be charged.

Scenario 2: Power produced by a wind turbine (PT) is < overall load demand (PL). In this situation, the BESS (PS) will be discharged.

The two scenarios are analyzed in detail in Section 6 and related to a simulation and results.

3.6 Simulation and result

To provide an adequate amount of energy to consumers, a wind speed of 10 ms^{-1} must be maintained in the turbine. In this case, the diesel generator is idled. The synchronous machine runs as a synchronous condenser when the mechanical power (P_m) input of the synchronous machine is fixed to zero. When the wind turbine operates at a velocity of 10

ms^{-1}, an output power of 206 kW is obtained. Hence, the wind turbine produces 200 kW due to the losses in ASM.

3.6.1 Power produced by wind turbine (P_T) is > overall load demand (P_L). In this situation, the BESS (P_S) will be charged

To analyze the dynamic stability of wind power flow, a comparison of the performance of the fuzzy logic controller over the PID controller was carried out. Figure 3.11a shows that the transient time of wind power is greatly reduced, and its fluctuation rate at 2.5 s is improved from 256 kW to 244 kW due to the additional load of 50 kW when using the fuzzy logic control compared to the PID controller. The synchronous condenser supplies reactive power at a rate of 15 kVA to maintain an acceptable level of voltage to the power network. Figure 3.11b reveals the transient time of reactive power flow produced by the synchronous condenser was also reduced using the fuzzy logic controller.

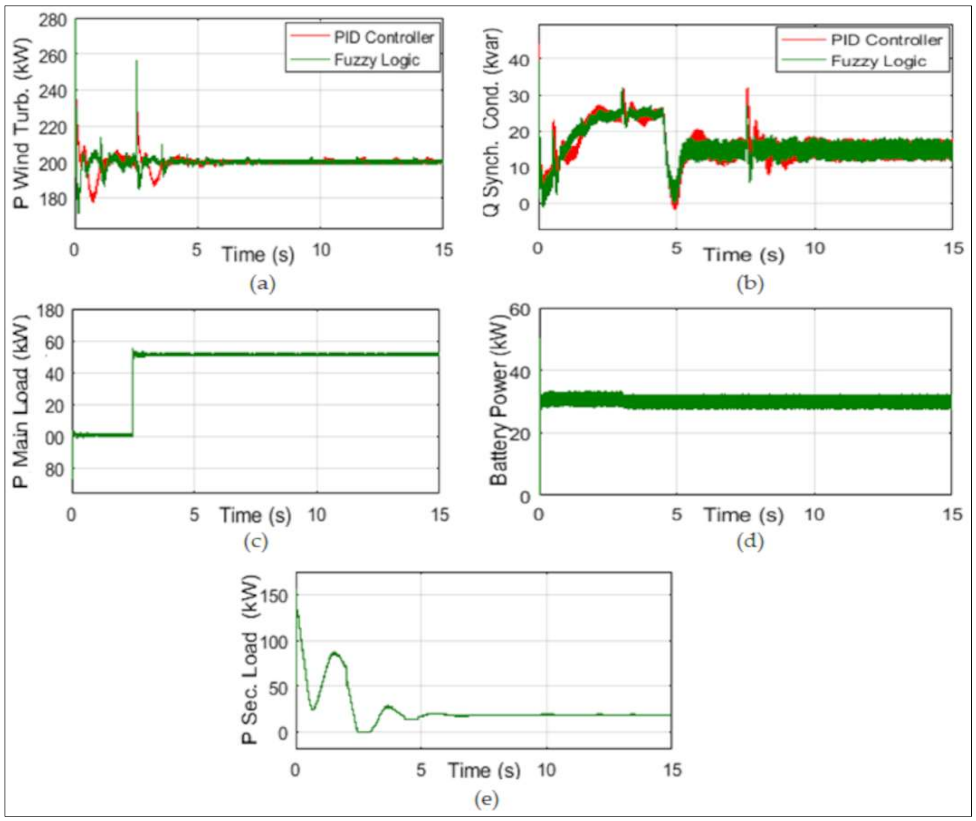

Figure 3.11 (a) The power produced by the wind turbine. (b) Reactive power supply from the synchronous condenser. (c) Power consumed by consumer load. (d) Power supplied from the BESS. (e) Power consumed by SL, when the battery is charged.

Figure 3.11c indicates that the main consumer load is 100 kW. An excess load of 50 kW has been connected at 2.5 s to observe the power stability and fluctuation of frequency in the network. Then, the total load of the network is 150 kW, which is less than the wind power produced with respect to the load demand. Therefore, without sending the excess power to the SL, the BESS was charged at the rate of charge 30 kW in 3 s as shown in Figure 11d. Figure 11e shows the SL only absorbed 20 kW that the battery cannot store to regulate the frequency of 60 Hz.

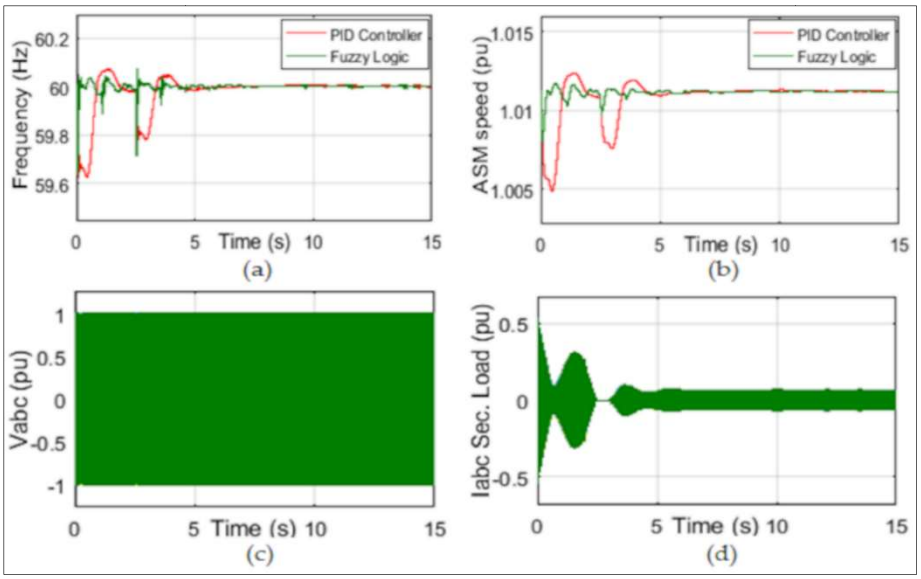

Figure 3.12 (a) Network frequency conditions. (b) Speed generated by ASM generator. (c) Voltage at load bus. (d) The current at SL, when the BESS is charged.

Figure 3.12a shows the transient time of network frequency is significantly reduced. Additionally, the frequency fluctuation rate at 2.5 s due to the excess load of 50 kW is improved from 59.68 Hz to 59.75 Hz using the fuzzy logic controller compared to the PID controller. The velocity of the ASM is reached at 1.01 pu and runs in generator mode. The transient time of ASM velocity is also reduced using the fuzzy logic controller shown in Figure 3.12b. Figure 3.12c shows the system voltage stays at 1 pu. For more observations, data was collected from 10 s to 14 s. The current of the SL decreased at 2.5 s due to an excess load of 50 kW. The SL also decreases at 3 s due to the BESS (rate of 30 kW) charging state, shown in Figure 3.12d.

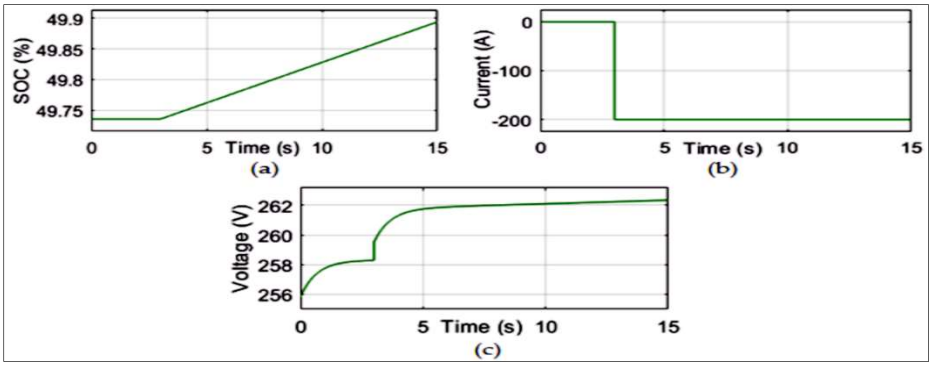

Figure 3.13. (a) BESS SOC condition, (b) BESS current condition and, (c) BESS voltage condition, where the BESS is charged.

Figure 3.13a presents the State of Charge (SOC) of the BESS at 50%. At this point, the BESS is charged from 49.7% to 49.9%. The BESS current situation is shown in Figure 3.13b. The BESS current was zero before 3 s, but after 3 s, the BESS received a −200 A current to charge and consumed 30 kW energy from the network. The voltage of the BESS is increased at 3 s and stays at 262 V during the simulation, as shown in Figure 3.13c.

3.6.2 Power produced by wind turbine (P_T) is < overall load demand (P_L). In this situation, the BESS (P_S) will be discharged

To analyze the dynamic stability of wind power flow, the fuzzy logic controller is compared to the PID controller. Figure 3.14a shows that, by using the fuzzy logic controller compared to the PID controller, the transient time of wind power flow is significantly reduced. Additionally, the wind power fluctuation rate at 0.5 s, 3 s, and 7.5 s due to the excess load of 50 kW, 30 kW, and 45 kW are improved from 256 kW to 244 kW, 232 kW to 225 kW, and 257.5 kW to 245 kW, respectively. The synchronous condenser supplies reactive power at a rate of 15 kVA to maintain an acceptable level of voltage to the power network. Figure 3.14b presents the transient time of reactive power flow produced by the synchronous condenser; this was also reduced using the fuzzy logic controller. Figure 3.14c shows the main consumer load is 100 kW. Excess loads of 50 kW, 30 kW, and 45 kW were connected at 0.5 s, 3 s, and 7.5 s, respectively, to analyze the wind power stability and fluctuation of the frequency in the network. Here, the total load of the network was 230 kW. This is more than the total load demand with respect to wind power generation. Therefore, the BESS has been discharged at a rated power of 50 kW in 4.5 s, as shown in Figure 3.14d, to maintain the high load demand

in the network. Figure 3.14e shows the SL only absorbed 20 kW to regulate the frequency of 60 Hz.

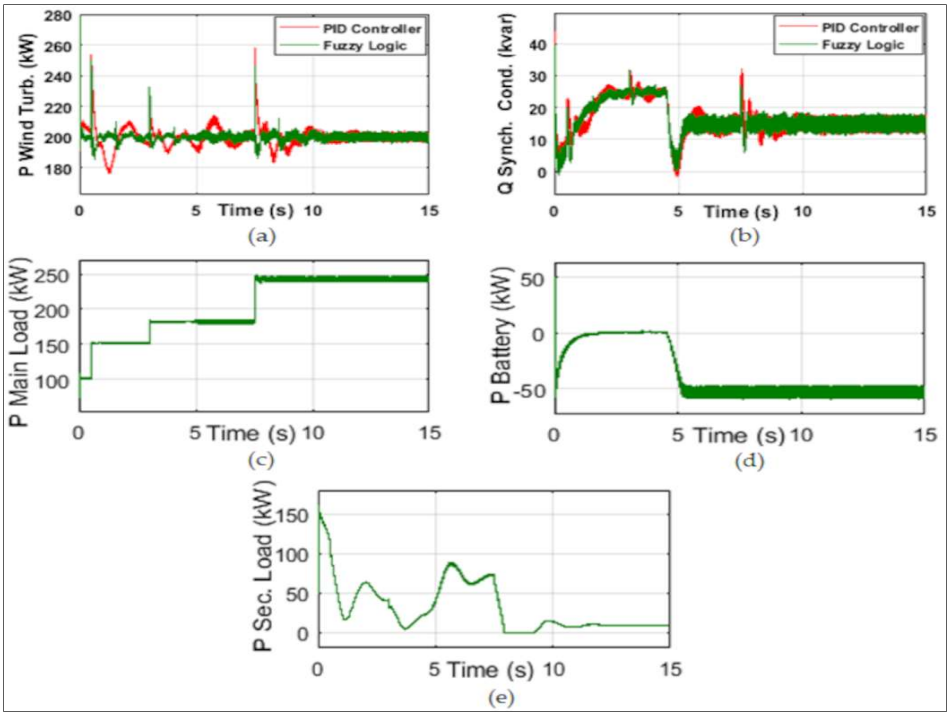

Figure 3.14 (a) The power produced by the wind turbine. (b) Reactive power supply from the synchronous condenser. (c) Power consumed by consumer load. (d) Power supplied from BESS. (e) Power consumed by SL, when the battery is discharged.

Figure 3.15a shows by using the fuzzy logic controller, compared to the PID controller, the transient time of the network frequency is significantly reduced. Additionally, the frequency fluctuation rate due to the excess loads of 50 kW, 30 kW and 45 kW at 0.5 s, 3 s, and 7.5 s improved from 59.53 kW to 59.72 kW, 59.82 kW to 59.84 kW, and 59.68 kW to 59.74 kW, respectively. The velocity of the ASM was reached at 1.01 pu and ran in a generator mode. The transient time of the ASM velocity also reduced using the fuzzy logic controller; as shown in Figure 3.15b,c, the system voltage remained at 1 pu. For more observations, data was collected from 10 s to 14 s. Figure 3.15d indicates the current of the SL decreased due to the excess loads of 50 kW, 30 kW, and 45 kW at 0.5 s, 3 s, and 7.5 s, respectively. The SL also decreases at 4.5 s due to the BESS (rated power of 50 kW) discharging state.

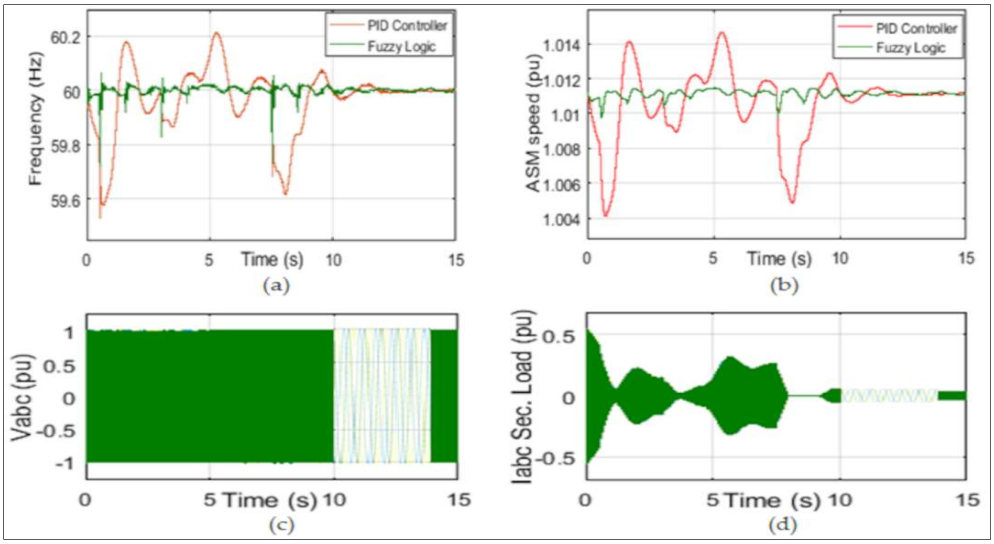

Figure 3.15 (a) Network frequency conditions. (b) Speed generated by ASM generator. (c) Voltage at load bus. (d) Current at SL, where the BESS is discharged.

Figure 3.16a represents the SOC of the BEES at 50%, where the BESS is discharged from 49.73% to 49.60%. The BESS current situation is shown in Figure 3.16b. The BESS current was 0 A before 4.5 s, but after 4.5 s, the BESS received 200 A to discharge itself and supply 50 kW energy to maintain the load demand in the network. The voltage of the BESS decreases at 4.5 s and remains at 254 V during the simulation, as shown in Figure 3.16c.

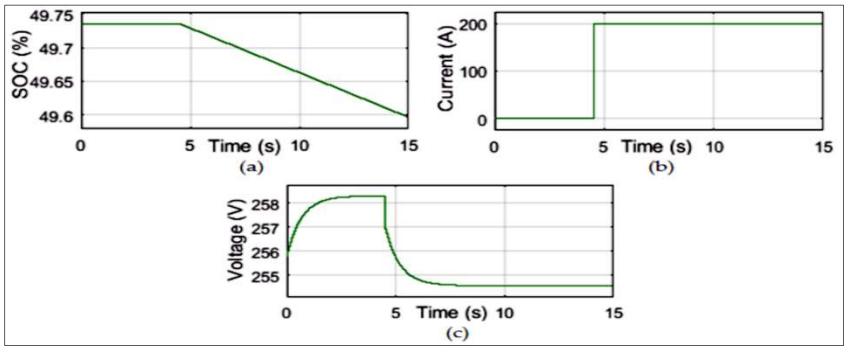

Figure 3.16 (a) The BESS SOC condition, (b) BESS current condition and, (c) BESS voltage condition, where the BESS is discharged.

3.7 Discussion

From the above simulation, the result shows that, when using a fuzzy logic controller over a PID controller, the variation of wind power flow and the fluctuation of frequency reduced significantly compared to previous research. It is also observed that to maintain an acceptable

level of frequency, a storage system (battery) was used to store energy without losing the surplus wind power in an SL. This energy is then consumed when there is a lack of wind power.

3.8 Conclusions

The technologies associated with wind-based DG, the fluctuating behavior of frequency in a wind turbine with a BESS and SL were analyzed and simulated in this paper. The wind power stability and frequency control techniques were analyzed elaborately. Power-sharing methods between the BEES and SL are presented with a high penetration-based DG using a logical algorithm. Furthermore, to maintain an acceptable level of frequency, a storage system (battery) was used to store the excess wind power and avoid loss through the SL. This stored power can be used when there is insufficient wind power generation compared to the total load demand. The response of the BESS usually depends on the technology used and its dynamics which can cause a wide variation in the power network (i.e., power flow, voltage, and, frequency). Finally, the simulation shows that the fuzzy logic controller offers better performance compared to the PID controller to analyze the dynamic stability of the wind power flow and the frequency fluctuation behavior with the load variation at different times.

3.9 References

1. Masson-Delmotte, V.; Zhai, P.; Pörtner, H.O.; Roberts, D.; Skea, J.; Shukla, P.R.; Pirani, A.; Moufouma-Okia, W.; Péan, C.; Pidcock, R.; et al. *Global warming of 1.5 °C.An IPCC Special Report on the Impacts of Global Warming of 1.5 °C Above Pre-Industrial Levels and Related Global Greenhouse Gas Emission Pathways, in the Context of Strengthening the Global Response to the Threat of Climate Change, Sustainable Development, and Efforts to Eradicate Poverty*; Intergovernmental Panel on Climate Change (IPCC): Geneva, Switzerland, 2017; ISBN 978-92-9169-151-7.
2. Al-Sakkaf, S.; Kassas, M.; Khalid, M.; Abido, M. An Energy Management System for Residential Autonomous DC Microgrid Using Optimized Fuzzy Logic Controller Considering Economic Dispatch. *Energies* 2019, *12*, 1457.
3. Hirsch, A.; Parag, Y.; Guerrero, J. Microgrids: A review of technologies, key drivers, and outstanding issues. *Renew. Sustain. Energy Rev.* 2018, *90*, 402–411.
4. Kowalczyk, A.; Wlodarczyk, A.; Tarnawski, J. Microgrid Energy Management System. In Proceedings of the 21st International Conference on Methods and Models in Automation and Robotics (MMAR), Międzyzdroje, Poland, 29 August–1 September 2016; pp. 157–162.

5. Zhang, H.; Davigny, A.; Colas, F.; Poste, Y.; Robyns, B. Fuzzy logic based energy management strategy for commercial buildings integrating photovoltaic and storage systems. *Energy Build.* 2012, *54*, 196–206.
6. Chen, Y.-K.; Wu, Y.-C.; Song, C.-C.; Chen, Y.-S. Design and Implementation of Energy Management System With Fuzzy Control for DC Microgrid Systems. *IEEE Trans. Power Electron.* 2013, *28*, 1563–1570.
7. Hosseinzadeh, M.; Salmasi, F.R. Power management of an isolated hybrid AC/DC micro-grid with fuzzy control of battery banks. *Iet Renew. Power Gener.* 2015, *9*, 484–493.
8. García, P.; Torreglosa, J.P.; Fernández, L.; Jurado, F. Optimal energy management system for stand-alone wind turbine/photovoltaic/hydrogen/battery hybrid system with supervisory control based on fuzzy logic. *Int. J. Hydrog. Energy* 2013, *38*, 14146–14158.
9. Kyriakarakos, G.; Dounis, A.; Arvanitis, K.; Papadakis, G. A fuzzy logic energy management system for polygeneration microgrids. *Renew. Energy* 2012, *41*, 315–327.
10. Abadlia, I.; Bahi, T.; Bouzeria, H. Energy management strategy based on fuzzy logic for compound RES/ESS used in stand-alone application. *Int. J. Hydrog. Energy* 2016, *41*, 16705–16717.
11. Arcos-Aviles, D.; Pascual, J.; Marroyo, L.; Sanchis, P.; Guinjoan, F. Fuzzy Logic-Based Energy Management System Design for Residential Grid-Connected Microgrids. *IEEE Trans. Smart Grid* 2018, *9*, 530–543.
12. Cheng, Y.-S.; Liu, Y.-H.; Hesse, H.; Naumann, M.; Truong, C.; Jossen, A. A PSO-Optimized Fuzzy Logic Control-Based Charging Method for Individual Household Battery Storage Systems within a Community. *Energies* 2018, *11*, 469.
13. Pan, I.; Das, S. Fractional Order Fuzzy Control of Hybrid Power System with Renewable Generation Using Chaotic PSO. *ISA Trans.* 2016, *62*, 19–29.
14. Vairavasundaram, I.; Ravi, L.; Vairavasundaram, S.; Varadharajan, V.; Siarry, P.; Uden, L. Multi-objective optimization and energy management in renewable based AC/DC microgrid. *Comput. Electr. Eng.* 2018, *70*, 179–198.
15. Fossati, J.P.; Galarza, A.; Martín-Villate, A.; Echeverria, J.M.; Fontan, L. Optimal scheduling of a microgrid with a fuzzy logic controlled storage system. *Int. J. Electr. Power Energy Syst.* 2015, *68*, 61–70.
16. Choudhury, S.; Bhowmik, P.; Rout, P. Economic load sharing in a D-STATCOM Integrated Islanded Microgrid based on Fuzzy Logic and Seeker Optimization Approach. *Sustain. Cities Soc.* 2018, *37*, 57–69.
17. Chaiyatham, T.; Ngamroo, I. A bee colony optimization based-fuzzy logic-pid control design of electrolyzer for microgrid stabilization. *Int. J. Innov. Comput. Inf. Control* 2012, *8*, 6049–6066.
18. Chaiyatham, T.; Ngamroo, I.; Pothiya, S.; Vachirasricirikul, S. Design of optimal fuzzy logic-PID controller using bee colony optimization for frequency control in an isolated wind-diesel system. In Proceedings of the Transmission & Distribution Conference & Exposition, Asia and Pacific, Seoul, Korea, 26–30 October 2009; pp. 1–4.

19. Impram, S.; Nese, S.V.; Oral, B. Challenges of renewable energy penetration on power system flexibility: A survey. *Energy Strategy Rev.* 2020, *31*, 100539.
20. Nazari, M.; Ilić, M.; Lopes, J. Dynamic stability and control design of modern electric energy systems with large penetration of distributed generators. In Proceedings of the IREP Symposium Bulk Power System Dynamics and Control—VIII (IREP), Rio de Janeiro, Brazil, 1–6 August 2010; pp. 1–7.
21. Rahman, J. Frequency Control in the Presence of Renewable Energy Sources in the Power Network. Master's Thesis, École de Technologie Supérieure, Montreal, Canada, 2017.
22. Rahman, M.J.; Tafticht, T.; Doumbia, M. Frequency Control for a High Penetration Wind-Based Energy Storage System in the Power Network. In Proceedings of the IEEE Electric Power and Energy Conference (EPEC), Kyiv, Ukraine, 9–10 November 2020; pp. 1–6.
23. Lingamuthu, R.; Mariappan, R. Power flow control of grid connected hybrid renewable energy system using hybrid controller with pumped storage. *Int. J. Hydrog. Energy* 2019, *44*, 3790–3802.
24. Zhao, C.; Topcu, U.; Li, N.; Low, S. Design and Stability of Load-Side Primary Frequency Control in Power Systems. *IEEE Trans. Autom. Control* 2014, *59*, 1177–1189.
25. Polydoros, C.; Vita, V. Design of an Offshore Wind Farm: Connection to the Main Electrical Grid. In Proceedings of the 11th Engineering Faculty Conference (BulEF), Bourgas, Bulgaria, 3–6 June 2020; pp. 1–6.
26. Vita, V.; Alimardan, T.; Ekonomou, L. The Impact of Distributed Generation in the Distribution Networks' Voltage Profile and Energy Losses. In Proceedings of the IEEE European Modelling Symposium (EMS), Madrid, Spain, 6–8 October 2015; pp. 260–265.
27. Sebastián, R.; Quesada, J. Distributed control system for frequency control in a isolated wind system. *Renew. Energy* 2006, *31*, 285–305.
28. Zamee, M.A.; Mitra, D.; Tahhan, S.Y. Load frequency control of interconnected hydro-thermal power system using conventional pi and fuzzy logic controller. *Int. J.Energy Power Eng.* 2013, *2*, 191.
29. Amano, H.; Oshiro, Y.; Kawakami, T.; Inoue, T. Utilization of battery energy storage system for load frequency control toward large-scale renewable energy penetration. In Proceedings of the 3rd IEEE PES Innovative Smart Grid Technologies Europe (ISGT Europe), Berlin, Germany, 14–17 October 2012; pp. 1–7.
30. Blaabjerg, F.; Yang, Y.; Yang, D.; Wang, X. Distributed Power-Generation Systems and Protection. *Proc. IEEE* 2017, *105*, 1311–1331.
31. Ahshan, R.; Saleh, S.; Al-Badi, A. Performance Analysis of a Dq Power Flow-Based Energy Storage Control System for Microgrid Applications. *IEEE Access* 2020, *8*, 178706–178721.

32. Salama, H.S.; Aly, M.M.; Abdel-Akher, M.; Vokony, I. Frequency and voltage control of microgrid with high WECS penetration during wind gusts using superconducting magnetic energy storage. *Electr. Eng.* 2019, *101*, 771–786.
33. Wang, Z.; Luo, D.; Li, R.; Zhang, L.; Liu, C.; Tian, X.; Li, Y.; Su, Y.; He, J. Research on the active power coordination control system for wind/photovoltaic/energy storage. In Proceedings of the IEEE Conference on Energy Internet and Energy System Integration (EI2), Beijing, China, 26–28 November 2017; pp. 1–5.
34. Syamala, J.; Naidu, I. Load Frequency Control of Multi-AreaPower Systems Using PI, PID, and FuzzyLogic Controlling Techniques. *Int. J.Innov. Res.Sci. Eng.Technol.* 2014, *3*, 128–1288.
35. Nguyen, T.-T.; Martin, V.; Malmquist, A.; Silva, C. A review on technology maturity of small scale energy storage technologies. *Renew. Energy Environ. Sustain.* 2017, *2*, 36.
36. Kouba, N.E.L.Y.; Menaa, M.; Hasni, M.; Boudour, M. Load Frequency Control in multi-area power system based on Fuzzy Logic-PID Controller. In Proceedings of the IEEE International Conference on Smart Energy Grid Engineering (SEGE), Oshawa, ON, Canada, 17–19 August 2015; pp. 1–6.
37. Vidyanandan, K.V.; Senroy, N. Primary frequency regulation by deloaded wind turbines using variable droop. *In IEEE Trans. Power Syst.* 2013, *28*, 837–846.
38. Bangash, K.N.; Farrag, M.; Osman, A. Investigation of Energy Storage Batteries in Stability Enforcement of Low Inertia Active Distribution Network. *Technol. Econ. Smart Grids Sustain. Energy* 2019, *4*, 1–12.
39. Obaid, Z.A.; Cipcigan, L.; Abrahim, L.; Muhssin, M.T. Frequency control of future power systems: Reviewing and evaluating challenges and new control methods. *J. Mod. Power Syst. Clean Energy* 2019, *7*, 9–25.
40. Sockeel, N.; Gafford, J.; Papari, B.; Mazzola, M. Virtual Inertia Emulator-Based Model Predictive Control for Grid Frequency Regulation Considering High Penetration of Inverter-Based Energy Storage System. *IEEE Trans. Sustain. Energy* 2020, *11*, 2932–2939.
41. Magdy, G.; Mohamed, E.A.; Shabib, G.; Elbaset, A.; Mitani, Y. Microgrid dynamic security considering high penetration of renewable energy. *Prot. Control Mod. Power Syst.* 2018, *3*, 1–11.
42. Can, S.D.L.R.D.; Leventis, G.; Phadke, A.; Gopal, A.R. Design of incentive programs for accelerating penetration of energy-efficient appliances. *Energy Policy* 2014, *72*, 56–66.
43. Zhao, D.; Ma, J.; Qian, M.; Zhu, L.; Yao, L.; Ding, K.; Han, H. Construction of an example system for AC/DC hybrid power grid with high proportion renewable energy. *J. Eng.* 2019, *16*, 1117–1121.
44. Mott, L.; Saulnier, B. Commercial Wind-Diesel Project, St. Paul Island, Alaska. In Proceedings of the 14th Prime Power Diesel Inter-Utility Conference, Winnipeg, MB, Canada, 28 May–2 June 2014.

CHAPTER 4

OPTIMAL INVERTER CONTROL STRATEGIES FOR A PV POWER GENERATION WITH BATTERY STORAGE SYSTEM IN MICROGRID

Md Jahidur Rahman[1], Tahar Tafticht[1], Mamadou Lamine Doumbia[2] and Iqbal Messaïf [3]

[1] Department of Engineering, Université du Québec en Abitibi-Témiscamingue, Rouyn-Noranda, QC J9X 5E4, Canada
[2] Department of Electrical and Computer Engineering, Université du Québec à Trois-Rivières, Trois-Rivières, QC G8Z 4M3, Canada
[3] Department of Electrical Engineering, Université des Sciences et de la Technologie Houari Boumediene, Alger 16111, Algeria

Paper published in *Energies,* May 2023

Abstract

Power generation from Renewable Energy Sources (RESs) is unpredictable due to climate or weather changes. Therefore, more control strategies are required to maintain the proper power supply in the entire microgrid. This paper presents a simulation scheme utilizing a solar system instanced by Photovoltaic (PV) panels coupled to the grid, loads, and an energy storage device. At first, modeling the PV panels cell and their operation were analyzed. The synthesis of the adaptive notch filter was designed to compensate for the input currents. The power converter's/inverter's efficiency and control facility allowed us to link the energy storage system with an electrical grid. Several simulations were accomplished consistently with nonlinear control techniques for the simple inverter, multi-variable filter, notch filter, and without a filter. Finally, the performances of the nonlinear controller with various filters were carried out to regulate the DC bus of the proposed grid. The advantage of these controllers is compensating the reactive power and harmonic currents to obtain a disturbance-free power network. The overall installations and simulations were established using the Matlab/Simulink software.

Keywords: photovoltaic energy; storage system; nonlinear control; power converter/inverter;

harmonic currents; reactive power

4.1 Introduction

The current structure of electrical grids is a centralized architecture wherein energy production is concentrated at specific points and then distributed to consumers [1, 2, 3]. During the last three decades, renewable energies have increased on the surface of our planet. This trend has gradually accelerated, particularly following the signing of the Kyoto Protocol, which requires many countries to limit their gas emission. Indeed, solar energy production in the world has increased 20-fold in ten years [4]. Efforts are underway to improve the competitiveness of solar panels in terms of performance and cost. The materials used in the manufacture are evolving, with the panels possessing a more critical yield. The main disadvantage of solar energy is that it varies irremediably according to weather conditions [5]. For example, the power provided by the PV panels is noticeably reduced in winter, night, or rainy weather. However, the development of photovoltaic systems has highlighted several factors directly affecting the performance of this technology. Studies have made it possible to emphasize the influence of partial shading and the impact of the increase in temperature on the efficiency of photovoltaic solar systems [6]

Many researchers have proposed technical solutions to reduce or eliminate these phenomena. The ultimate goal is to make the photovoltaic panels work at their maximum power points under any environmental conditions [7]. The partial shading on solar panels is usually caused by obstacles close to photovoltaic installations, such as trees, tall chimneys, walls, etc. Most of these obstacles are permanent, predictable, and detected at certain times of the year due to the sun's path [8, 9]. We also notice short-lived and unpredictable partial shading due to passing clouds, bird droppings, snow, dust, etc. When the solar radiation is constant, the photovoltaic cell is likened to a diode that operates in direct bias. Since it's connected in series, the cells are required to drain the current. However, they cannot do so because some PV cells receive partial shading. Once partial shading occurs, the short circuit current of the shaded cells drops dramatically, which leads shaded cells to operate in reverse bias [3]. In the reverse bias region, the PV solar cell will dissipate power in the form of heat that creates a hot spot and can damage the shaded PV solar cells [9]. Advanced MPPT methods have been

developed to detect the global maximum point when partial shading occurs with high accuracy and acceptable speed. Speed and accuracy are essential parameters when choosing the MPPT techniques [3]. These methods can be listed in three categories: linear search methods, artificial intelligence methods, and the metaheuristic approach [10]. The combination of the two steps generally develops linear search methods. The first step allows a sweep to find the region that contains the global maximum point. The second step uses one of the conventional MPPT techniques to find the location of the maximum power point with high accuracy.

The experimental results show that technology is more effective, particularly when weather conditions change suddenly. The disadvantage of this technology is that it does not guarantee rapid convergence during permanent partial shading. We can also mention the Global Maximum Power Point Tracking (GMPPT) algorithm. The advantage of this technique is that it can be applied in photovoltaic systems whose electrical characteristics are unknown. According to [11], this technique is better suited to building-integrated photovoltaic systems with inverters mostly mounted in strings. Artificial intelligence methods such as artificial neural networks and fuzzy logic controllers are also used. The technique using artificial neural networks can effectively track the global maximum point under any sunlight condition. Its advantage is that depending on the weather conditions, it can use some or all of its input parameters. The disadvantage of this technique is that it is not accurate under all partial shade conditions without periodic adjustment [3]. The fuzzy logic controller method allows fast and precise convergence even when the sunshine varies suddenly. The advantage of the method is that it does not require mathematical modeling of the system.

However, according to [12], the table of logic rules described in [13] largely depends on the designer’s experience and prior knowledge of how the photovoltaic system works. The metaheuristic approach has the well-known Particle Swarm Optimization (PSO) technique. This technique finds a function’s optimal value in a predefined search space. It is inspired by the social behavior of a large group of birds and a fish gathering [11, 12]. The PSO is estimated to be relatively fast and accurate, with an error of 4% from experimental results. An improved version of this method, called Adaptive Perceptive PSO, has been proposed, providing more accurate results (3% error).

The other exciting technique is the Fibonacci Search method. It uses the sequence of Fibonacci numbers to track the global maximum point under uniform and non-uniform insulation conditions. Its tracking rate is acceptable according to the experimental results, but it sometimes fails when we have a power-voltage characteristic curve $P_{pv} = f(V_{pv})$ with multiple peaks. On the other hand, its slowness constitutes a limit for its implementation. We can also quote that the Modified Firefly Algorithm [13] can significantly reduce the global maximum tracking time even though its efficiency is slightly lower than that of the Firefly Algorithm. Many other techniques have recently been listed in the literature. In [14], the following methods are mentioned: Evolutionary algorithm, Genetic Algorithm, and Differential Evolution. There are also other lesser-known techniques for reconfiguring photovoltaic panels that allow maximum power to be achieved. However, these techniques require the installation of sensors, switches, and complex control algorithms to dynamically reconfigure the photovoltaic field [15] during partial shading conditions. These reconfigurations can be partial or complete. The Partial reconfiguration foresees part of the photovoltaic cells of the solar field being fixed, and the other part can be reconfigured. The entire reconfiguration predicts that all the photovoltaic cells of the solar area are reconfigurable. Research has already been carried out in the past and proposed partial or complete reconfiguration algorithms. We can name the unbalanced topology of photovoltaic cells [16], the model using mathematical formulas [17], and the dynamic programming algorithm [18]. However, all these methods use switches, which generate power losses. The algorithm for determining optimal connections [19], a new approach, uses busbars to change the positions of the photovoltaic cells between them. This has the advantage of minimizing power losses for switches. Other more recently developed techniques, such as the Futoshiki configuration, are based on the logic of puzzles. In this approach, the physical location of the photovoltaic modules changes, but the electrical connections of the modules are unchanged. The study results show that the Futoshiki technique generates greater power for all shading conditions than the total-cross-tied configuration [20, 21]. The disadvantage of the method is that it cannot extract the maximum power from the photovoltaic system. It will be necessary to develop an algorithm that allows this technique to optimize the pursuit of the global maximum point [14].

Control strategies of an inverter are also developed to minimize the harmful effects of partial shading, especially in high-power photovoltaic systems. The control strategy named Mitigation Control Against Partial Shading Effects (MICAPAS) allows isolated photovoltaic power plants to regulate the frequency of partial shading without resorting to energy storage. However, according to [22], this strategy is only effective for huge photovoltaic power plants. We have noted in the literature that a more practical version of the sub-Module Integrated Converters (MICs) control strategy has been implemented. It also makes it possible to minimize power losses due to partial shading and mismatch between solar panels [23]. Sliding mode control is also a widely used strategy. Its principle consists of bringing a system's state trajectory towards the sliding surface and making it commute around this one until the point of equilibrium. It has the advantage of being stable and easy to implement [24, 25]. To improve the robustness of this technique, the Proportional-integral Control and the sliding mode control have been developed [26]. Sliding mode control is one of the nonlinear control techniques. Another nonlinear technique is drop control. Although it has limitations, it is one of the most widely used techniques to guarantee the reliability of the power network [27, 28]. Thus variants of this control technique have been implemented to optimize it [29, 30].

In PV power generation, the inverter systems introduce some energy losses during the conversion of DC power generated by the PV panels to AC power used in most electrical systems. These losses can reduce the overall efficiency of the system. Furthermore, the efficiency of inverters can vary depending on their design, size, and load conditions [31]. In some cases, PV systems are oversized by installing inverters with higher capacities than necessary to accommodate future expansions or increase system flexibility. However, oversizing the inverter without appropriate load management or battery storage can lead to inefficient utilization of generated power and may result in increased costs without proportional benefits [5, 9, 32]. The inverter-based PV systems rely on grid-connected operation to ensure stable voltage and frequency levels. However, sudden variations in PV power generation can introduce voltage and frequency fluctuations, and increase the Total Harmonic Distortion (THD) of the inverter which has a huge impact on maintaining the stability of the local grid [33]. This issue becomes more pronounced when a significant

number of PV systems are connected to the same grid. The grid codes and standards are in place to address these challenges, but they can impose additional requirements and costs on PV system installations [34]. Also, inverter-based PV systems with battery storage often rely on the grid as a backup source of power or to supply excess electricity during periods of high demand. If the grid experiences an outage, these systems may not be able to operate independently unless they incorporate additional equipment such as backup generators or specialized grid-forming inverters. Grid dependence can limit the system's resilience and reliability, especially in areas with unreliable or weak grid infrastructure [32, 35]. It's worth noting that these deficiencies mostly are in inverter-based PV power generation systems with battery storage and can vary depending on the specific components, system design, and grid conditions. Ongoing research and technological advancements continue to address these limitations and improve the performance and reliability of inverter-based PV systems.

Thus, this paper presents photovoltaic technology, extracting electrical energy using the boost converter to determine the MPPT. The power generated by the PV panel was connected to the grid with a battery storage system ensured by the DC/AC converter to maintain the unbalanced nonlinear load. This converter interfaced with the grid, which corrected the components and blocked the pollution of the grid through its control strategies. The simulation tests were carried out with a simple nonlinear controller and integrated into the multi-variable and notch filters. Finally, we simulated the inverter using a nonlinear controller without a filter and compared the results to determine the best controller that performs better. The main contributions of this paper are designing the control scheme for an inverter/rectifier to help the batteries store/supply a desired amount of energy at maximum speed; designing DC/AC converters to maintain the unbalanced nonlinear load of the PV-based battery storage system; modifying the adaptive notch filter to adequately compensate the input currents and perform an inverse transformation before injecting them at the output; and reducing the (THD) rate of the inverters to enhance the efficiency of the power grid.

The rest of the paper is organized as follows: Section 4.2 describes the modeling of a solar photovoltaic cell. Section 4.3 presents the photovoltaic system connected to the power grid. The simulation results and performance of the nonlinear controller with different types of

filters are presented in Section 4.4. The comparison of nonlinear controllers with various filters is analyzed in Section 4.5 and Section 4.6 concludes the paper.

4.2 Modeling of a solar photovoltaic cell

A single photovoltaic cell cannot provide enough power to supply a load or the electrical grid. Therefore, it is necessary to combine these solar cells to generate more power. A series combination of the cells will increase the solar panel output voltage, while a parallel combination will increase the current supplied to the load. Here, N_P and N_S represent the number of cells in parallel and series. Now the expression of the current I_{PV} becomes [36].

$$I_{pv} = N_P I_{SC} - \left(e^{\frac{I_{pv}R_S}{N_P V_T} + \frac{V_{pv}}{N_S V_T}} - 1 \right) I_0 - I_{pv} \frac{R_S}{R_p} - \frac{V_{pv}}{R_p} \tag{4.1}$$

where I_{pv} represents the current for a photovoltaic cell; I_{sc} represents the short-circuit current of a cell; I_0 represents the diode reverse bias current; V_{pv} represents the voltage for a photovoltaic cell; V_T represents the thermal voltage of a cell; N_P and N_S represent the number of cells in parallel and series; R_p represents the resistance losses by recombination of the carriers due to the structural defects of the material; R_s represents the resistance losses by joule effects in the semiconductor and the losses through the grids and the bad ohmic contacts of the cell. The amount of solar radiation affects the production of carrier charge in the PV module, subsequently affecting the generated current.

The following equation describes the current I_{pv} with the influence of the cell temperature:

$$I_{pv} = I_{sct} - \left(e^{\frac{\frac{I_{pv}R_S}{N_P} + \frac{V_{pv}}{N_S}}{V_T}} - 1 \right) I_{0s} N_p - I_{pv} \frac{R_S}{R_p} - \frac{V_{pv}}{R_p} \tag{4.2}$$

$$I_{os} = \left(\frac{T}{T_t} \right)^3 I_{or} - \left(e^{\left(\frac{1}{T_r} - \frac{1}{T} \right) \frac{qE_{G0}}{k\beta}} - 1 \right) \tag{4.3}$$

$$I_{sct} = \frac{G}{1000} [(T - 298.15) K_I + I_{sc}] \tag{4.4}$$

where T is the cell's operating temperature in Kelvin and T_r is the reference temperature (298.18 K); E_{G0} is the silicon's bandwidth (1.12 eV); β is the ideality factor (1740); I_{os} is the

reverse saturation current of the cell; I_{or} is the saturation current of the cell; q is the charge of electrons.

The selection of solar cells significantly contributes to better efficiency in the overall power grid. Indeed, the temperature and the level of sunlight can affect the solar panel's performance. In order to distinguish the modified value of the current and the voltage of the solar panel due to a temperature change, the following characteristic curves $I_{pv} - V_{pv}$ and $P_{pv} - V_{pv}$ are plotted using Equations (2) – (4) and can also be written as follows:

$$P_{pv} = V_{pv} I_{pv} = V_{pv} \left(I_{sct} - \left(e^{\frac{I_{pv} R_S + \frac{V_{pv}}{N_S}}{V_T}} - 1 \right) I_{0s} N_p - I_{pv} \frac{R_S}{R_p} - \frac{V_{pv}}{R_p} \right) \quad 4.5$$

The following curves are obtained (with 15 photovoltaic modules in series and 50 in parallel). Figure 4.1 shows the I-V and P-V curves of PV modules with a temperature variation. It is observed that the power produced by the panel decreases at high temperatures. The characteristics of the solar panel according to the radiation $G =$ 600, 800, and 1000 W/m^2 are shown in Figure 4.2.

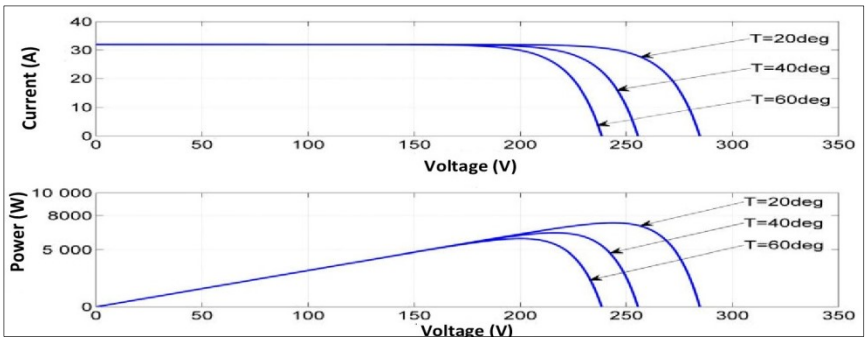

Figure 4.1 I-V and P-V curves of PV modules with temperature variation.

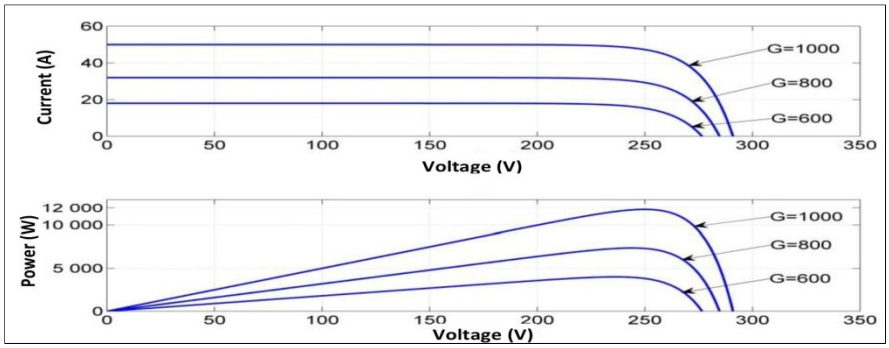

Figure 4.2 I-V and P-V curves of PV modules with the variation of sun radiation.

4.3 Photovoltaic system connected to the power grid

The MPPT is a principle technique for tracking the maximum power point of a nonlinear power generator. This control technique forces the generator to work at its Maximum Power Point (MPP). Indeed, this operation makes it possible to obtain the best power efficiency of the photovoltaic system. A photovoltaic generator has a nonlinear characteristic of $I = f(U)$. Consequently, the power supply will differ according to the load for the same lighting. Therefore, an MPPT controller makes it possible to control the static converter connecting to the load and the photovoltaic panel to supply the maximum power to the load permanently. There are different methods to get to this point. Generally, each of these methods has been made for a specific application. The accuracy and robustness of these controllers depend on some parameters (i.e., sampling rate, system voltage, temperature compensation, noise, and filtering). For our application, the Perturb and Observe (P&O) method is used to get MPPT from the PV panel. Here, the inverter is placed downstream from the boost converter and upstream from the grid. Its principal function is to deliver the alternating currents and voltages from a DC power source. Figure 4.3 shows the generic circuit diagram of a boost converter. This DC-DC converter, also called a parallel chopper, is a switching power supply that increases the initial DC voltage. Therefore it makes it possible to impose a current, which will be determined by the MPPT algorithm.

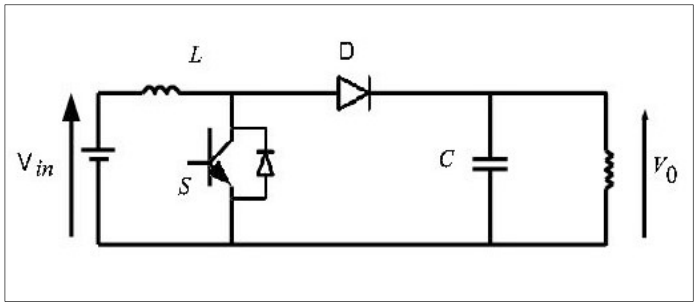

Figure 4.3 Generic circuit diagram of a boost converter.

For current regulations, we will use the dynamic current equation:

$$V_{in} - (1-d)v_c = L\frac{dI_L}{dt} \qquad 4.6$$

We use a proportional-integral (PI) controller to regulate the current, the new input u (which represents the output of the regulator), and it is defined as follows:

$$u = L\frac{dI_L}{dt} \quad 4.7$$

Using the Laplace transform, we obtain

$$u = S.L.I_L \quad 4.8$$

Let *G* be the open loop current transfer function defined as follows:

$$G = \frac{1}{SL} = \frac{I_L}{u} \quad 4.9$$

The controller will generate the boost command from the signal corresponding to the difference evaluated between the set point I_{Lref} and the current in the inductor I_L. The transfer function of the controller is given by the following:

$$Cs = \frac{K_i}{S} + K \quad 4.10$$

The closed-loop transfer function of the controller associated with the PV system is given by the following:

$$\frac{I_{PV}}{I_{PV}^*} = \frac{\frac{K_i + K_P S}{L}}{\frac{K_i}{L} + S^2 + S\frac{K_P + R_C}{L}} = \frac{\frac{K_i + K_P S}{L}}{\frac{2}{i} + S^2 + 2S\ {}_i\zeta} \quad 4.11$$

where I_{PV} is the current error, and I^*_{PV} is the reference current of the PV. This allowed us to determine, by identification, the coefficients *Kp* and *Ki*:

$$K_P = 2L\ {}_i\xi - R_c \quad 4.12$$

And:

$$K_i = L\ \frac{2}{i} \quad 4.13$$

To regulate the boost converter, the control law was considered:

$$L\frac{dI_L}{dt} = V_{in} - (1-d)v_c = u \quad 4.14$$

$$d = \frac{-V_{in} + u}{v_c} + 1 \quad 4.15$$

where *d* is the duty cycle of the converter

The PWM modulation technique was then used to generate the trigger pulses to control the converter switch. The control scheme is given in Figure 4.4.

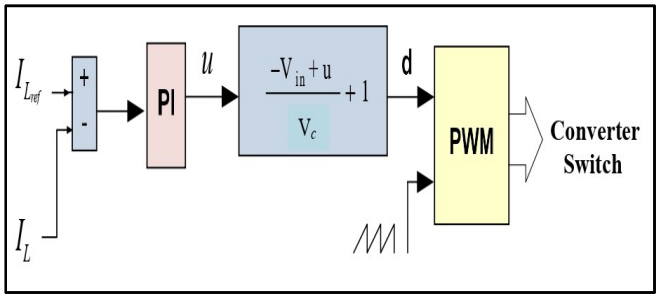

Figure 4.4 The control scheme of a boost converter.

To validate the results, Matlab simulation software was used to test the behavior of the photovoltaic system connected to the power grid. The disturbances were added to the system with variations of loads, solar radiation, and the rate of charge and discharge of the battery. Figure 4.5 shows the proposed diagram of PV connected to the grid.

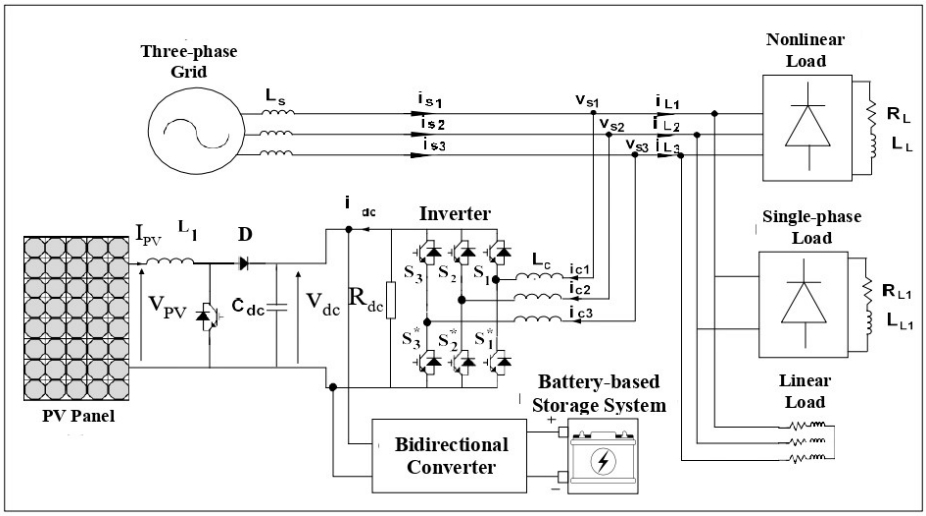

Figure 4.5 Proposed diagram of PV connected grid.

4.3.1 Nonlinear control technique of an inverter

The inverter was placed downstream from the boost converter and upstream from the grid. Its principal function is to deliver the alternating currents and voltages from a DC power source. A nonlinear control technique was used to compensate for the harmonic currents generated by the nonlinear load, maintain the imbalance load, regulate the DC bus voltage, and compensate for the reactive power consumed by the load. Reactive power compensation is a technique used to manage and mitigate the reactive power in an electrical system. The range of power factor (cos φ) within which reactive power compensation can be achieved depends

on the design and capabilities of the controller. In general, a controller such as SVC or STATCOM can operate over a wide range of power factors, typically ranging from lagging (inductive loads) to leading (capacitive loads). The control algorithm employed in these controllers is often based on voltage or current measurement feedback and utilizes closed-loop control techniques. The controller monitors the system voltage and current and adjusts the reactive power output accordingly to maintain a desired power factor or to compensate for reactive power fluctuations. A model of the active filter using these differential equations (park transformation) that passes from the '*abc*' plane to the '*dq*' plane.

4.3.1.1 Modeling the '*abc*' plane transformation

At first, we used Kirchhoff's laws for each phase of the connection point of the inverter: The equations can be written as:

$$\begin{cases} v_1 = V_{MN} + V_{1M} + R_C i_1 + L_C \frac{di_1}{dt} \\ v_2 = V_{MN} + V_{2M} + R_C i_2 + L_C \frac{di_2}{dt} \\ v_3 = V_{MN} + V_{3M} + R_C i_3 + L_C \frac{di_3}{dt} \end{cases} \quad 4.16$$

It's assumed that the voltages are balanced here, and the zero-sequence component is zero. After simplification, the systems of equations become:

$$\begin{cases} v_1 - d_{n1} V_{DC} - R_C i_1 = L_C \frac{di_1}{dt} \\ v_2 - d_{n2} V_{DC} - R_C i_2 = L_C \frac{di_2}{dt} \\ v_3 - d_{n3} V_{DC} - R_C i_3 = L_C \frac{di_3}{dt} \end{cases} \quad 4.17$$

At the DC bus terminal, we have the equality of:

$$i_{DC} = C_{DC} \frac{dV_{DC}}{dt} \quad 4.18$$

Now we give the state representation of the active filter in the plane of '*abc*' in the current system without taking into account the absence of the zero-sequence component:

$$\begin{cases} v_1 - d_{n1} V_{DC} - R_C i_1 = L_C \frac{di_1}{dt} \\ v_2 - d_{n2} V_{DC} - R_C i_2 = L_C \frac{di_2}{dt} \\ i_1 (d_{n2} + 2d_{n1}) \frac{1}{C_{DC}} = \frac{dV_{DC}}{dt} \end{cases} \quad 4.19$$

The active filters help reduce THD source current and are linked to the inverter to maintain the grid control strategies. Two control strategies of the inverter (voltage source active filter) are studied here.

4.3.1.2 Modeling the filter '*abc/dq*' plane transformation

The filter model *d-q* stationary plane is transformed to accelerate the implementation and reduce the computation time. By using Equations (18) and (19) the model gives a relation in the following form:

$$C_{DC}\frac{dV_{DC}}{dt} = d_{n1}i_1 + d_{n2}i_2 + d_{n3}i_3 = [d_{n1} + d_{n2} + d_{n3}]\begin{bmatrix} i_1 \\ i_2 \\ i_3 \end{bmatrix} \quad 4.20$$

Based on Equation (20), the transition performs from the '*abc*' plane to the '*dq0'* plane.

$$C_{dq}^{123} f_{dq0} = f_{123} \quad 4.21$$

$$C_{dq}^{123} = \sqrt{\frac{2}{3}\begin{bmatrix} Cos\theta & Cos(\theta - {}^{2\pi}/_{3}) & Cos(\theta - {}^{4\pi}/_{3}) \\ -Sin\theta & -Sin(\theta - {}^{2\pi}/_{3}) & Sin(\theta - {}^{4\pi}/_{3}) \end{bmatrix}} \quad 4.22$$

$$\frac{dV_{DC}}{dt} = \frac{d_{nd}i_d}{C_{DC}} + \frac{d_{nq}i_q}{C_{DC}} + \frac{d_{n0}i_0}{C_{DC}} \quad 4.23$$

Without taking the zero sequence components into account:

$$\frac{dV_{DC}}{dt} = \frac{d_{nd}i_d}{C_{DC}} + \frac{d_{nq}i_q}{C_{DC}} \quad 4.24$$

$$L_C\frac{di_d}{dt} = V_d - R_C i_d + L_C\omega i_d - d_{nd}V_{DC} \quad 4.25$$

$$L_C\frac{di_q}{dt} = V_q - R_C i_q - L_C\omega i_q - d_{nq}V_{DC} \quad 4.26$$

$$C_{DC}\frac{dV_{DC}}{dt} = d_{nd}i_d + d_{nq}i_q \quad 4.27$$

In order to carry out a good follow-up of the instructions, we must have current loops on the axes of *d* and *q* that are relatively fast. The first two differential equations of the model (4.18) are established and can be rewritten in the following form:

$$u_d = R_C i_d + L_C\frac{di_d}{dt} = V_d + L_C\omega i_q - d_{nd}V_{DC} \quad 4.28$$

$$u_q = R_C i_q + L_C\frac{di_q}{dt} = V_q - L_C\omega i_d - d_{nq}V_{DC} \quad 4.29$$

These equations represent the dynamics of the active filter's nonlinear current of *id*, and *iq*. The currents *id* and *iq* can be controlled independently by inputs u_d and u_q. The Proportional-

Integrator controllers are used for rapid dynamic response to canceling the steady-state error. PI controllers have the following expressions:

$$u_d = \widetilde{I_d} K_p + K_i \int \widetilde{I_d}\, dt \quad 4.30$$

$$u_q = \widetilde{I_q} K_p + K_i \int \widetilde{I_q}\, dt \quad 4.31$$

The closed loop current transfer function is given by the following:

$$\frac{I_d(s)}{I_d^*(s)} = \frac{I_q(s)}{I_q^*(s)} = \frac{s+\frac{k_i}{k_p}}{s^2+\frac{(R_c+k_p)}{L_c}+\frac{k_i}{L_c}} \cdot \frac{k_P}{L_c} \quad 4.32$$

where $I\tilde{d}$ and $I\tilde{q}$ are represent the errors of the currents and Id^* and Iq^* are represent the references of the currents. The current regulator parameters are as follows:

$$K_p = 2\xi L_c \omega_{ni} - R_c \text{ and } K_i = \omega_{ni}^2 L_c \quad 4.33$$

where $\xi = \frac{\sqrt{2}}{2}$; ω_{ni} must be selected less than $\omega_{nis} = 2\pi f_s$; f_s is switching frequency. From Equations (4.28) and (4.29), we determined the control laws as follows:

$$d_{nd} = \frac{V_d - u_d + L_C \omega i_q}{V_{DC}} \quad 4.34$$

$$d_{nq} = \frac{V_q - u_q - L_C \omega i_d}{V_{DC}} \quad 4.35$$

The analysis of the voltage loop is based on Equations (4.25)–(4.27), defined as the equivalent input of:

$$u_{DC} = d_{nd} i_d + d_{nq} i_q = \frac{dv_{DC}}{dt} C_{DC} \quad 4.36$$

The transfer function of the regulator is written as follows:

$$G_v = \frac{U_{DC}}{\widetilde{V_{DC}}} = \frac{\frac{K_{iv}}{k_{pv}}+S}{S} . k_{pv} \quad 4.37$$

The closed-loop transfer function is given by the following:

$$\frac{V_{DC}(S)}{V_{DC}^*(S)} = \frac{\frac{K_{pv}S + K_{iv}}{C_{DC}}}{S^2+\frac{(K_{pv})}{C_{DC}} . S+\frac{K_{iv}}{C_{DC}}} = \frac{\frac{\omega}{2\xi}+s}{S^2+2\xi\omega S+\omega^2} . 2\xi \quad 4.38$$

where $\widetilde{V_{DC}}$is the voltage error and V_{DC}^* is the voltage reference of V_{DC}; $k_{pv} = 2\xi\omega C_{DC}$ and $K_{iv} = \omega^2 C_{DC}$. To regulate the DC bus voltage and to compensate for the losses in the dissipative elements of the filter, an active current i_{d0} is added to the reference current i_d.

We have:

$$i_{d0} = \frac{u_{DC} V_{DC} - d_{nq} V_{DC} i_q}{d_{nd} V_{DC}} = \frac{u_{DC} - d_{nq} i_q}{d_{nd}} \quad 4.39$$

$$d_{nq}V_{DC} \approx V_q = 0 \tag{4.40}$$

$$d_{nd}V_{DC} \approx V_q = \sqrt{\frac{2}{3}}\, V_{smax} \tag{4.41}$$

$$i_{d0} \approx u_{DC}\sqrt{\frac{2}{3}}\,\frac{V_{DC}}{\hat{V}} \tag{4.42}$$

The following transfer function has been used in the filter:

$$H(s) = \frac{s+2s\omega}{s^2+2s\omega\xi+\omega^2} \tag{4.43}$$

By plotting it to the Bode diagram for different cutoff frequencies, with f_c =15 Hz, and 65 Hz, we get the following graph:

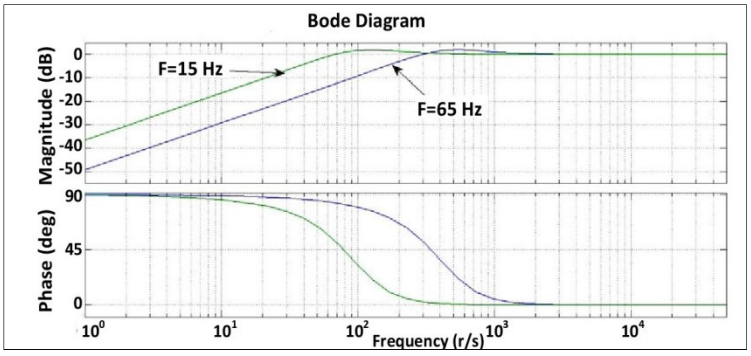

Figure 4.6 Bode diagram of the filter for different cutoff frequencies.

Figure 4.6 shows that for a frequency greater than 60 Hz, the harmonic current will be higher than ω = 377 rd/s. For a cutoff frequency f = 15 Hz, the modulus in dB is almost zero, demonstrating no amplitude modification between the input and the output of the high pass filter. Moreover, the phase is also zero, indicating no phase shift between the input and the output of the high-pass filter. For a cutoff frequency f = 65 Hz, the modulus in dB is approximately 2 dB, demonstrating a modification of amplitude between the input and the output of the high pass filter. Moreover, the phase is not zero, showing a phase difference between the input and the output of the high-pass filter. It is evident that the cutoff frequency at 15 Hz is suitable for compensating for the unbalanced load since there is no change in the input and output signal, neither in amplitude nor phase.

It is seen that the current of the grid is more disturbed for the higher frequency. Figure 4.7 shows the block diagram of the *dq* command. The currents supplied by the active filter are controlled in the *dq* plane using an equivalent control strategy based on synchronous *dq*. The

harmonic references current i_{Ld} and i_{Lq} are extracted from the load currents. A PI Controller is used for the current loops (inner loops) in order to allow the filter currents to follow their references quickly. For the external loop (voltage loop), a PI controller is also used to bring the DC voltage V_{DC} back to its set value. The compensated error is added to the output of the reference current along with the *d*-axis.

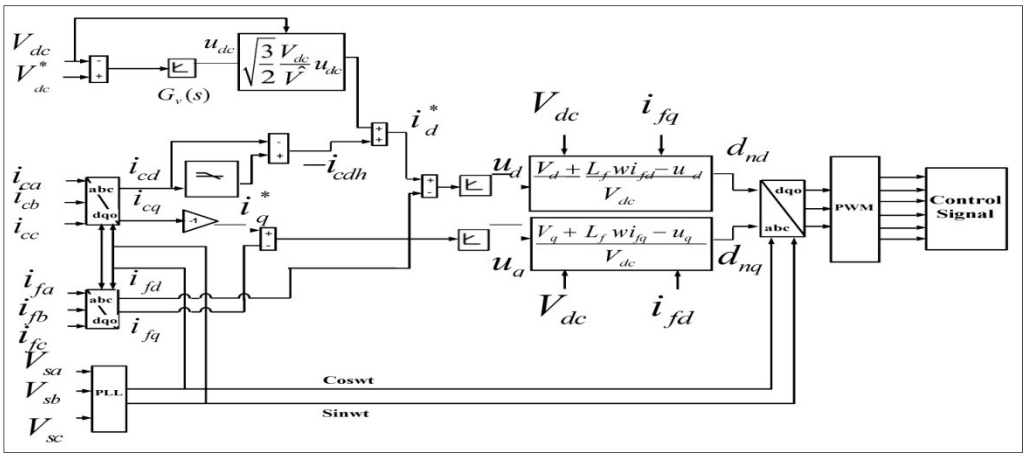

Figure 4.7 Block diagram of nonlinear control.

4.3.2 Nonlinear control with adaptive notch filter

This method is used to analyze the filter inspired by the work carried out by Karimi-Ghartemani in 2006 [37].

$$u(t) = u_1(t) + u_0(t) \tag{4.44}$$

$$u_0(t) = A_0 sin(d_0 + w_0 t) \tag{4.45}$$

The undesired signal can be assimilated to noise, transient disturbances, and sinusoidal components with a frequency different from ω_0 (center frequency). We wish to obtain an estimate of $u_0(t)$, designated by $y(t)$, from the signal $u(t)$. The least-squares error between the input signal $u(t)$ and output $y(t)$ is minimized by a method called gradient descent. It is the starting point for various adaptive algorithms, such as the linear least squares method. The cost function is defined by:

$$J(t, Q) = \frac{1}{2}[u(t) - y(t, Q)]^2 = \frac{1}{2}e^2(t, Q) \tag{4.46}$$

The system comprises a conventional phase-locked loop associated with an amplitude estimator and an adjustment unit. The dynamic system receives the input signal $u(t)$ and

provides a real-time estimate of the fundamental component $y(t)$, the amplitude $V(t)$ of $y(t)$, the frequency and the phase $\Delta\omega(t)=\omega(t)-\omega_0$ and the phase $\varphi(t)$ of $y(t)$. The estimated time derivative of the amplitude, phase, and frequency is then estimated. The error signal $e(t) = u(t) - y(t)$ is the input distortion signal. The speed and accuracy of the response are determined by the parameters of k_1, k_2, and k_3. It controls the behavior of the response both at the transient level and at the steady state. This system has the ability to be inherently adaptive and follows variations in amplitude, phase angle, and frequency of the input signal. It can provide an accurate estimate of the fundamental component of the polluted signal. Its simple structure makes this notch filter suitable for real-time applications. Therefore, the derivatives of A, ω, and φ can be formulated by the equations.

$$\begin{aligned} \dot{A}(t) &= k_1 e(t) sin\varphi(t) \\ \dot{\omega}(t) &= k_2 e(t) cos\varphi(t) \\ \dot{\varphi}(t) &= \omega(t) + k_2 k_3 e(t) cos\varphi(t) \\ y(t) &= A(t) sin\varphi(t) \end{aligned} \qquad 4.47$$

The block diagram of the Adaptive Notch Filter is shown in Figure 4.8.

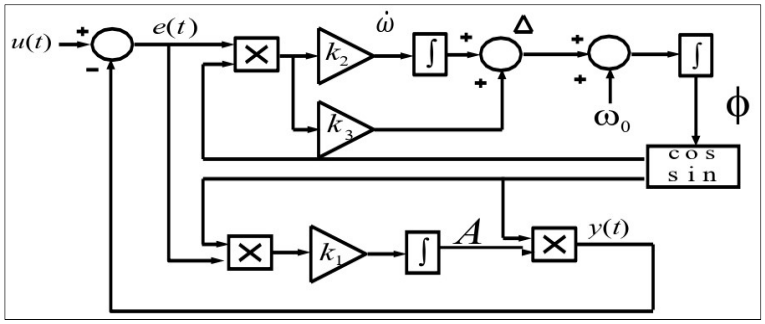

Figure 4.8 The operational block diagram of the adaptive notch filter.

Therefore, we integrated this filter into the simple nonlinear control proposed by using it as an input signal of load currents. Our simulations show that the inverter control does not adequately compensate for the currents. Hence we need to introduce the inverse component in a control system to correct this imperfection. We will therefore capture the input currents and perform an inverse transformation before injecting them at the output. The equation governs the negative sequence component of the load current.

$$I_{inv} = L_{La} + aL_{Lc} + a^2 L_{Lb} \qquad 4.48$$

By integrating it into the global diagram of the filter, we obtain the final diagram of the modified Adaptive Notch Filter shown in Figure 4.9.

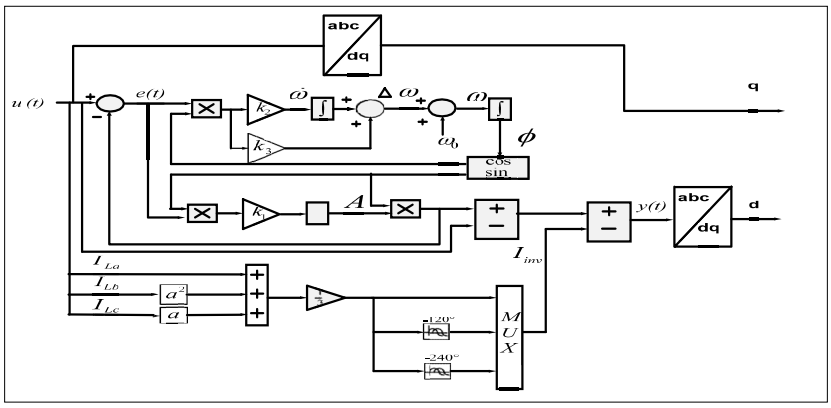

Figure 4.9 Final diagram of the modified adaptive botch filter.

4.3.3 Nonlinear control with multi-variable filter

The main objective of this control strategy is to improve the performance of the nonlinear control by using a multi-variable filter. This filter can directly extract the direct fundamental component of input signals in a voltage or current, along with the *dq* axes. It can also isolate a harmonic in a particular order (direct or inverse). The following equation expresses a method to recover the transfer function from integrating the synchronous reference signal [38].

$$x_{\alpha\beta}(t) = e^{jwt} \int V_{xy}(t)\, e^{-jw}\, dt \tag{4.49}$$

$$H(s) = \frac{x_{\alpha\beta}(s)}{\hat{x}_{\alpha\beta}(s)} = \frac{s+\omega j}{s^2+\omega^2} \tag{4.50}$$

This transfer function makes it possible to demonstrate the input signal in phase with the output signal. Integrating the signal amplitude with the input signal affects its magnitude. We add two constants k_1 and k_2, to the previous transfer function to obtain the following equation:

$$H(s) = \frac{x_{\alpha\beta}(s)}{\hat{x}_{\alpha\beta}(s)} = \frac{(k_1+s)+\omega_c j}{(k_1+s)^2+\omega_c^2}.k_2 \tag{4.51}$$

To obtain $H(s) = 0$ dB, we must take $K = k_1 = k_2$. Therefore, the Laplace transforms transfer function of the multi-variable filter *H(s)* becomes:

$$H(s) = \frac{x_{\alpha\beta}(s)}{\hat{x}_{\alpha\beta}(s)} = \frac{(K+s)+\omega_c j}{(K+s)^2+\omega_c^2}.K \tag{4.52}$$

where K is a positive constant, $x_{\alpha\beta}$ is an input signal, and $\hat{x_{\alpha\beta}}$ is an output signal of the multi-variable filter. We draw the Bode diagram of the transfer function directly from Simulink using 'linear control design' for three values for K = 1500, 15,000, and 150,000, shown in Figure 4.10.

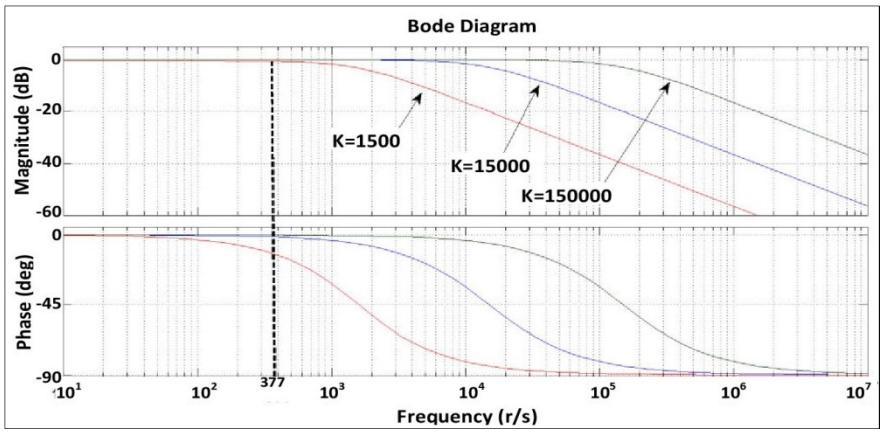

Figure 4.10 Bode diagram representation of different values of K.

We are looking for the value of K, which gives us a zero phase shift and dB modulus at the frequency of the electrical grid, f = 60 Hz or ω = 377 rd/s. The values retained are those greater than 15,000. The amplitude remains high for a higher value of K, and the phase remains equal to zero. Figure 4.11 shows the Total Harmonic Distortion (THD) of the grid for different values of K in the transfer function.

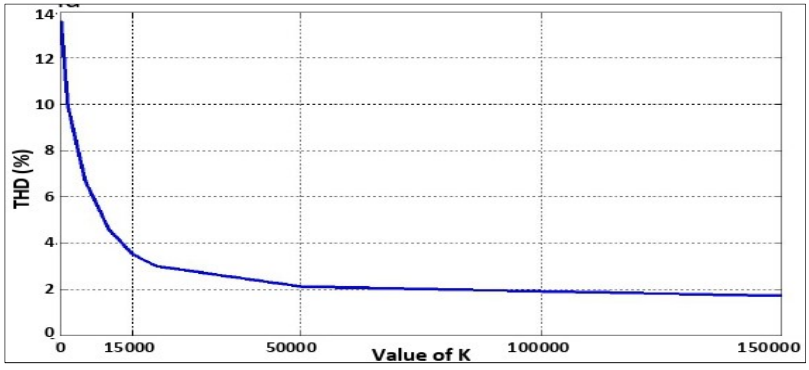

Figure 4.11 THD of the grid for different values of K.

We can conclude from this figure that when we increase the value of K, the rate of harmonic distortion in the grid is reduced. The THD of the grid remains below 5% when the value of K is increased from K = 10,000. Thus, by using a multi-variable filter, the direct or inverse fundamental and harmonic components of the input signals (voltage or current) can be

extracted directly along the *dq* axes without phase shift or amplitude change. From the transfer function, we obtain the following equations.

$$\hat{x}_\alpha(s) = x_\alpha(s)\frac{(K+s).K}{(K+s)^2+\omega_c^2} - x_\beta(s)\frac{\omega_c K}{(K+s)^2+\omega_c^2} \quad 4.53$$

$$\hat{x}_\beta(s) = x_\alpha(s)\frac{\omega_c K}{(K+s)^2+\omega_c^2} + \frac{(K+s).K}{(K+s)^2+\omega_c^2}\, x_\beta(s) \quad 4.54$$

$$\hat{x}_\alpha(s) = [x_\alpha(s) - \hat{x}_\alpha(s)]\frac{K}{s} - \hat{x}_\beta(s).\frac{\omega_c}{s} \quad 4.55$$

$$\hat{x}_\beta(s) = \left[x_\beta(s) - \hat{x}_\beta(s)\right]\frac{K}{s} + \hat{x}_a(s).\frac{\omega_c}{s} \quad 4.56$$

Therefore, we integrated this filter into the proposed nonlinear controller by using it as input signals of the load currents of the grid.

4.3.4 Nonlinear control without filter

A simple nonlinear control is proposed to extract the grid's current harmonics to avoid using a traditional high-pass filter. This control is based on using the positive sequence of the load current. The inverter has the ability to compensate for all undesired current harmonics, unbalanced load currents, and reactive power consumed by the loads [39].

$$L_c\omega i_{cq} - d_{nd}v_{dc} + v_d = L_c\frac{di_{cd}}{dt} \quad 4.57$$

$$-L_c\omega i_{cd} - d_{nq}v_{dc} + v_q = L_c\frac{di_{cq}}{dt} \quad 4.58$$

$$d_{nd}i_{cd} + d_{nd}i_{cq} = C_{dc}\frac{dv_{dc}}{dt} + \frac{v_{dc}}{R_{dc}} \quad 4.59$$

$$\begin{cases} L_cL_c\frac{di_{Ld}}{dt} - L_c\omega i_{Lq} + L_c\omega i_{sq} - d_{nd}v_{dc} + v_d = L_c\frac{di_{sd}}{dt} \\ L_c\frac{di_{Lq}}{dt} + L_c\omega i_{Ld} - L_c\omega i_{sd} - d_{nq}v_{dc} + v_q = L_c\frac{di_q}{dt} \end{cases} \quad 4.60$$

To maintain V_{dc} equal to its reference, the DC bus voltage regulator uses a proportional-integral PI as an output component i_{d0} to maintain the DC bus voltage and reduce the losses in the converter.

$$i_{d0} = \frac{v_{dc}u_{dc}}{v_{dc}d_{nd}} = \frac{u_{dc}}{d_{nd}} = \sqrt{\frac{2}{3}}\, u_{dc}\frac{v_{dc}}{\hat{v}} \quad 4.61$$

$$d_{nd} = \frac{L_c\frac{di_{Ld}}{dt} - L_c\omega i_{Lq} + L_c\omega i_{sq} - d_{nd}v_{dc} + v_d - u_d}{v_{dc}} \quad 4.62$$

$$d_{nq} = \frac{L_c\frac{di_{Lq}}{dt} + L_c\omega i_{Ld} - L_c\omega i_{sd} - d_{nq}v_{dc} + v_q - u_q}{v_{dc}} \quad 4.63$$

The diagram of the nonlinear controller without an inverter filter is shown in Figure 4.12.

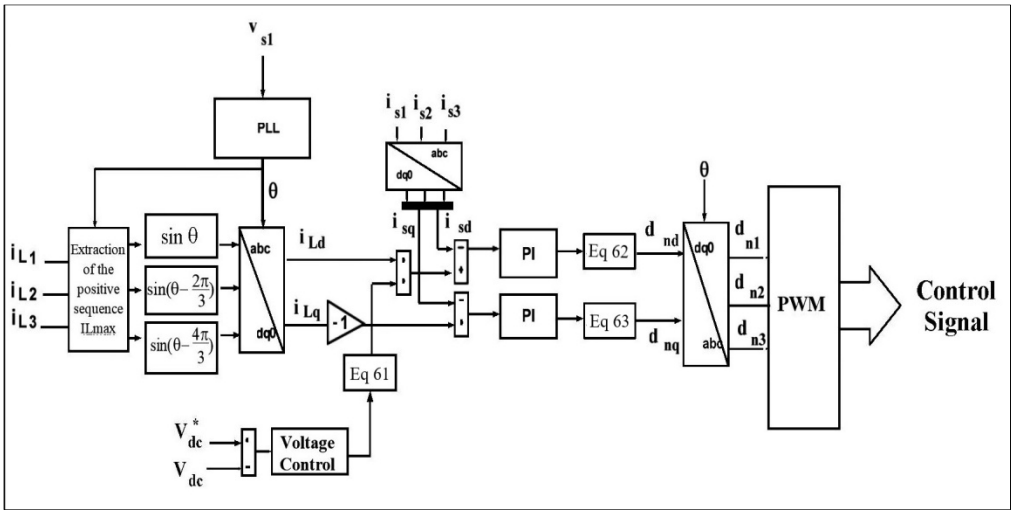

Figure 4.12 Diagram of the nonlinear controller without an inverter filter.

The following values will be used for the simulation of the grid as shown in Table 4.1.

Table 4.1 Simulation data of the proposed grid.

Sources	Symbols/Parameters
Solar Panel	Radiation 800 W/m^2, Current I_{PV} = 40 A, Voltage V_{PV} = 150V, Power P_{PV} = 6000 W
Bidirectional Converter	Inductance L = 5 mH, Capacitance C = 200.10^{-6} F
Loads	Nonlinear load R_L=30 Ω, L_L=10 mH; Single-phase load: R_{L1} = 50 Ω, L_{L1} = 10 mH; Linear load R_{L2} = 30 Ω, L_{L2} = 10 mH
Inverter/Rectifier	Lc = 5 mH, Ls = 0.5 mH
Three-Phase Grid	Frequency 60 Hz and a Voltage phase 208 V
Storage System	Li-ion- 20Ah, SOC 70%

4.4 Simulation results

4.4.1 Using a sample nonlinear controller

4.4.1.1 Assembled with loads, solar radiation, and without a battery system

Using Matlab/Simulink software, we analyzed a system consisting of a photovoltaic panel connected to the three-phase grid with an unbalanced nonlinear load. At t = 0.1 s, solar

radiation is fixed at G = 800 W/m2. We obtained the powers, currents, and voltage curves at a certain point level to understand the effect of each subsystem of the entire grid. The THD rate of the grid and loads are also considered here. Figure 4.13 and Figure 4.14 show the dynamic response of the grid and power flow in the grid with solar radiation of G = 800 W/m2 without a storage system. Figure 4.15 shows the harmonic spectrum of the grids and load current.

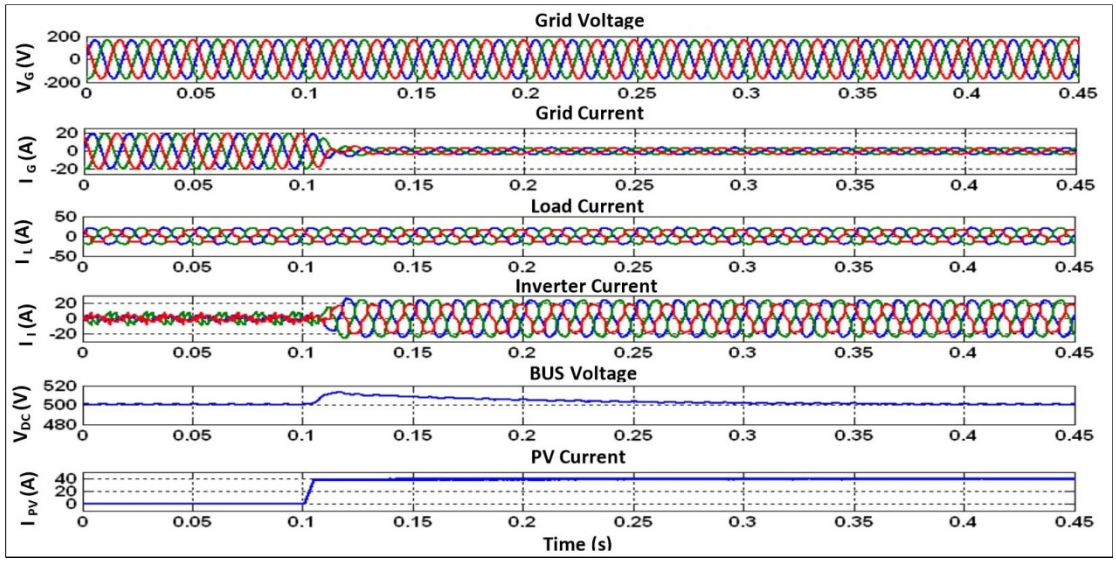

Figure 4.13 Dynamic response of the grid with solar radiation of G = 800 W/m2.

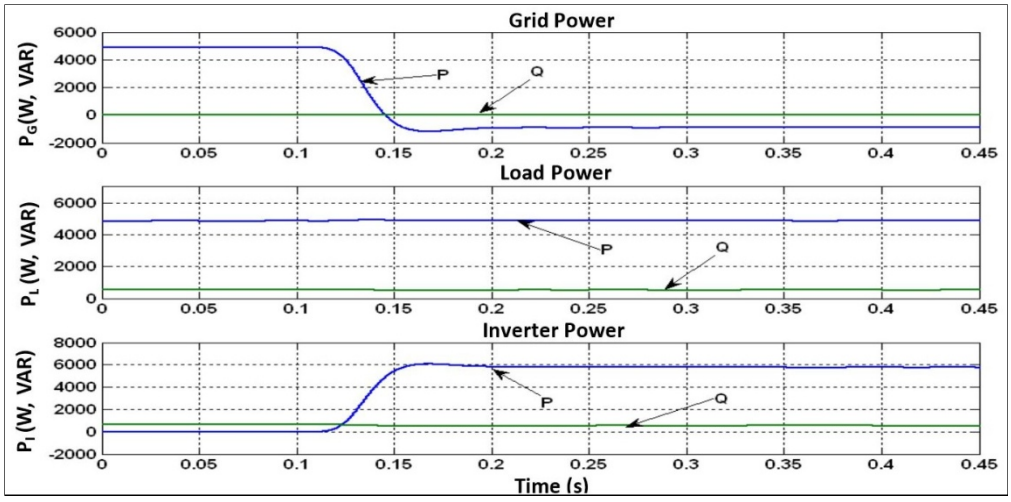

Figure 4.14 Power flow in the grid with solar radiation G = 800W/m2.

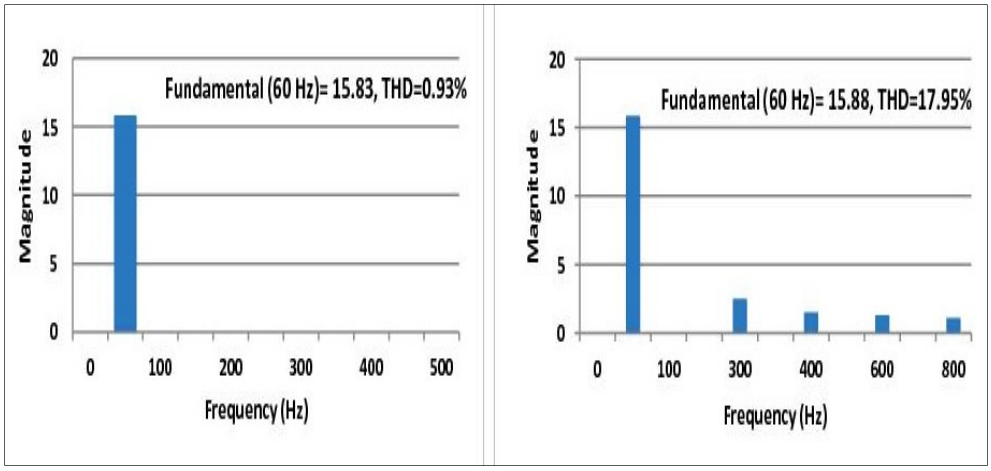

Figure 4.15 Harmonic spectrum of the grids and load current with solar radiation of G = 800 W/m2.

From the above simulation, we analyzed that the grid's current is in phase with the voltage. As a result, the current provides a part of the power to the battery and loads. In the presence of solar radiation, the current is out of phase with the voltage. Therefore it receives power. The V_{dc} is adequately regulated here. With G = 800 W/m^2, we observe a current of 40 A generated by the solar panel. The power curves confirm that the load is supplied at 5000 W at first entirely by the grid, then the solar panel provides 6000 W under sunny conditions. At the same time, it can also feed the grid up to 1000 W. We also observed a grid THD of 0.93%.

4.4.1.2 Assembled with load, solar radiation, and variation of the battery charge

For this simulation, we use the same assembly as before to allow the storage system to compensate for the variations of power generated by the solar panel due to climatic conditions. At t = 0 s, the solar radiation is fixed at G = 800 W/m2. On the other hand, the current of the battery is varied. Indeed, through the control of the DC-DC converter, we imposed a current to charge battery Iin = 20 A from t = 0 to t = 0.1 s, then discharged from t = 0.1 to 0.3 s with Iin = −20 A, and again charged from t = 0.3 s with Iin = 20 A. The current, voltage, and power curves are observed in Figure 4.16 and Figure 4.17, respectively. The simulation results we obtained are shown as follows.

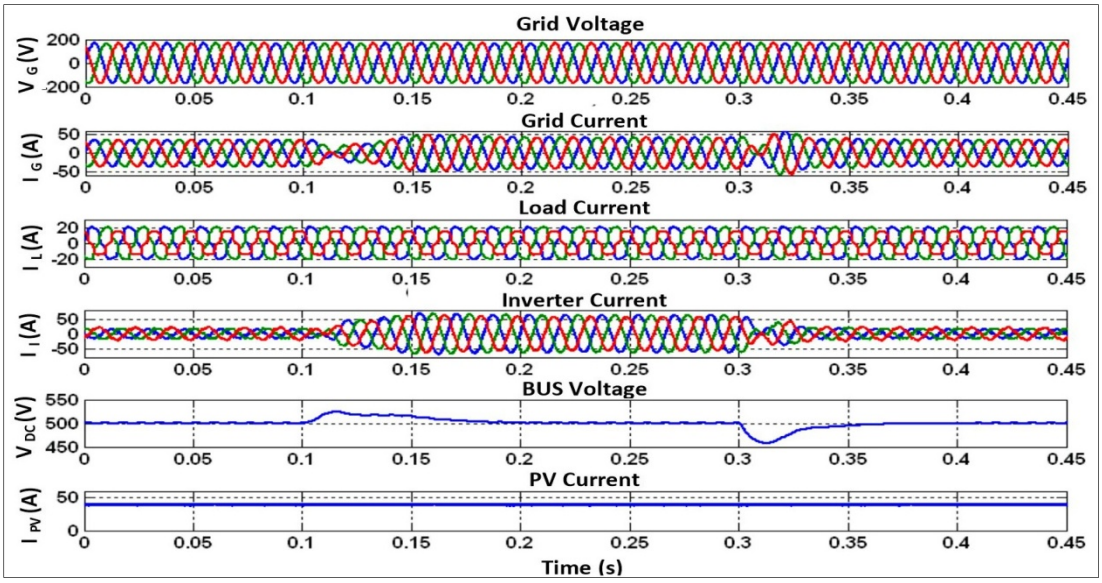

Figure 4.16 Dynamic state response with battery charge variation.

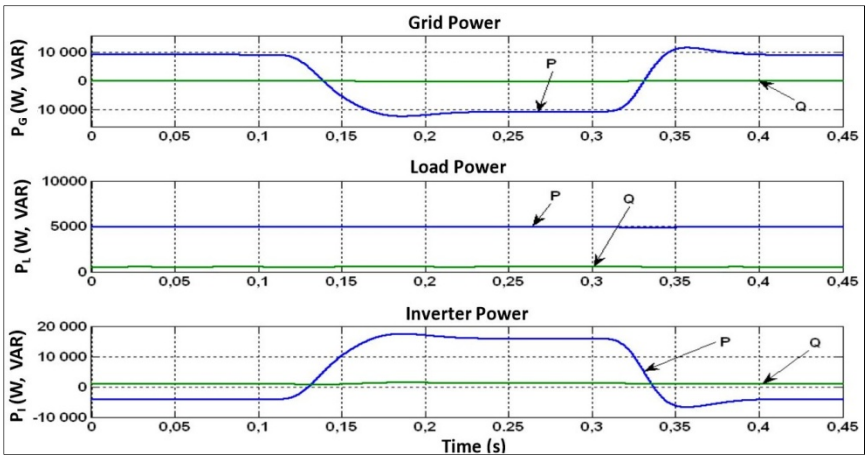

Figure 4.17 Power flow with battery charge variation.

The current in the inverter increases at t = 0.1 to 0.3 s because of the battery discharges shown in Figure 4.18. The results show phase opposition between the current and the grid voltage, indicating that the grid receives power. Power curves confirmed that the inverter is negative when the battery absorbs current and positive when the battery discharges the current. The DC bus voltage is regulated here, and the current in the solar panel is constant at 40 A. The power supplied to the load is up to 5000 W. The curves relating to the battery indicate when the current imposed is negative, the battery is charged. When it is positive, it is discharged. The voltage decreases when the current increases and vice versa.

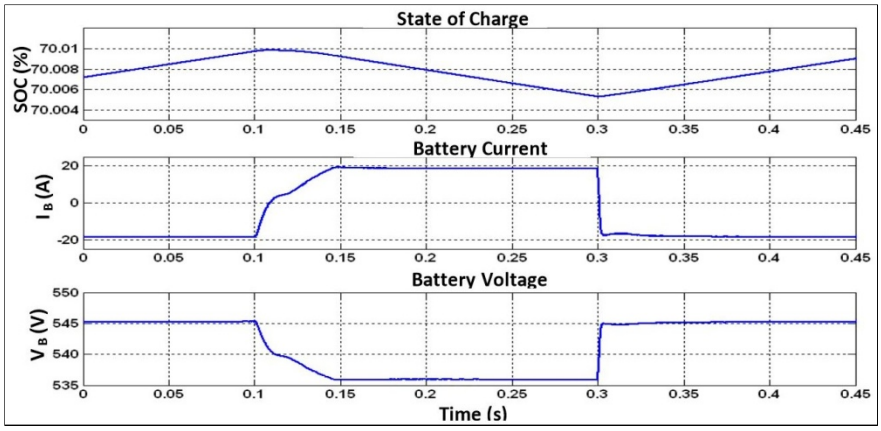

Figure 4.18 Battery state of charge.

4.4.1.3 Assembled with solar radiation, battery charge, and variation of the load

For this simulation, we use the same setup as the second simulation, except for the varied unbalanced load. The purpose of this operation is to analyze the assembled grid reaction to this modification. We can imagine a city as a load that needs to be supplied and requires more or less energy. The system must adapt to these variations. At t = 0 s, the solar radiation is set at G = 800 W/m2. Between t = 0.1 and 0.2 s, we increase the load. At t = 0.3 s, we fix the load as at t = 0 s. The other parameters (radiation, battery charge) are constant. The same current, voltage, and power curves are observed in Figure 4.19 and Figure 4.20 respectively, as in the first simulation. Here are the results we obtained from the simulation.

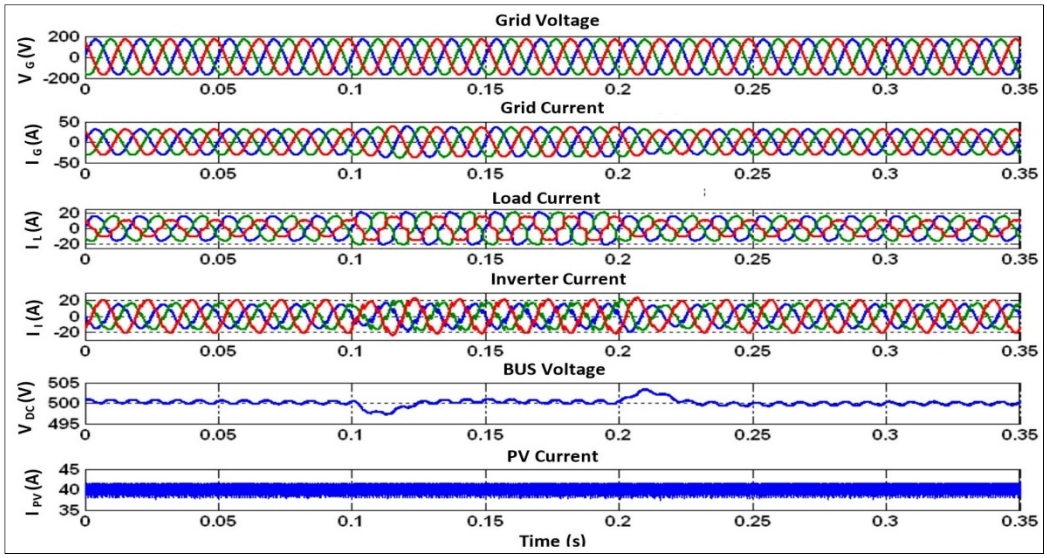

Figure 4.19 Dynamic response with load variation.

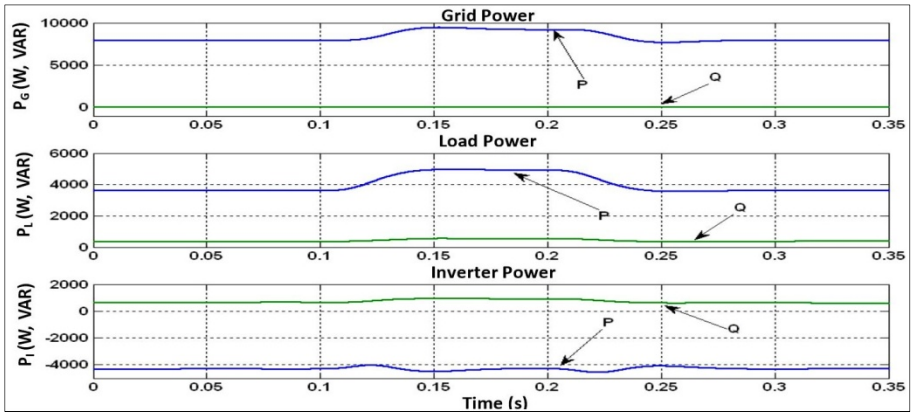

Figure 4.20 Power flow with load variation.

From the above-shown power curve, we observed the PV and grid that supply power to the load. When the load power increases at t = 0.1 s, the current in the grid increases due to the power of the grid. With solar radiation of G = 800 W/m2, the PV can't support the grid to supply power to the load.

4.4.1.4 Assembled with battery charge, load, and with variation of the solar radiation

For this simulation, we used the same setup as the second simulation, except the varied solar radiation at t = 0 s, G = 600 W/m2, at t = 0.1 s, G = 800 W/m2, and at t = 0.3 s, G = 1000 W/m2. The other parameters (load, battery charge) are constant. The same current, voltage, and power curves are observed in Figure 4.21 and Figure 4.22, respectively, as in the first simulation. The simulation results we obtained are shown as follows:

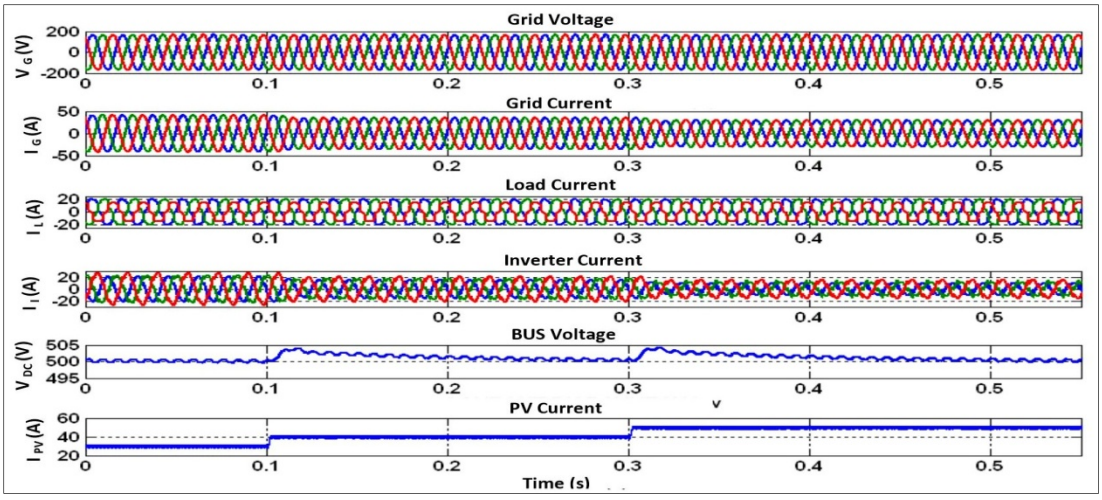

Figure 4.21 Dynamic response with the variation of solar radiation.

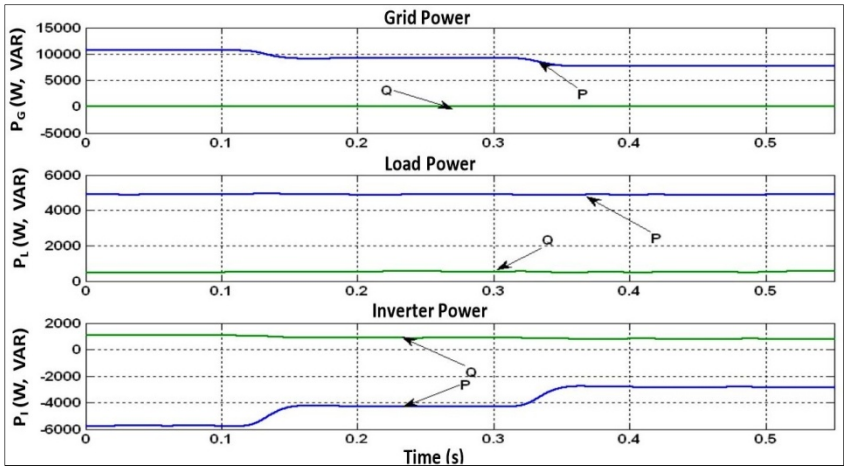

Figure 4.22. Power flow with a variation of solar radiation.

This simulation shows that the grid current decreases when solar radiation increases. This increment in solar radiation causes to increase in PV current from 25 A to 40 A and finally to 50 A. From the above power curve, we observed the grid power decreases, inverter power increases and the load becomes constant.

4.4.2 Using nonlinear controller with multi-variable filter

4.4.2.1 Assembled with loads, solar radiation, and without a battery system

The same simulation is carried out as in Section 4.4.1.1 by replacing the simple nonlinear controller of the inverter with the nonlinear controller with a multi-variable filter. Here are the results we obtained:

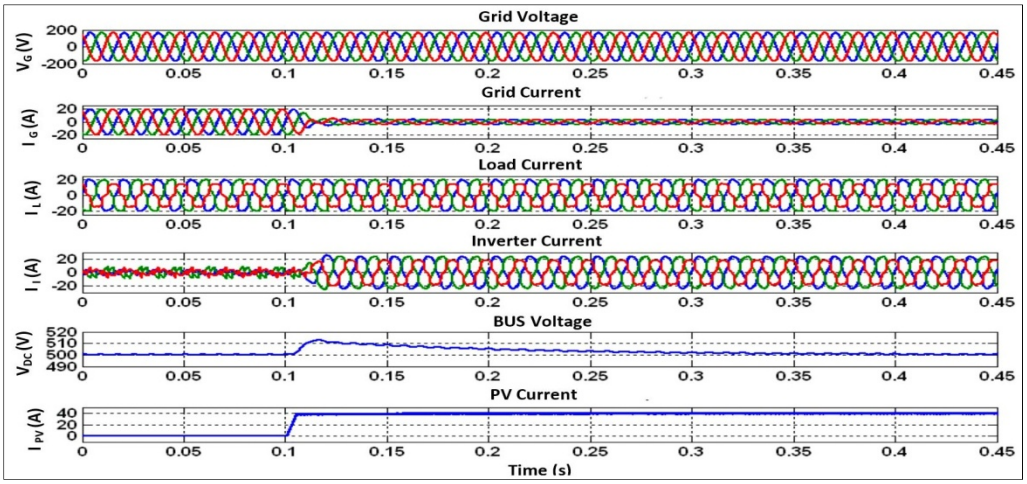

Figure 4.23 Dynamic response with solar radiation of G=800W/m2 using multi-variable filter

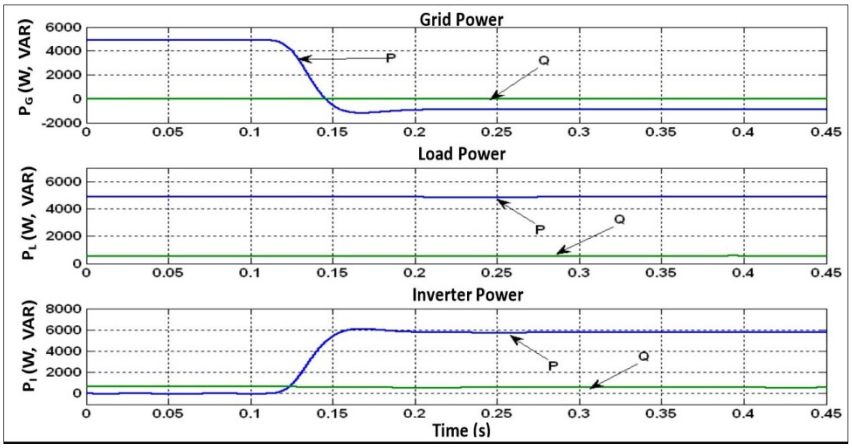

Figure 4.24 Power flow with the variation of solar radiation G = 800W/m2 using multi-variable filter.

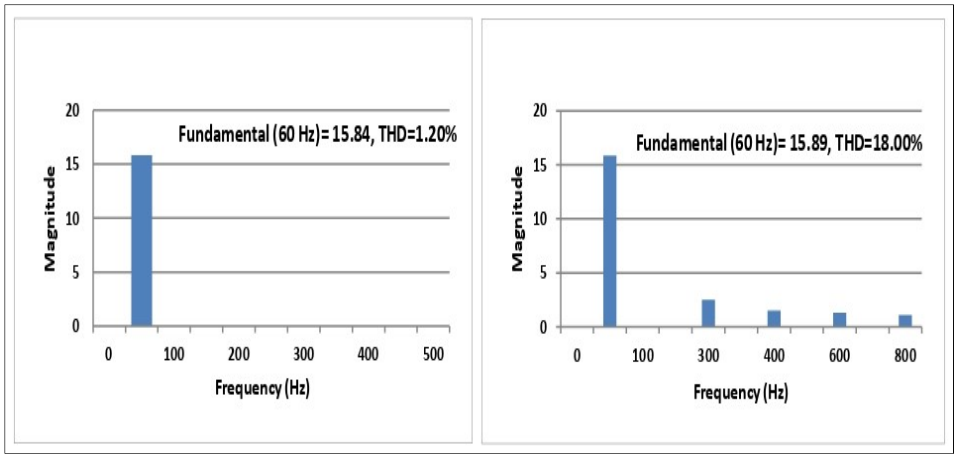

Figure 4.25 Harmonic spectrum of the grid and load current using a multi-variable filter.

We analyzed from Figure 4.23 that the grid current significantly decreased when solar radiation increased. In the absence of solar radiation, the current is in phase with the voltage. Therefore it supplies current. On the other side, the current is out of phase with the voltage with solar radiation. Thus it receives current. The Vdc is adequately regulated here. With G = 800 W/m2, we observe a current of 40 A generated by the solar panel. Figure 4.24 shows that the power curves confirm that the load is supplied at 5000 W entirely by the grid, then the solar panel provides 6000 W under sunny conditions. At the same time, it can also feed the grid up to 1000 W. We also observed from Figure 4.25 that a grid THD of 1.20% is a steady-state condition.

4.4.2.2 Assembled with loads, solar radiation, and variations of the battery charge

The same simulation is carried out as in Section 4.4.1.2 by replacing the simple nonlinear controller of the inverter with the nonlinear controller with a multi-variable filter. Here are the results we obtained:

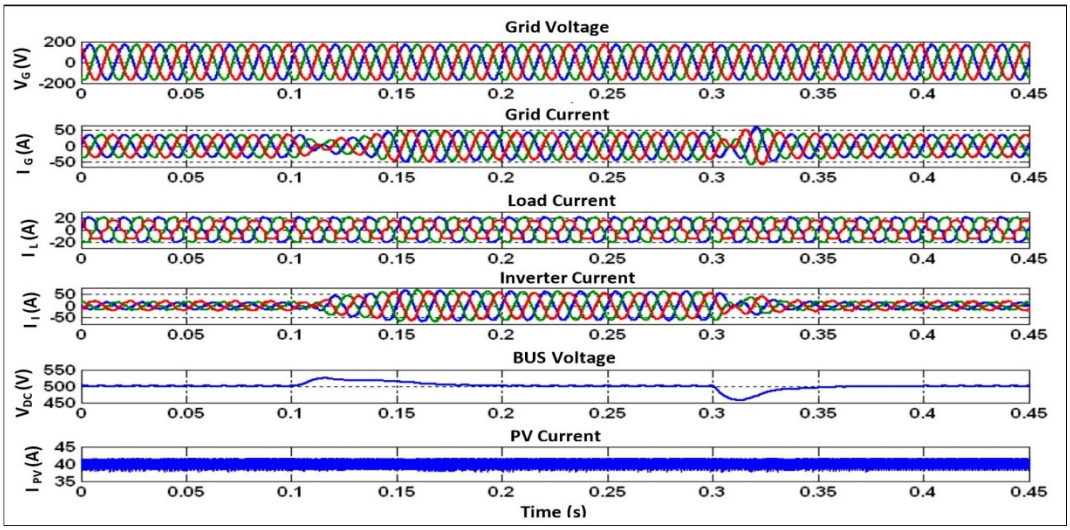

Figure 4.26 Dynamic response with battery charge variation using a multi-variable filter.

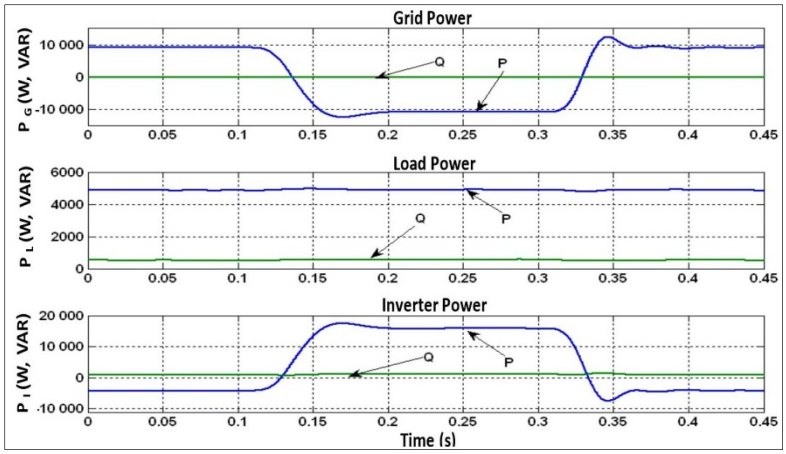

Figure 4.27 Power flow with battery charge variation using a multi-variable filter.

Figure 4.26 shows the current in the inverter increases at t = 0.1 to 0.3 s because of the battery discharges. The results show phase opposition between the current and the grid voltage, indicating that the grid receives power. Figure 4.27 shows the power curves confirming that the inverter is negative when the battery absorbs current and positive when the battery discharges the current shown in Figure 4.28. The DC bus voltage is regulated

here, and the current in the solar panel is constant at 40 A. The power supplied to the load is up to 5000 W. The curves relating to the battery indicate when the current imposed is negative, the battery is charged. When it is positive, it is discharged. The voltage decreases when the current increases and vice versa.

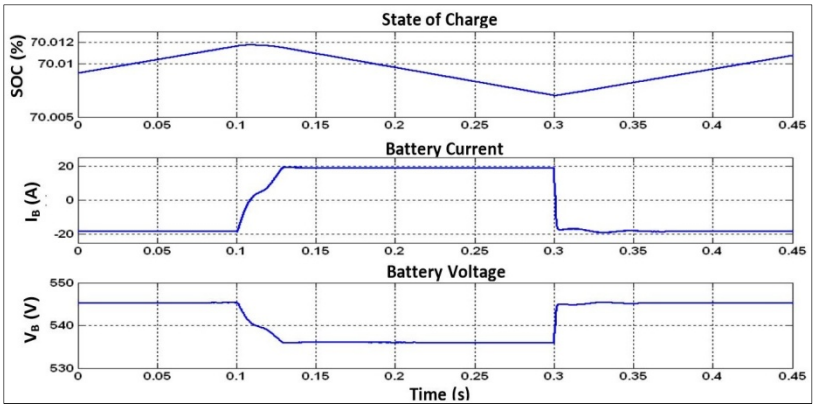

Figure 4.28 Battery state of charge using multi-variable filter.

4.4.2.3 Assembled with solar radiation, battery charge, and variation of the loads

The same simulation is carried out as in Section 4.4.1.3 by replacing the simple nonlinear controller of the inverter with the nonlinear controller with a multi-variable filter. Here are the results we obtained.

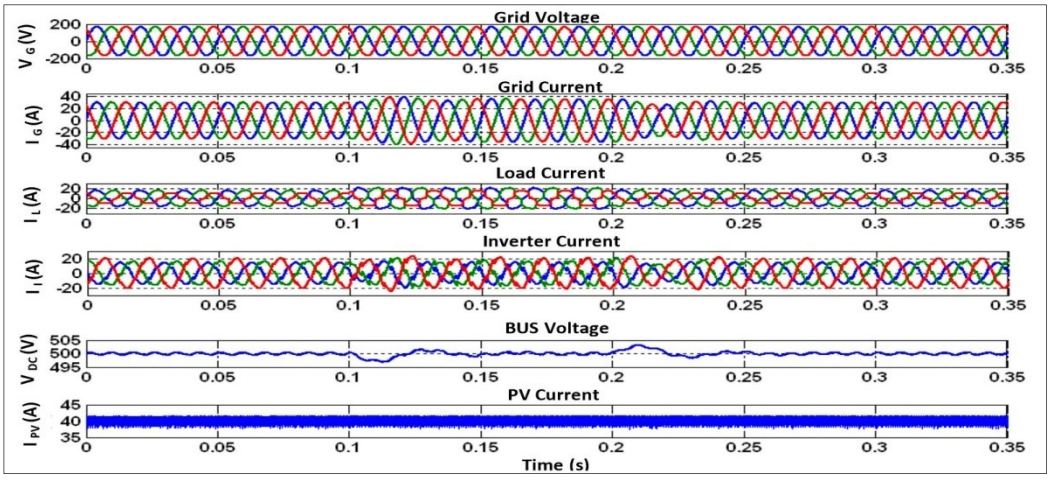

Figure 4.29 Dynamic response with load variation using a multi-variable filter.

From the above power curve, we observed the PV and grid that supply power to the load. Figure 4.29 and Figure 4.30 show when the load power increases at t = 0.1 s, the current in

the grid increases due to the power of the grid. With the solar radiation of G = 800 W/m2, the PV can't support the grid to supply power to the load.

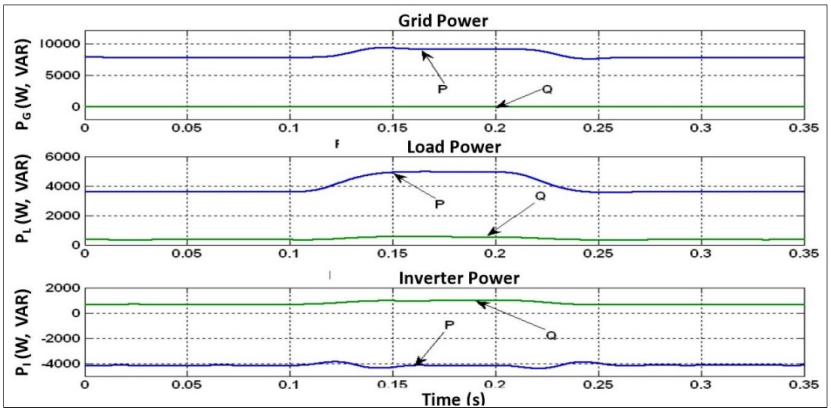

Figure 4.30 Power flow with a load variation multi-variable filter.

4.4.2.4 Assembled with battery charge, load, and variation of the solar radiation

The same simulation is carried out as in Section 4.4.1.4 by replacing the simple nonlinear controller of the inverter with the nonlinear controller with a multi-variable filter. Here are the results we obtained.

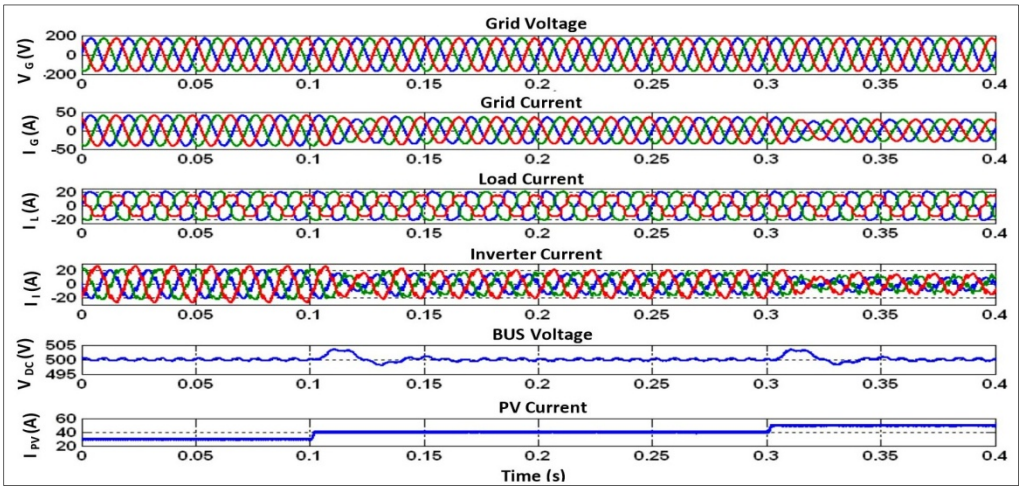

Figure 4.31 Dynamic response with a variation of solar radiation using a multi-variable filter.

This simulation shows that the grid current decreases when solar radiation increases. This increment in solar radiation causes to increase in PV current from 25 A to 40 A and finally to 50 A shown in Figure 4.31. From the above power curve, we observed that the grid power decreases, inverter power increases and the load becomes constant, as shown in Figure 4.32.

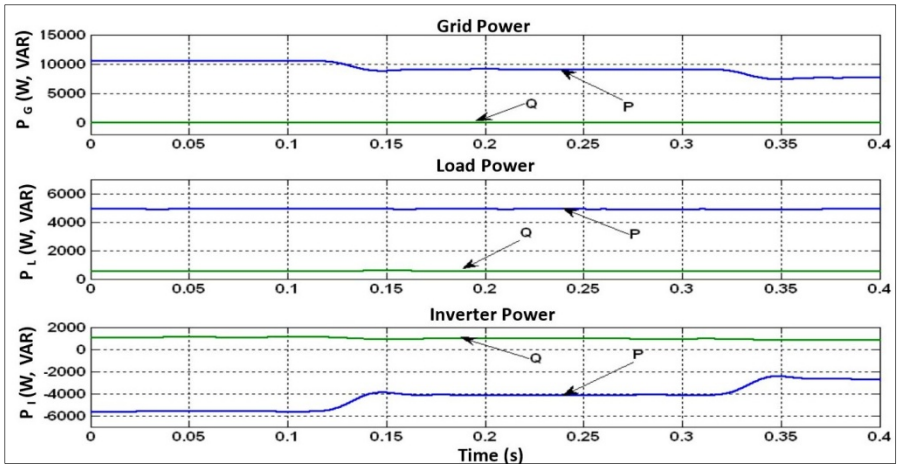

Figure 4.32 Power flow with a variation of solar radiation using a multi-variable filter.

4.4.3 Using nonlinear controller with notch

4.4.3.1 Assembled with loads, solar radiation, and without a battery system

The same simulation is carried out as in Section 4.4.1.1 by replacing the simple nonlinear controller of the inverter with the nonlinear controller with a notch filter. For the balanced load, no anomaly is seen in the grid current. In this case, the load is unbalanced. Thus inverter control system does not compensate for the currents correctly. Hence we need to introduce an inverse component in the control system to correct this abnormality. Adding this component gives us the expected results shown below.

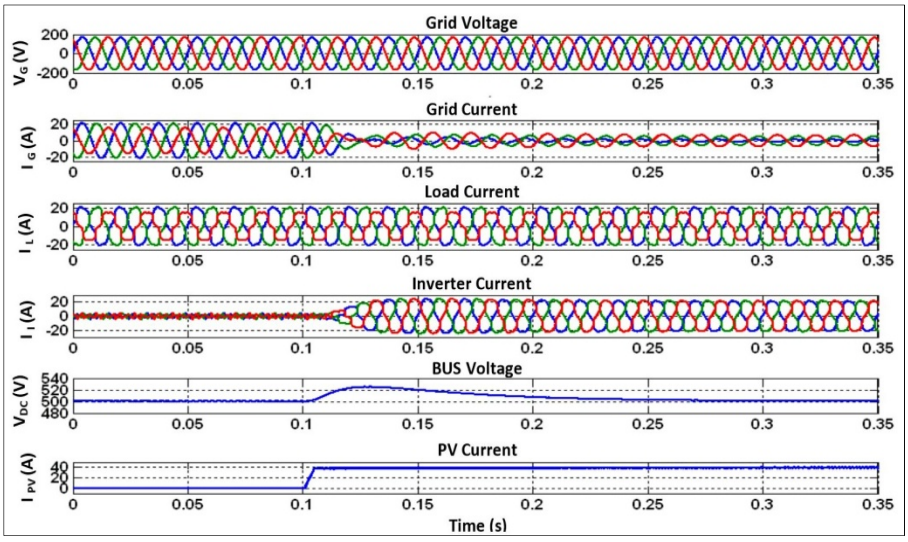

Figure 4.33 Dynamic response with solar radiation of G = 800 W/m^2 using a notch filter.

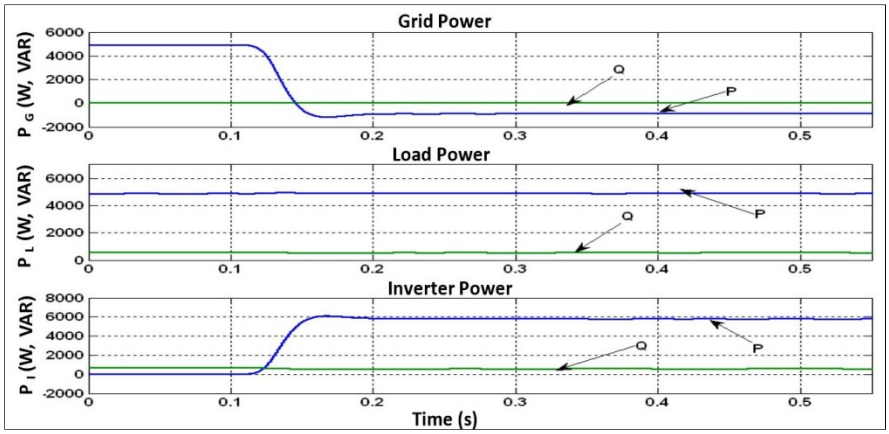

Figure 4.34 Power flow with solar radiation G = 800 W/m^2 using a notch filter.

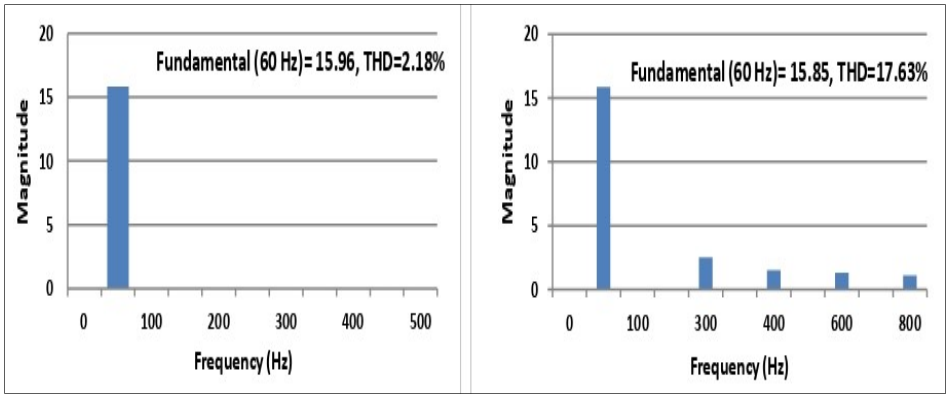

Figure 4.35. Harmonic spectrum of the grid and load current using a notch filter.

We analyzed from Figure 4.33 that the grid current significantly decreased when solar radiation increased. In the absence of solar radiation, the current is in phase with the voltage. Therefore it supplies current. On the other side, the current is out of phase with the voltage with solar radiation. Thus it receives current. The Vdc is adequately regulated here. With G = 800 W/m2, we observe a current of 40 A generated by the solar panel. Figure 4.34 shows that the power curves confirm that the load is supplied at 5000 W entirely by the grid, then the solar panel provides 6000 W under sunny conditions. At the same time, it can also feed the grid up to 1000 W. In Figure 4.35, we also observed a grid THD of 2.18% in a steady state.

4.4.3.2 Assembled with loads, solar radiation, and without a battery system

The same simulation is carried out as in Section 4.1.2 by replacing the simple nonlinear controller of the inverter with the nonlinear controller with a notch filter.

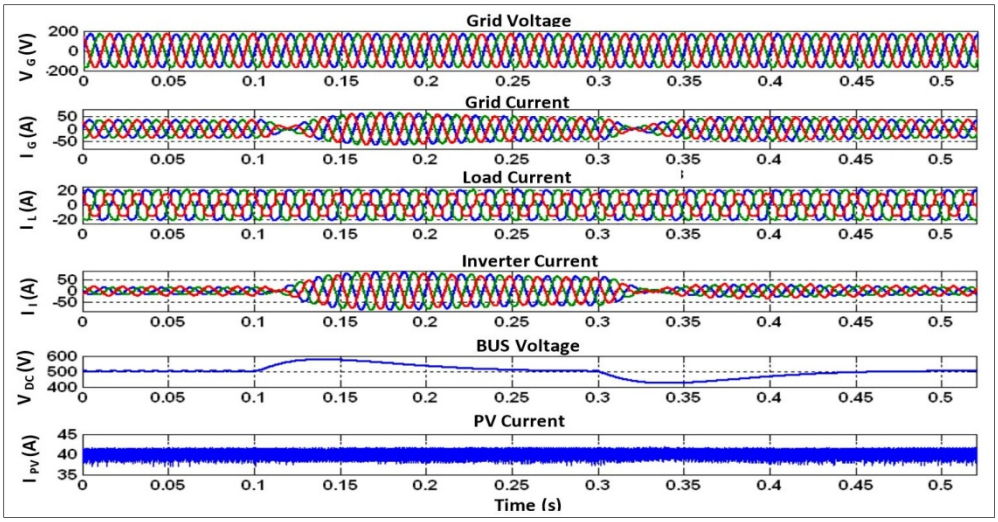

Figure 4.36 Dynamic state response with battery charge variation using a notch filter.

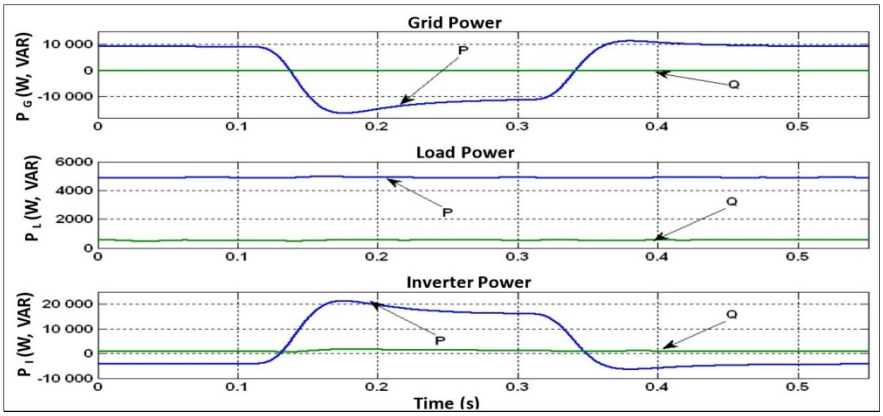

Figure 4.37 Power flow with battery charge variation using a notch filter.

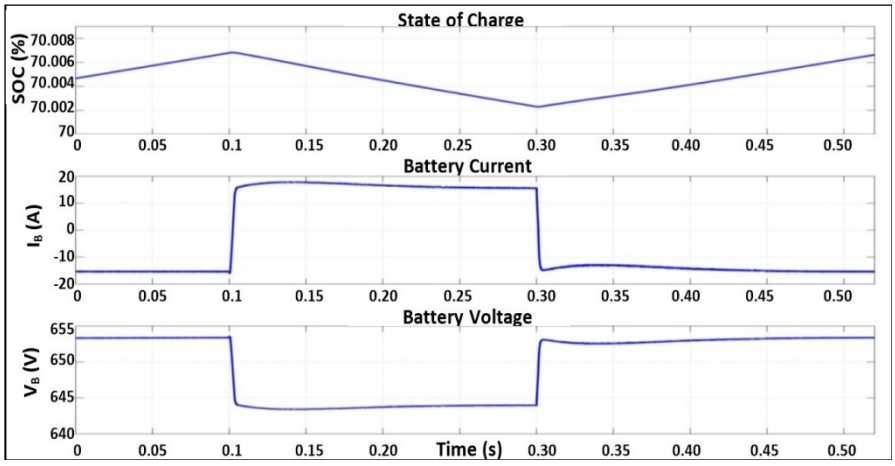

Figure 4.38 Battery state of charge using a notch filter.

Figure 4.36 shows that the current in the inverter increases at t = 0.1 to 0.3 s because the battery discharges are shown in Figure 4.37. The results show phase opposition between the current and grid voltage, indicating that the grid receives power. Power curves confirmed that the inverter is negative when the battery absorbs current and positive when the battery discharges the current. In Figure 4.38, the curves relating to the battery indicate that when the current imposed is negative, the battery is charged. When it is positive, it is discharged.

4.4.3.3 Assembled with solar radiation, battery charge, and variation of the loads

The same simulation is carried out as in Section 4.1.3 by replacing the simple nonlinear controller of the inverter with the nonlinear controller with a notch filter. Here are the results we obtained.

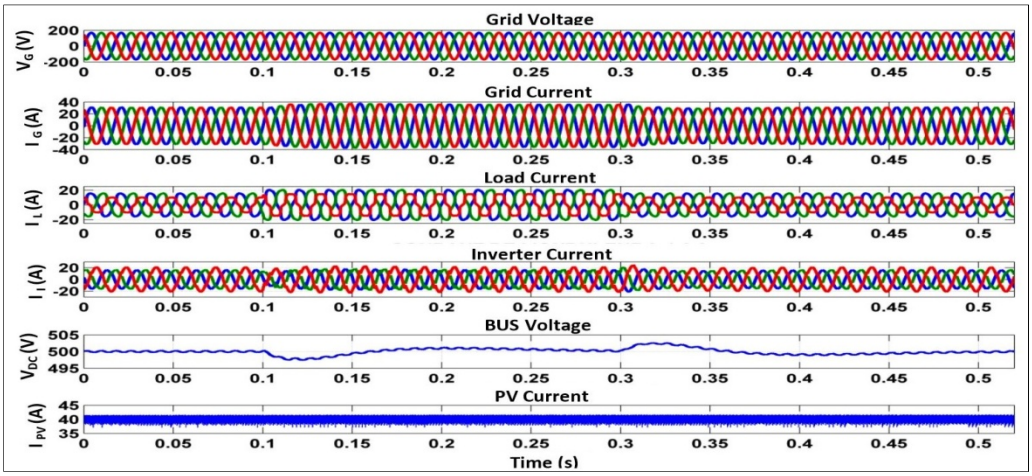

Figure 4.39 Dynamic response with load variation using a notch filter.

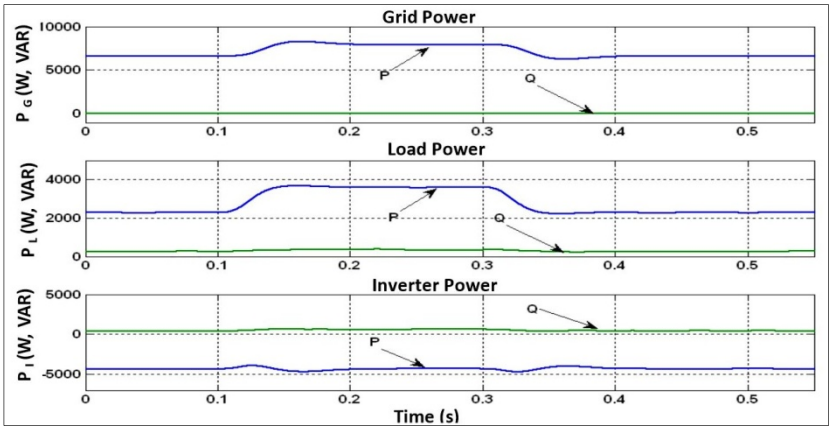

Figure 4.40 Power Flow with load variation using a notch filter.

4.4.3.4 Assembled with battery charge, load, and with variation of the solar radiation

The same simulation is carried out as in Section 4.4.1.4 by replacing the simple nonlinear controller of the inverter with the nonlinear controller with a notch filter. Here are the results we obtained.

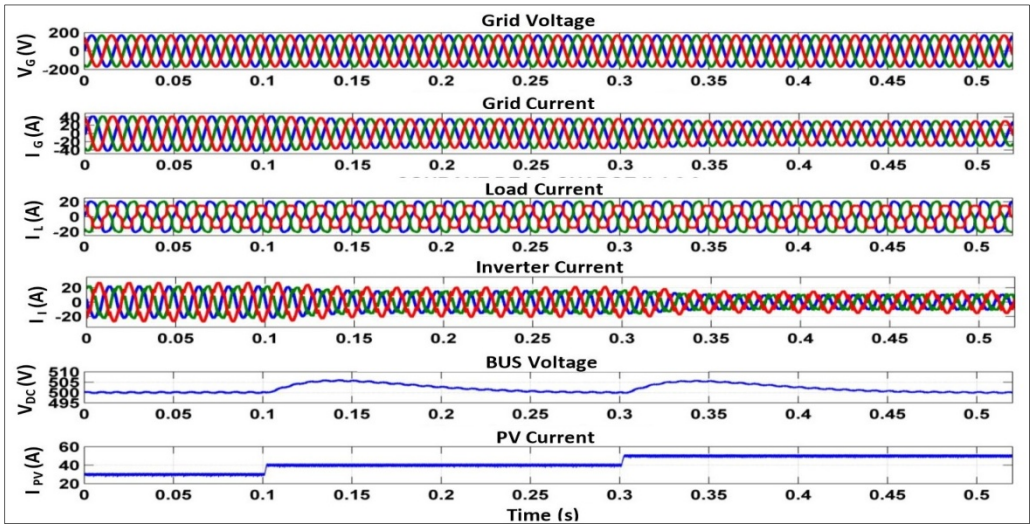

Figure 4.41 Dynamic response with a variation of solar radiation using a notch filter.

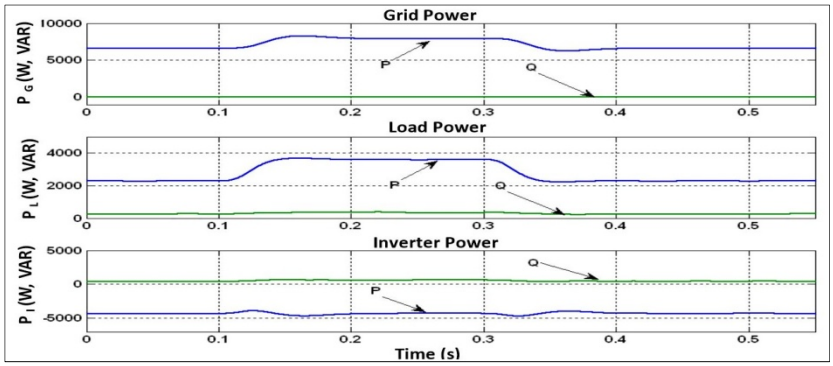

Figure 4.42 Power flow with a variation of solar radiation using a notch filter.

Figure 4.41 shows that the grid current decreases when solar radiation increases. This increment in solar radiation causes to increase in PV current from 25 A to 40 A and finally to 50 A. From the above power curve, we observed that the grid power decreases, inverter power increases and the load becomes constant, as shown in Figure 4.42.

4.4.4 Using nonlinear controller without filter

4.4.4.1 Assembled with loads, solar radiation, and without a battery system

The same simulation is carried out as in Section 4.4.1.1 by replacing the simple nonlinear controller of the inverter with the nonlinear controller without a filter. The dynamic responses with solar radiation of G = 800 W/m2 without filter are shown in Figure 4.43. Figure 4.44 shows the power curves confirm that the load is supplied at 5000 W at first entirely by the grid, then the solar panel provides 6000 W under sunny conditions. At the same time, it can also feed the grid up to 1000 W. We also observed a grid THD of 1.48%, shown in Figure 4.45, in a steady state.

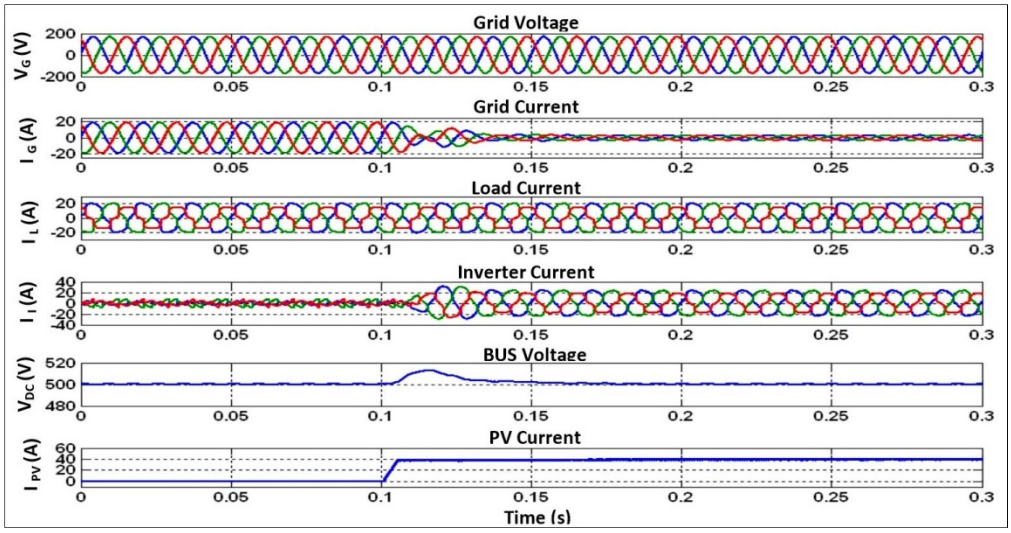

Figure 4.43 Dynamic response with solar radiation of G = 800 W/m2 without a filter.

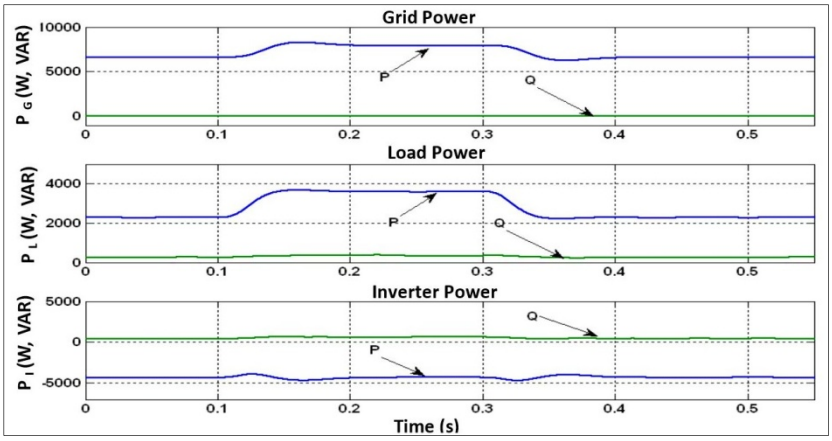

Figure 4.44 Power flow with solar radiation of G = 800 W/m2 without a filter.

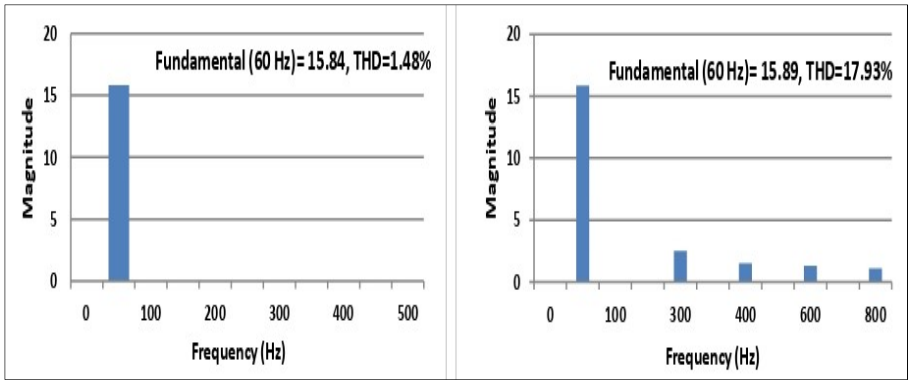

Figure 4.45 Harmonic spectrum of the grid and load current without a filter.

4.4.4.2 Assembled with loads, solar radiation, and without a battery system

The same simulation is carried out as in Section 4.4.1.2 by replacing the simple nonlinear controller of the inverter with the nonlinear controller without a filter. The dynamic responses with solar radiation of G = 800 W/m2 without filter are shown in Figure 4.46. The current in the inverter increases at t = 0.1 to 0.3 s because the battery discharges. The results show phase opposition between the current and the grid voltage, indicating that the grid receives power shown in Figure 4.47. Figure 4.48 shows the power curves confirming that the inverter is negative when the battery absorbs current and positive when the battery discharges the current.

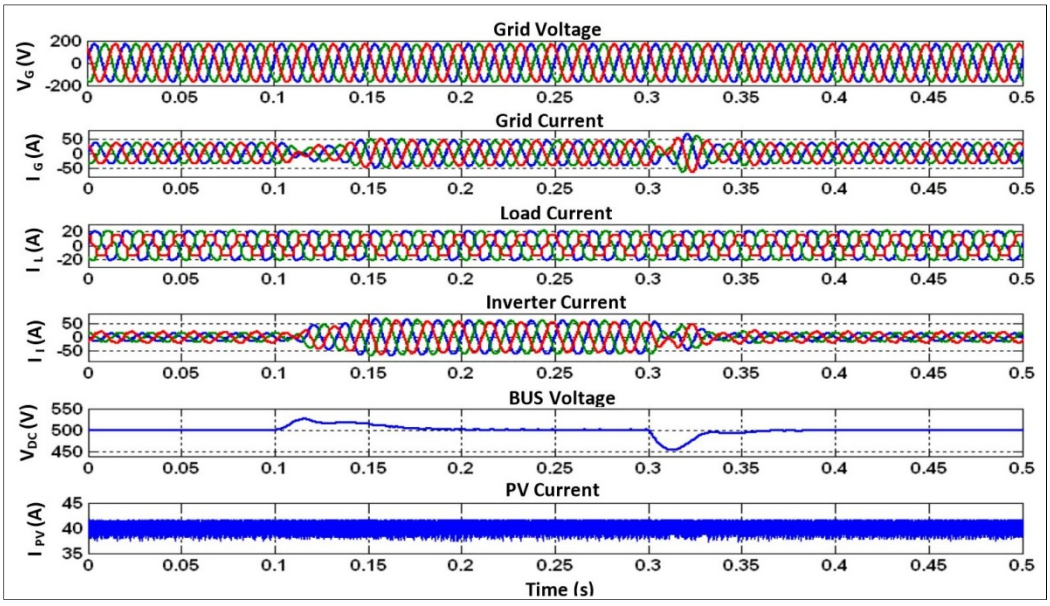

Figure 4.46 Dynamic state response with battery charge variation without a filter.

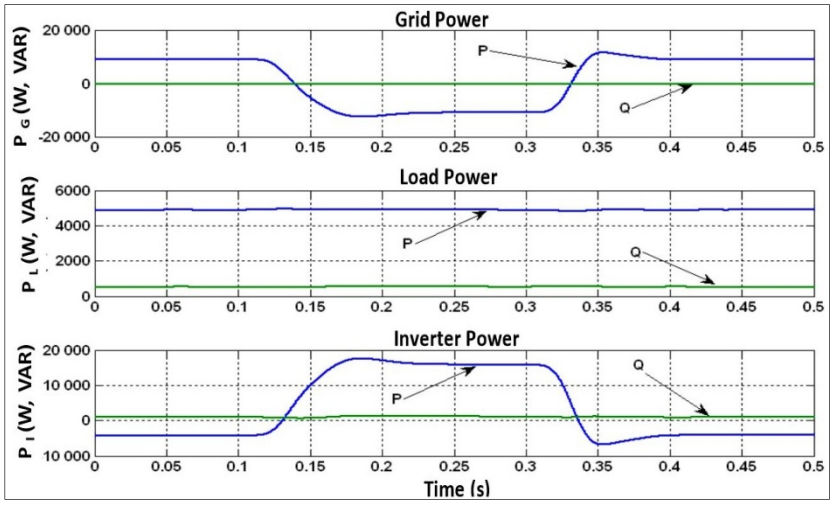

Figure 4.47 Dynamic state response with battery charge variation without a filter.

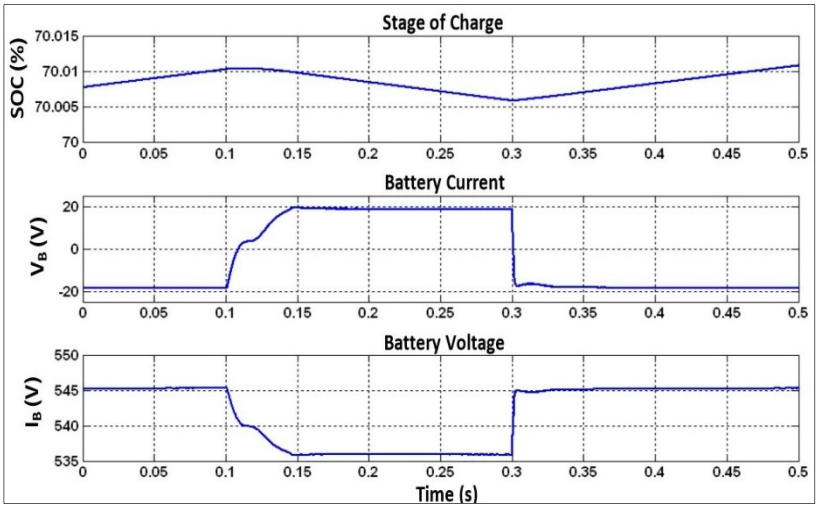

Figure 4.48 Battery state of charge using without a filter.

4.4.4.3 Assembled with solar radiation, battery charge, and variation of the loads

The same simulation is carried out as in Section 4.4.1.3 by replacing the simple nonlinear controller of the inverter with the nonlinear controller without a filter. Figure 4.49 shows the dynamic responses with solar radiation of G = 800 W/m2 without a filter. From the above power curve, we observed from Figure 4.50 that the PV and grid supply power to the load. When the load power increases at t = 0.1 s, the current in the grid increases due to the grid power. With solar radiation of G = 800 W/m2, the PV can't support the grid to supply the power to the load.

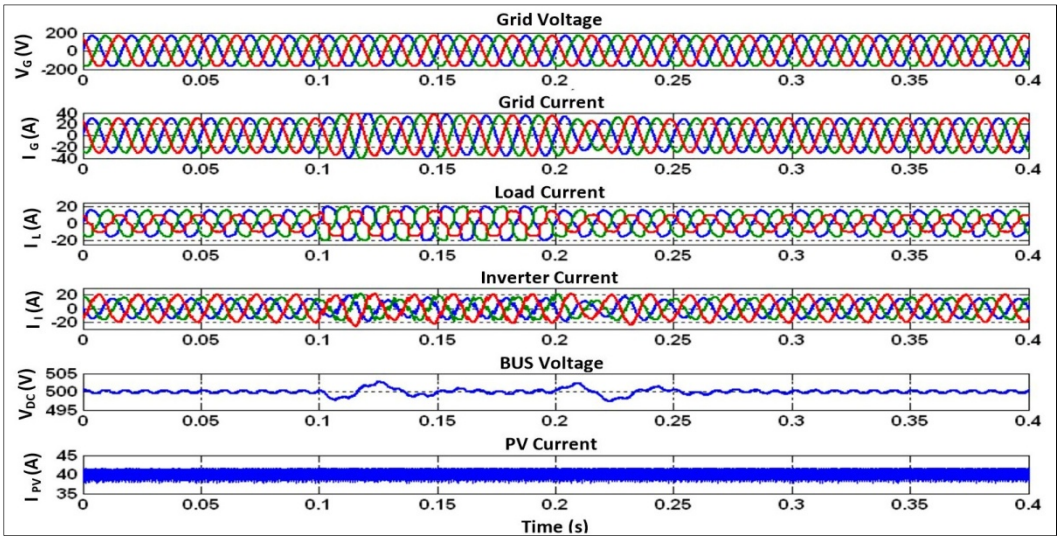

Figure 4.49 Dynamic response with load variation without a filter.

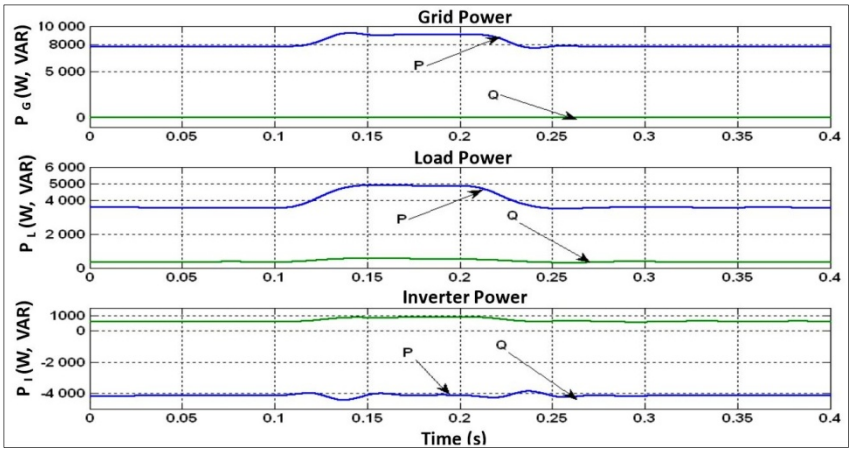

Figure 4.50 Power flow with load variation without a filter.

4.4.4.4 Assembled with battery charge, load, and with variation of the solar radiation

The same simulation is carried out as in Section 4.4.1.4 by replacing the simple nonlinear controller of the inverter with the nonlinear controller without a filter. The simulation results we obtained are shown as follows. Figure 4.51 shows that the grid current decreases when solar radiation increases. This increment in solar radiation causes to increase in PV current from 25 A to 40 A and finally to 50 A. From the above power curve, we observed from Figure 4.52 that the grid power decreases, inverter power increases, and the load becomes constant.

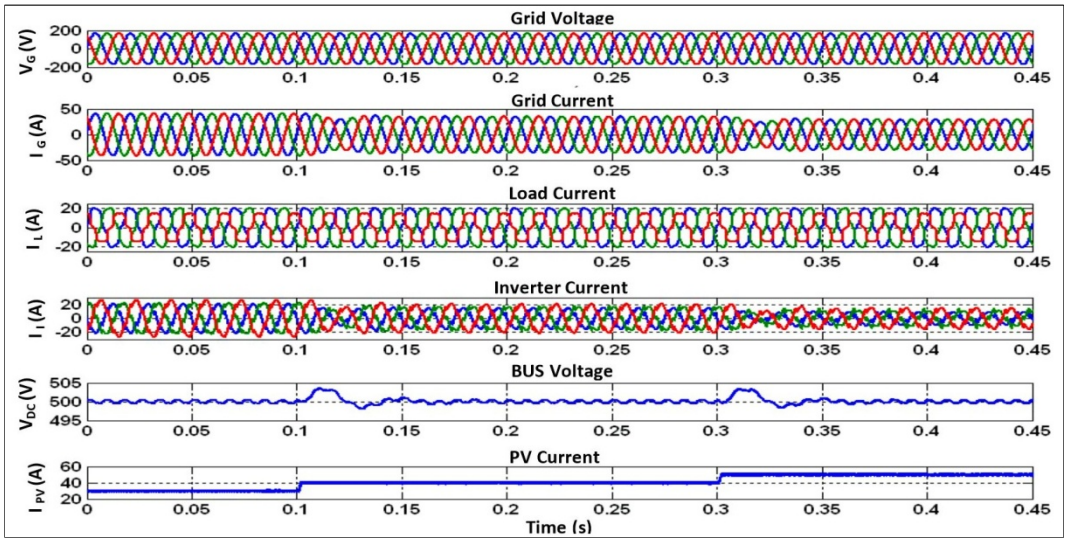

Figure 4.51 Dynamic responses with a variation of solar radiation without a filter.

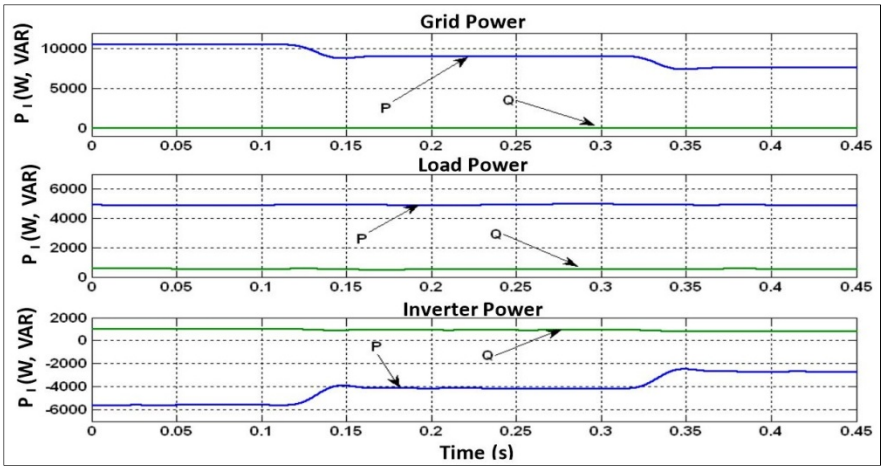

Figure 4.52 Power flow with a variation of solar radiation without a filter.

4.5 Comparison of nonlinear controllers with various filters

A final simulation is carried out to compare the performances of nonlinear controllers with various filters regarding the regulation of the DC bus. We simulate the overall system without the PV and battery for each controller, with a load variation from 4000 W to 5000 W between t = 0.1 s and 0.3 s. Figure 4.53 shows the result we obtained by grouping the curves for each of the controllers on the same figure:

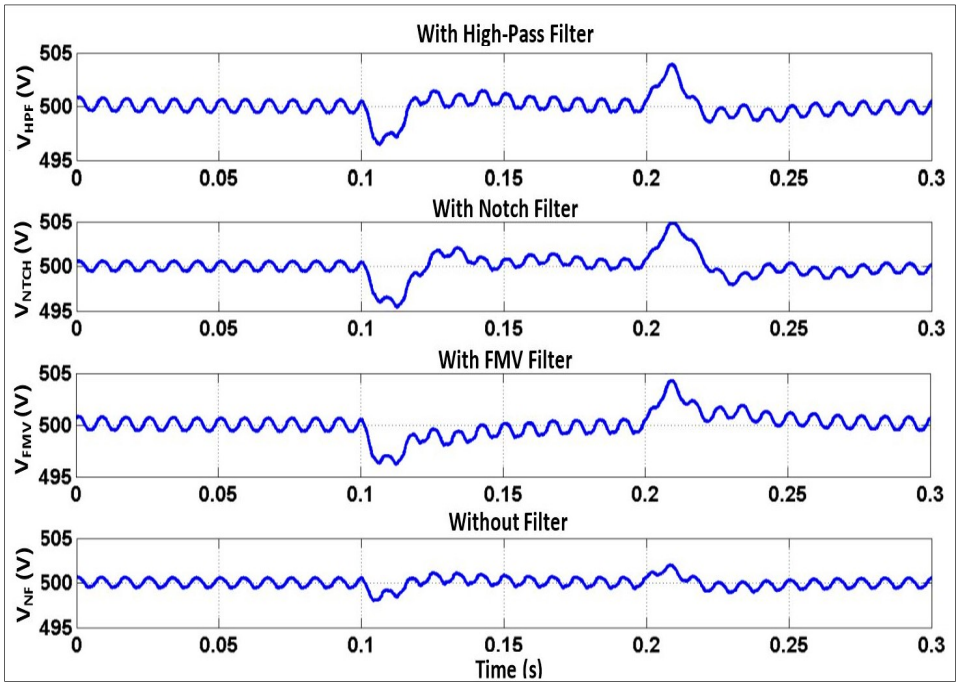

Figure 4.53 DC bus regulation with various controllers.

Finally, let us note that the nonlinear control without a filter obtains the best regulation, followed by the simple nonlinear control (high pass filter) and the control with a multi-variable filter. The nonlinear control with a Notch filter has the worst result. Table 4.2 summarizes the performance of the different simulations of the various controllers used for the inverter.

Table 4.2 Ranking of controllers according to their performance.

Types of Controllers	**Simple Nonlinear Controller**	**Nonlinear Controller with Multi-variable Filter**	**Nonlinear Controller with Notch Filter**	**Nonlinear Controller without filter**
THD of grid without the PV and Battery	1.43%	1.70%	1.61%	1.33%
V_{dc} Regulation Time with Load Variation	0.025 s	0.07 s	0.05 s	0.015 s
V_{dc} Exceeded with Load Variation	0.6%	0.8%	1%	0.2%

4.6 Conclusions

During this research, we presented a study on photovoltaic panels connection to the electrical grid and a load. The operation of a storage device was also inserted into the assembly, which was carried out via Matlab simulation. The comprehensive study of solar energy has been carried out with the interface of a step-up converter equipped with a PI regulator and the MPPT implemented by the P&O method. At first, we connected the photovoltaic system and its storage device to the grid with an unbalanced nonlinear load. The inverter, which delivers alternating voltages and currents from a direct source of electrical energy, will play the role of interface between the panel and the grid. The inverter acts as a filter and makes it possible to compensate for the currents that pollute the network. Then several controllers were studied, modeled, and simulated. First, we use a simple nonlinear control with a traditional high-pass filter. Then we replaced it with a multi-variable filter and a Notch filter in another simulation. Finally, we used a nonlinear control without a filter. During our simulations, we obtained the expected results, proving each controller's performance. Therefore, we can affirm that this global topology is an exciting alternative for using solar energy, mainly its simplicity, performance, and speed. It turns out that during our simulations, the filterless nonlinear control obtained the best performance. For economic considerations, the energy produced by the solar panel should be prioritized by the grid and not the battery. We use an intelligent MPPT to get the maximum power from the connected solar panels with different capacities. Finally, we observed that the filterless nonlinear control provides the best results for THD correction (1.33%), Vdc regulation time with load variation (0.015 s), and Vdc exceeded with load variation (0.2%). The controller with the notch filter has the worst results for THD correction (1.61%), Vdc regulation time with load variation (0.05 s), and Vdc exceeded with load variation (1%). Following the Vdc regulation times, we see that the controller without the filter has the fastest and the notch controller has the slowest performance. It is noted that the controller with the notch filter has the worst results for the overshoot of the Vdc, and the multi-variable filter has the poorest outcomes for the regulation speed of the Vdc (0.07 s) with the THD correction (1.70%). The simple nonlinear controller provides the THD correction (1.43%), Vdc regulation time with load variation (0.025 s), and Vdc exceeded with load variation (0.6%). Finally, the multi-variable filter is ranked fourth,

the Notch filter is third, the simple nonlinear controller is second, and the nonlinear controller without the filter is ranked first. In summary, the nonlinear controller without a filter is the best for the operation. Concerning the quality of the electrical grid, the controllers used for the inverter ensure that the harmonic distortion rate remains below 5%, complying with the IEEE519-1992 standard for grid quality. This indicates that the proposed system maintains the required power quality levels while integrating renewable energy sources. This research highlights the prioritization of energy produced by the solar panel for the grid rather than the battery, considering economic factors. This approach optimizes the utilization of solar energy and enhances the cost-effectiveness of the system.

To continue this research work, the proposed system and controllers can be implemented in a real-world setup to verify the performance and effectiveness of the studied approaches under practical conditions. This will provide more robust and reliable results; The study by comparing the performance of the proposed controllers can be expanded with other existing control strategies for photovoltaic systems; The efficiency, stability, and dynamic response of different controllers can be evaluated to identify potential improvements or alternative approaches; Parameter tunings or advanced control algorithms such as Model Predictive Control (MPC) or Adaptive Control can be considered to enhance the response, accuracy, and stability of the system under varying operating conditions; The reliability and resilience of the proposed system can be assessed in the face of various disturbances and uncertainties. By considering these recommendations, the research work can be extended to further enhance the understanding, performance, and applicability of photovoltaic systems connected to the electrical grid, ultimately contributing to the advancement and adoption of renewable energy technologies.

4.7 References

1. Ajabnoor, A.; Kwasinski, A. Photovoltaic Maximum Power Point Tracker for a Multiple-Input SEPIC Under Partial Shading Condition. In Proceedings of the 2022 IEEE 13th International Symposium on Power Electronics for Distributed Generation Systems (PEDG), Kiel, Germany, 26–29 June 2022; pp. 1–6.
2. Rahman, M.J.; Tafticht, T.; Doumbia, M.L. Power Stability and Frequency Control Techniques of DG for a High Penetration Wind-Based Energy Storage System Using Integral–Derivative Controller. *IEEE Can. J. Electr. Comput. Eng.* 2022, *45*, 232–241.
3. Rahman, M.J.; Tafticht, T.; Doumbia, M.L.; Mutombo, N.M.-A. Dynamic Stability of Wind Power Flow and Network Frequency for a High Penetration Wind-Based Energy Storage System Using Fuzzy Logic Controller. *Energies* 2021, *14*, 4111
4. Purevdorj, G.; Enkjargal, K. Ecological, economic and social aspects from the renewable energy and energy conservation. In Proceedings of the 2007 International Forum on Strategic Technology, Ulaanbaatar, Mongolia, 3–6 October 2007; pp. 20–23.
5. Bineeta, M.; Das, D. Multi-objective dynamic and static reconfiguration with optimized allocation of PV-DG and battery energy storage system. *Renew. Sustain. Energy Rev.* 2020, *124*, 109777.
6. Kermadi, M.; Salam, Z.; Ahmed, J.; Berkouk, E.M. A High-Performance Global Maximum Power Point Tracker of PV System for Rapidly Changing Partial Shading Conditions. *IEEE Trans. Ind. Electron.* 2021, *68*, 2236–2245.
7. Hernández, J.C.; Sanchez-Sutil, F.; Muñoz-Rodríguez, F.J. Design criteria for the optimal sizing of a hybrid energy storage system in PV household-prosumers to maximize self-consumption and self-sufficiency. *Energy* 2019, *186*, 115827.
8. Li, X.; Wang, L.; Yan, N.; Ma, R. Cooperative Dispatch of Distributed Energy Storage in Distribution Network With PV Generation Systems. *IEEE Trans. Appl. Supercond.* 2021, *31*, 0604304.
9. Alivarani, M.; Nayak, B.; Das, P.; Mohanty, K.B. A review on MPPT techniques of PV system under partial shading condition. *Renew. Sustain. Energy Rev.* 2017, *80*, 854–867.
10. Winston, D.; Prince, S.; Kumaravel, B.; Kumar, P.; Devakirubakaran, S. Performance improvement of solar PV array topologies during various partial shading conditions. *Solar Energy* 2020, *196*, 228–242.
11. Bidram, A.; Davoudi, A.; Balog, R.S. Control and Circuit Techniques to Mitigate Partial Shading Effects in Photovoltaic Arrays. *IEEE J. Photovolt.* 2012, *2*, 532–546.
12. Teshome, D.F.; Lee, C.H.; Lin, Y.W.; Lian, K.L. A Modified Firefly Algorithm for Photovoltaic Maximum Power Point Tracking Control Under Partial Shading. *IEEE J. Emerg. Sel. Top. Power Electron.* 2017, *5*, 661–671.
13. Zengin, S.; Boztepe, M. Modified dual active bridge photovoltaic inverter for solid state transformer applications. In Proceedings of the 2014 International Symposium on

Fundamentals of Electrical Engineering (ISFEE), Bucharest, Romania, 28–29 November 2014; pp. 1–4.

14. Ishaque, K.; Salam, Z. A Review of Maximum Power Point Tracking Techniques of PV System for Uniform Insolation and Partial Shading Condition. *Renew. Sustain. Energy Rev.* 2013, *19*, 475–488.
15. Adam, G.P.; Alajmi, B.; Ahmed, K.H.; Finney, S.J.; Williams, B.W. New flying capacitor multilevel converter. In Proceedings of the 2011 IEEE International Symposium on Industrial Electronics, Gdansk, Poland, 27–30 June 2011; pp. 335–339.
16. Roberts, M.B.; Bruce, A.; MacGill, I. Impact of shared battery energy storage systems on photovoltaic self-consumption and electricity bills in apartment buildings. *Appl. Energy* 2019, *245*, 78–95.
17. Sahu, H.S.; Nayak, S.K.; Mishra, S. Maximizing the Power Generation of a Partially Shaded PV Array. *IEEE J. Emerg. Sel. Top. Power Electron.* 2016, *4*, 626–637.
18. Lin, H.; Veda, S.S.; Shukla, S.S.; Mili, L.; Thorp, J. GECO: Global Event-Driven Co-Simulation Framework for Interconnected Power System and Communication Network. *IEEE Trans. Smart Grid* 2012, *3*, 1444–1456.
19. Okan, B.; Özkaya, B. Analysis and comparison of different PV array configurations under partial shading conditions. *Solar Energy* 2018, *160*, 336–343.
20. Wang, Y.; Lin, X.; Kim, Y.; Chang, N.; Pedram, M. Architecture and Control Algorithms for Combating Partial Shading in Photovoltaic Systems. *IEEE Trans. Comput.-Aided Des. Integr. Circuits Syst.* 2014, *33*, 917–930.
21. Teo, J.C.; Tan, R.H.; Mok, V.H.; Ramachandaramurthy, V.K.; Tan, C. Impact of partial shading on the PV characteristics and the maximum power of a photovoltaic string. *Energies* 2018, *11*, 1860.
22. Rahmann, C.; Vittal, V.; Ascui, J.; Haas, J. Mitigation Control Against Partial Shading Effects in Large-Scale PV Power Plants. *IEEE Trans. Sustain. Energy* 2016, *7*, 173–180.
23. Xiao, W.; El Moursi, M.S.; Khan, O.; Infield, D. Review of grid-tied converter topologies used in photovoltaic systems. *IET Renew. Power Gener.* 2016, *10*, 1543–1551.
24. Tafticht, T.; Tchakala, M.; Rahman, M.J. GMPPT Approach for Photovoltaic Systems under Partial Shading Conditions Using Genetic Algorithm. *Int. J. Power Electron. Drive Syst.* 2022, *13*, 1238–1245.
25. Salem, R.; Mendalek, N.; Al-Haddad, K. Experimental design of a nonlinear control technique for three-phase shunt active power filter. *IEEE Trans. Ind. Electron.* 2010, *57*, 3364–3375.
26. Ahmed, B.; Hamadi, A.; Ndtoungou, A.; Javadi, A.; Rahmani, S.; Al-Haddad, K. Modified droop control to improve performances of two single-phase parallel inverters. In Proceedings of the IECON 2017-43rd Annual Conference of the IEEE Industrial

Electronics Society, Beijing, China, 29 October–1 November 2017; IEEE: New York City, NY, USA, 2017; pp. 6470–6475.

27. Ali, E.; Cingoz, F.; Sozer, Y. Smart loads management using droop-based control in integrated microgrid systems. *IEEE J. Emerg. Sel. Top. Power Electron.* 2017, *5*, 1142–1153.
28. Egwebe, M.; Fazeli, M.; Igic, P.; Holland, P.M. Implementation and Stability Study of Dynamic Droop in Islanded Microgrids. *IEEE Trans. Energy Convers.* 2016, *31*, 821–832.
29. Abdelsalam, K.; Massoud, A.M.; Ahmed, S.; Enjeti, P.N. High-Performance Adaptive Perturb and Observe MPPT Technique for Photovoltaic-Based Microgrids. *IEEE Trans. Power Electron.* 2011, *26*, 1010–1021.
30. Banu, I.V.; Istrate, M. Comparative Analysis of the Perturb-and-Observe and Incremental Conductance MPPT Methods. In Proceedings of the 2013 8th International Symposium on Advanced Topics in Electrical Engineering (ATEE), Bucharest, Romania, 23–25 May 2013.
31. Park, C.-Y.; Hong, S.-H.; Lim, S.-C.; Song, B.-S.; Park, S.-W.; Huh, J.-H.; Kim, J.-C. Inverter Efficiency Analysis Model Based on Solar Power Estimation Using Solar Radiation. *Processes* 2020, *8*, 1225.
32. Blanco, H.; Faaij, A. A review at the role of storage in energy systems with a focus on Power to Gas and long-term storage. *Renew. Sustain. Energy Rev.* 2018, *81 Pt 1*, 1049–1086.
33. Du, Y.; Lu, D.D.-C.; James, G.; Cornforth, D.J. Modeling and analysis of current harmonic distortion from grid connected PV inverters under different operating conditions. *Solar Energy* 2013, *94*, 182–194.
34. Al-Shetwi, A.Q.; Hannan, M.A.; Jern, K.P.; Alkahtani, A.A.; PG Abas, A.E. Power Quality Assessment of Grid-Connected PV System in Compliance with the Recent Integration Requirements. *Electronics* 2020, *9*, 366.
35. Rocchetta, R. Enhancing the resilience of critical infrastructures: Statistical analysis of power grid spectral clustering and post-contingency vulnerability metrics. *Renew. Sustain. Energy Rev.* 2022, *159*, 112185.
36. Chim, C.S.; Neelakantan, P.; Yoong, H.P.; Teo, K.T. Fuzzy Logic Based MPPT for Photovoltaic Modules Influenced by Solar Irradiation and Cell Temperature. In Proceedings of the 13th International UkSim Conference on Modelling and Simulation, Cambridge, UK, 30 March–1 April 2011; pp. 376–381.
37. Karimi-Ghartemani, M.; Mokhtari, H. Extraction of Harmonics and Reactive Current for Power Quality Enhancement. In Proceedings of the 2006 IEEE International Symposium on Industrial Electronics, Montreal, QC, Canada, 9–13 July 2006; pp. 1673–1678.

38. Chaoui, A.; Gaubert, J.-P.; Bouafia, A. Experimental Validation of Active Power Filtering with a Simple Robust Control. *Electr. Power Compon. Syst.* 2016, *44*, 1163–1176

39. Rampradesh, T.; Rajan, C.C.A. Performance assessment of NMPC based MPPT controller and extended Kalman filter for a Wind/PV hybrid system. In Proceedings of the 2021 Fourth International Conference on Electrical, Computer and Communication Technologies (ICECCT), Erode, India, 15–17 September 2021; pp. 1–4.

CHAPTER 5

POWER CONVERTERS ANALYZED IN ENERGY STORAGE SYSTEMS TO ENHANCE THE PERFORMANCE OF THE SMART GRID APPLICATION

Md Jahidur Rahman[1], Tahar Tafticht[1], Mamadou Lamine Doumbia[2]

[1] Department of Engineering, Université du Québec en Abitibi-Témiscamingue, Rouyn-Noranda, Canada
[2] Department of Electrical and Computer Engineering, Université du Québec à Trois-Rivières, Trois-Rivières, Canada

Paper published in *International Journal of Power Electronics and Drive Systems,* March 2024

Abstract

This paper implements and compares the existing power supply converters for an energy storage system to determine the best suited for the smart grid application. A survey of different DC-DC converters is carried out to analyze the battery's overall performance. The main objective is to identify this application's most appropriate energy storage device. The advantages of this technology have high efficiency and reliability, which can connect various energy sources and reduce conduction losses in the power converters. Through the converter control, reference currents are imposed to charge the battery. The battery nominal voltage needs to change to see which type of converter is the most suitable and robust. Simulation results show that the operating ranges of boost-buck, buck-boost, and buck-boost converters with negative output voltage enhance the efficiency of battery and renewable energy sources and compare the DC converters to know the functional voltage for the energy storage system. The power converter's efficiency and control facility will allow us to link the energy storage system with the power grid. The overall installation is established using Matlab/Simulink software.

Keywords: storage system, DC converters, smart grid, battery performance, conduction losses

5.1 Introduction

The techniques for designing and producing power converters are mainly based on the association and assembly of discrete components. Thus a converter can be seen as a set of passive and active components interconnected to perform the desired function for a given specification. Each component must then be chosen according to the constraints that will be imposed on it by these specifications. This approach, therefore, requires a specific study for each function to be performed, which will have several consequences [1]. Each new application corresponds to a new converter, which systematically reviews and redesigns new conversion structures and proves costly in terms of time and money. Eventually, this can lead to specific technological developments that also affect the cost of developing power converter solutions [2] [3]. Regulating the conversion functions and the complex coupled electrical, magnetic, thermal, and mechanical phenomena involved in the operation of a power converter requires an excellent knowledge of power electronics reserved for specialists in this field only. Moreover, with the current integration process, this point becomes more critical. The three preceding points induce significant development times and costs, thus limiting the generalization of a power converter with high conversion efficiency in consumer and industrial applications [4] [5]. This leads to reducing the penetration of power converters in mass applications, which would reduce our consumers' energy bills.

Energy sources in local settings are excluded from use in low or medium-power applications, including micro-grids and industrial areas situated at higher power ranges[6] [7]. These regionally distributed energy sources present opportunities for enhancing load balancing among various power supply modules. Their operation relies primarily on the communication channel, resulting in a heightened risk of failures, reduced load regulation, and intricate implementation, all of which contribute to elevated manufacturing and maintenance expenses. Nonetheless, the progress of photovoltaic systems has drawn attention to numerous factors that have a direct impact on the performance of this technology [8] [9]. The power converters and storage devices (battery) are the disciplines in which we seek to design and analyze an electrical system ensuring the transfer of power from an energy source to a receiver and guaranteeing the highest possible energy efficiency while limiting losses as much as possible [9] [10]. The power converter is a device composed of electronically

controlled switches. This commute, i.e., oscillates between an on-state and an off-state. The frequency of these switching is generally relatively high, of the order of a few kilo-Hertz, or even a few tens of kilo-Hertz. Such a converter is commonly called a static converter because it does not include any moving mechanical component. Static converters are used to shape an electrical wave. They allow, for example, to modify the voltage or current waveform to adapt it to the receiver's needs. The power dissipated during the transfer is a loss due to the imperfections of its components which make up the converters [9].

Many research has been done on a multiple-power converter based on distributed power systems in other systems to handle multiple input sources. Most system configurations adopted from previous research rely solely on localized converters with extensive communication capabilities or on a decision agent mechanism technique, described in [11] [12]. Multi-converter systems designed for communication and battery applications exhibit exceptional load regulation and robust load-sharing capabilities [13] [14]. However, this particular system is specialized and tailored for specific tasks, rendering it unsuitable for the all-encompassing performance requirements of smart energy systems. The universal input converter emerges as an optimal choice for distributed generation and smart grid infrastructures, as it can seamlessly integrate and process energy sources and storage into a unified global unit. The universal keying technology topology boasts advantages such as cost-effectiveness, higher power density, and simplified management.

Extensive research conducted over the past decade has yielded a wide array of topologies for multi-input converters. Broadly, multi-input converters can be categorized into two groups: Magnetic Coupling Converters (MCC) and Electrically Coupled Converters (ECC). [15] pioneered the initial literature on single-output topologies after [16] [17] reached a consensus on an idea that applies to other topologies and multi-input versions. The tri-port converter employs various power flow control strategies [18] [5]. Nevertheless, the magnetic energy transfer method is sensitive to circuit parameters and may lead to potentially inaccurate performance, making current disposal capacity a critical consideration when interfacing with renewable energy sources like fuel cells. Alternatively, energy transfer methods not only focus on current regulation but primarily emphasize power flow control. MCCs offer higher power density and flexible output voltage levels, facilitated by

strong and soft switching techniques. However, MCC circuit devices entail a complex load-sharing implementation compared to other energy sources and storage elements. On the other hand, ECCs are straightforward and typically operate with less than 10KW of power [19]. ECCs are often associated with non-isolated converter topologies, such as Buck, Boost, and Buck-Boost. Their power flow control is relatively simple, and the peripheral circuitry is generally uncomplicated. ECC systems feature less flexible output voltage, a modular structure, and lower manufacturing costs, rendering them advantageous in various applications like automotive and communication systems.

In this context, we explored various implementations of multi-input topologies. [20] grouped diverse sources together to achieve high output voltage and employed a time-domain switching scheme for these channels with multiple inputs, offering a multiplex or a combination of multiplexing and simultaneous switching topology based on the boosted cell with stack input voltage. [21] introduced a step-down topology based on the multi-input ECC code, operating with a time-multiplexed switching model. [8] investigated sources with varying input levels and proposed a topology featuring Mix-Boost and Buck-Boost switching cells as a front-end application for microgrid conversion. The combination of Buck and Boost switching cells is integrated into a single unit to share power, with a bank of battery sources included for the negative output of the Buck-Boost switching cells. According to [22], the use of mixed switch mode and charge pump topology results in a multi-input ECC with all subsystems having a common point, enabling bi-directional power flow due to inductive coupling. This approach provides several benefits, such as the ability to transmit power individually or simultaneously from PV and wind turbines directly to the grid, the capacity to implement Maximum Power Point Tracking (MPPT) for solar systems and wind power, and an extended variable input voltage range for renewable energy power systems [23] [24]. [2] also concurred that similar Boost cells could constitute a multi-input converter system suitable for immobilizer systems, mobile applications, and switch cells capable of supplying power to various sources. [25] approached to operate a Buck-Boost converter as a bidirectional regulable power bridge between low and high-voltage buses. As a result, the battery's charge can be utilized and handle overload situations. A flexible and sustainable power generation scheme is proposed in [26] using flexible fuzzy goal

programming to increase the capacity of renewable sources and reduce emission levels on Earth. The optimal cost solution and flexibility of power demand are achieved by switching to renewable energy sources.

The DC–DC converters are presented in most applications of low, medium, and high voltage or current. Researchers in every sector are launching new research technology aiming to improve and solve many issues related to power converters to enhance new technology associated with challenges and requirements that have been brought recently in the power converters applications. Power electronics and converters always help to solve problems of industrial and residential power losses and support energy development, opening the gap for new opportunities and improving the quality of power supply. Thus, it is a reality that power converters and their technologies can be a major considerable research topic in power system engineering. In this paper, we present the study of the different types of existing converters and batteries to choose the most suitable for the smart grid system and can solve the problem of intermittency of the operation of renewable energy sources. We compared the different operating ranges of Boost-Buck, Buck-Boost, and Buck-Boost with negative output voltage using Matlab simulation. Then we studied the DC-DC converters capable of feeding the battery storage. Each converter's control strategy is determined and chosen for the best topology.

The primary contributions of this paper can be summarized as:

- Devising a control scheme for switched-mode converters aimed at facilitating rapid energy storage and delivery to batteries while meeting desired energy levels;
- Analyzing the operating ranges of Boost-Buck, Buck-Boost, and Buck-Boost ($-V_{out}$) converters to enhance the efficiency of battery and renewable energy sources;
- Comparing the DC converters to know the functional voltage for the energy storage system.

The rest of the paper is sorted as follows: Section 5.2 studies the converters used in an energy storage system. Section 5.3 describes the operational technique of different DC converters. Section 5.4 presents the simulation results of the proposed research work. Section 5.5

summarizes the functional voltage of the converters for the energy storage system, and Section 5.6 concludes the paper.

5.2 Study of converters used in energy storage systems

DC converters play a vital role in energy storage systems (ESS) by facilitating efficient power conversion and bidirectional energy flow between storage devices and the grid. As the demand for renewable energy integration and grid stability increases, the importance of energy storage systems and their associated DC converters becomes more significant. Energy storage systems have gained prominence as a crucial element in modern power systems due to their ability to mitigate renewable energy intermittency, support grid stabilization, and enhance overall system efficiency. DC converters serve as an interface between energy storage devices (e.g., batteries, supercapacitors) and the AC grid, allowing for efficient energy conversion and optimal power management. They are essential for converting the DC output of energy storage devices into usable AC power for the grid or vice versa. These converters enable bidirectional power flow, allowing energy to be stored in the system when there is excess generation or to be released to the grid when demand exceeds supply. A study has been done to compare the existing power supply converters for an energy storage system to determine the best suited for our application. This technology has many advantages [27], such as high efficiency and reliability, connecting various energy sources, and reducing conduction losses in power switches. The main disadvantages of this technology are Magnetic losses, eddy current losses, and losses in passive components. Despite its losses, switched-mode power supplies have an efficiency of between 65% and 90%, while linear power supplies reach between 35% and 55% [28]. Through the converter control, reference currents are imposed to charge the battery. We will also change the battery's nominal voltage to see which type of converter is the most suitable and robust.

5.3 Operational technique of different DC converters

5.3.1 Operational equations of the boost-buck converter

The DC-DC converter utilized in this system functions as a switching power supply capable of both stepping up and stepping down the output voltage. This converter is integrated with a

Li-ion battery. The battery model is linked to a DC voltage source through a series resistor. The equivalent circuit and the configuration of the bidirectional boost-buck converter can be observed in Figure 5.1. In its operation, the converter shifts into Boost mode for discharging and switches to Buck mode when charging the battery.

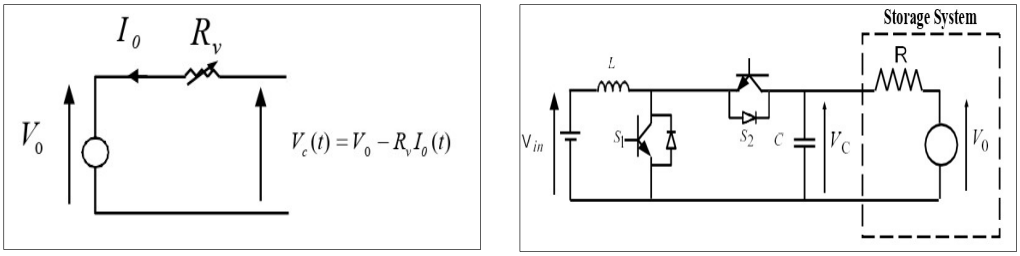

Figure 5.1. Equivalent circuit diagram of a battery with bidirectional boost-buck converter

The precise formula for $V_c(t)$ is:

$$V_C(t) = A \exp(-B \int_0^t I_0 dt) + V_0 - R_V I_0 - K \frac{Q}{Q - \int_0^t I_0 dt} \quad 5.1$$

Where V_0 is the nominal voltage, I_0 is the nominal current and K is the bias voltage of the battery. The following relationship represents the control source of voltage:

$$V_C = A \exp(-B \int_0^t I_0 dt) + V_0 \quad 5.2$$

Where A is the exponential voltage, and B is the exponential capacity of the battery.

And for the variable resistor

$$R_V = \mathrm{R} = R_i + k \frac{Q}{Q - \int_0^t I_0 dt} \quad 5.3$$

Where R_i is the number of resistors and Q is the capacity of the battery. We will now establish the equations with the fixed resistor R to extract the control law [29]. This converter comprises switches and diodes, each of which can be on or off. When the switch is on, the voltage V_{in} is entire across the inductor.

When S_1 and S_2 are on:

$$V_{in} = L \frac{dI_L}{dt} \quad 5.4$$

$$\frac{1}{L} V_{in} = \frac{dI_L}{dt} \quad 5.5$$

$$\frac{1}{R}(v_c - V_0) - C \frac{d_{v_c}}{dt} = 0 \quad 5.6$$

$$\frac{d_{v_c}}{dt} = \frac{1}{RC}(v_c - V_0) \quad 5.7$$

Then, we get the state model:

$$XA_1 + UB_1 = X \tag{5.8}$$

With

$$U = \begin{bmatrix} V_{in} \\ V_0 \end{bmatrix} \tag{5.9}$$

$$X = \begin{bmatrix} I_L \\ v_c \end{bmatrix} \tag{5.10}$$

This allows us to establish the following matrix:

$$\begin{bmatrix} \frac{dI_L}{dt} \\ \frac{d_{v_c}}{dt} \end{bmatrix} = \begin{bmatrix} V_{in} \\ V_0 \end{bmatrix} \begin{bmatrix} \frac{1}{L} & 0 \\ 0 & -\frac{1}{RC} \end{bmatrix} + \begin{bmatrix} I_L \\ v_c \end{bmatrix} \begin{bmatrix} 0 & 0 \\ 0 & \frac{1}{RC} \end{bmatrix} \tag{5.11}$$

When S_1 and S_2 are closed, the current flows through the circuit shown in Figure 5.2.

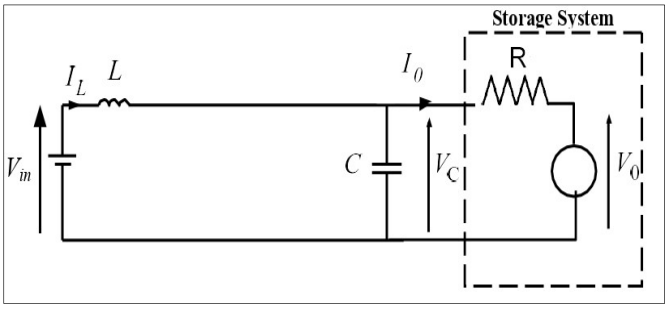

Figure 5.2 Diagram of the boost-buck converter when the switch is blocked

When S is blocked and D on:

$$V_{in} = v_c + L \frac{dI_L}{dt} \tag{5.12}$$

$$\frac{1}{L} V_{in} - \frac{1}{L} v_c = \frac{dI_L}{dt} \tag{5.13}$$

$$\frac{1}{R}(v_c - V_0) + C \frac{d_{v_c}}{dt} = I_L \tag{5.14}$$

$$\frac{1}{RC}(V_0 - v_c) + \frac{1}{C} I_L = \frac{d_{v_c}}{dt} \tag{5.15}$$

Then we get the state model:

$$XA_2 + UB_2 = X \tag{5.16}$$

This allows us to establish the following matrix:

$$\begin{bmatrix} \frac{dI_L}{dt} \\ \frac{d_{v_c}}{dt} \end{bmatrix} = \begin{bmatrix} V_{in} \\ V_0 \end{bmatrix} \begin{bmatrix} \frac{1}{L} & 0 \\ 0 & \frac{1}{RC} \end{bmatrix} + \begin{bmatrix} I_L \\ v_c \end{bmatrix} \begin{bmatrix} 0 & -\frac{1}{L} \\ \frac{1}{C} & -\frac{1}{RC} \end{bmatrix} \tag{5.17}$$

The following equality is used to determine the mean of the state model:

$$XA + UB = \dot{X} \tag{5.18}$$

As well:

$$A = d.A_1 + (1-d)A_2 \text{ And } B = d.B_1 + (1-d)B_2 \tag{5.19}$$

Where *d* is the duty cycle of the converter. We use the two matrices previously determined to obtain A and B:

$$A = (1-d)\begin{bmatrix} 0 & -\frac{1}{L} \\ \frac{1}{C} & -\frac{1}{RC} \end{bmatrix} + d\begin{bmatrix} 0 & 0 \\ 0 & \frac{1}{RC} \end{bmatrix} \tag{5.20}$$

And:

$$B = (1-d)\begin{bmatrix} \frac{1}{L} & 0 \\ 0 & \frac{1}{RC} \end{bmatrix} + d\begin{bmatrix} \frac{1}{L} & 0 \\ 0 & -\frac{1}{RC} \end{bmatrix} \tag{5.21}$$

Therefore we obtain:

$$A = \begin{bmatrix} 0 & -\frac{(1-d)}{L} \\ \frac{(1-d)}{C} & -\frac{1}{RC} \end{bmatrix} \tag{5.22}$$

And:

$$B = \begin{bmatrix} \frac{1}{L} & 0 \\ 0 & \frac{1}{RC} \end{bmatrix} \tag{5.23}$$

This can be written as:

$$V_{in} - (1-d)v_c = L\frac{dI_L}{dt} \tag{5.24}$$

$$\frac{1}{RC}V_0 + \frac{1-d}{L}I_L - \frac{1}{RC}V_C = C\frac{d_{v_c}}{dt} \tag{5.25}$$

We will only focus on current regulations so we will use the dynamic current equation:

$$V_{in} - (1-d)v_c = L\frac{dI_L}{dt} \tag{5.26}$$

To maintain current regulation, a proportional-integral (PI) controller is employed. The new input, denoted as *u* and representing the regulator's output, is defined as follows:

$$u = L\frac{dI_L}{dt} \tag{5.27}$$

By employing the Laplace transform, the following expression is derived:

$$u = S.L.I_L \tag{5.28}$$

Consider *G* as the open-loop current transfer function, defined as follows:

$$G = \frac{1}{SL} = \frac{I_L}{u} \tag{5.29}$$

The controller will produce the boost command based on the signal representing the difference between the setpoint I_{Lref} and the inductor current I_L. The transfer function of the controller is expressed as:

$$Cs = \frac{K_i}{S} + K \tag{5.30}$$

The transfer function in the closed-loop system of the controller linked with the PV system is defined as:

$$\frac{I_{PV}}{I_{PV}^*} = \frac{\frac{K_i + K_P S}{L}}{\frac{K_i}{L} + S^2 + S\frac{K_P + R_C}{L}} = \frac{\frac{K_i + K_P S}{L}}{\omega_i^2 + S^2 + 2S\omega_i\zeta} \tag{5.31}$$

In this context, I_{PV} stands for the current error, while I^*_{PV} represents the reference current for the PV system. This process facilitates the identification of the coefficients *Kp* and *Ki*:

$$K_P = 2L\omega_i\xi - R_c \tag{5.32}$$

And:

$$K_i = L\omega_i^2 \tag{5.33}$$

The control law is given by:

$$L\frac{dI_L}{dt} = V_{in} - (1-d)v_c = u \tag{5.34}$$

$$d = \frac{u - V_{in}}{v_c} + 1 \tag{5.35}$$

The PWM modulation method is employed for producing trigger pulses to manage the converter switch. The control schematic of the Boost-Buck converter is depicted in Figure 5.3. Through the utilization of the controlled voltage source *Vin*, the Boost-Buck converter is controlled by comparing the real-time current with the reference current, which can assume values of 10A, -10A, -20A, and 20A. The battery undergoes discharging when the reference current is negative and charging when the reference current is positive. Four simulations were carried out with this converter. For each simulation, the nominal voltage of the Lithium Ion battery used in the Matlab software, with the modified value V_{bat} =250V, V_{bat} =350V, V_{bat} =500V, and V_{bat} =650V. The input voltage V_{in} is fixed at 500V. The components of the boost-buck converter have the value of L=10mH and C=4500µF.

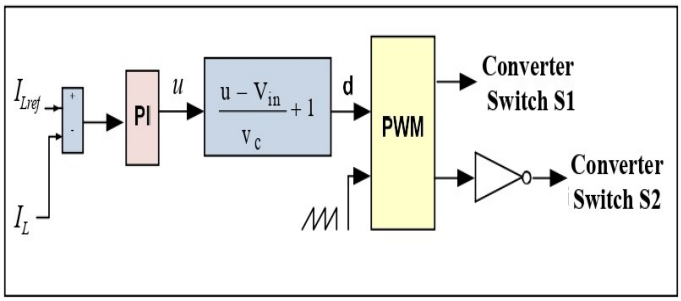

Figure 5.3 The control scheme of the boost-buck converter

5.3.2 Operational equations of the buck-boost converter

The DC-DC converter in use serves as a bidirectional switching power supply, capable of both stepping down and stepping up the output voltage as needed. This converter is paired with a Li-ion battery, with the battery model connected to a DC voltage source via a series resistor. Figure 5.4 provides a visual representation of the equivalent circuit and the configuration of the bidirectional buck-boost converter. In its operational modes, the converter charges the battery in buck mode and discharges it in boost mode.

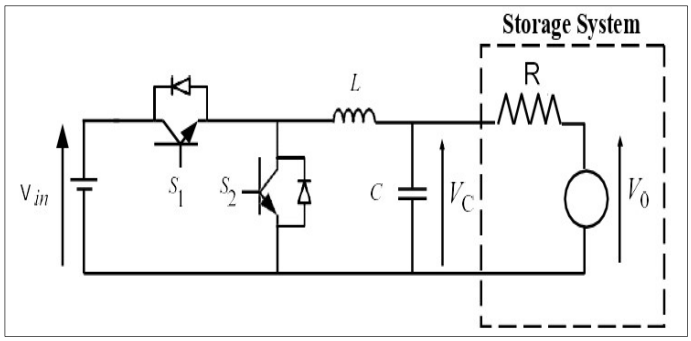

Figure 5.4 Circuit diagram of the buck-boost converter

The method employed here is PWM modulation, which generates the trigger pulses to manage the converter switch. Figure 5.5 illustrates the control diagram of the buck-boost converter. Utilizing the controlled voltage source V_{in}, the buck-boost converter is adjusted by comparing the real-time current with the reference current, which can assume values of 10A, -10A, -20A, and 20A. Charging occurs when the reference current is positive while discharging takes place when the reference current is negative.. Four simulations were carried out with this converter. For each simulation, the nominal voltage of the Lithium Ion battery used in the Matlab software, with the modified value V_{bat} =250V, V_{bat} =350V, V_{bat}

=500V, and V_{bat} =650V. The input voltage V_{in} is fixed at 500V. The components of the buck-boost converter have the values of L=10mH and C=4500µF.

The control law of the buck-boost converter using equation (5.35) is given by:

$$d = 1 - \frac{-u+V_{in}}{v_c} \qquad 5.36$$

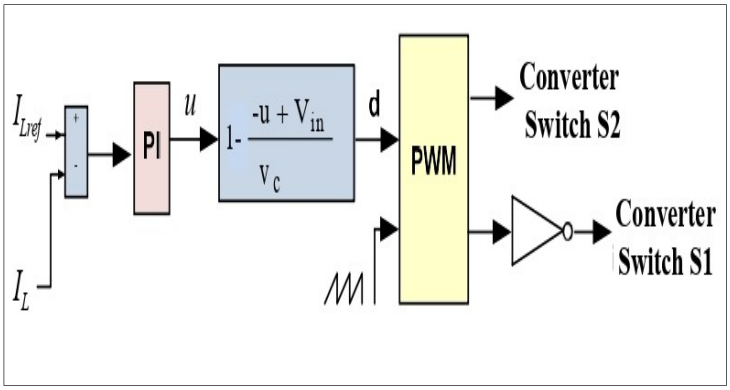

Figure 5.5 The control scheme of the buck-boost converter

5.3.3 Operational equations of the buck-boost converter with negative output voltage

The general topology of the Buck-Boost converter with negative output voltage is shown in Figure 5.6. Here, we used the control law (equation 5.36) previously analyzed for the buck-boost converter.

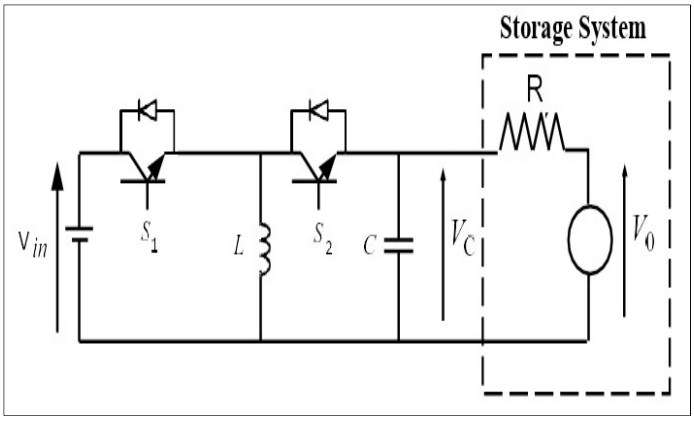

Figure 5.6 Circuit diagram of the buck-boost converter with negative output voltage

5.4 Simulation results

5.4.1 Simulation results using boost-buck converter

The simulation results show that the Boost-Buck converter cannot charge or discharge the battery at a nominal battery voltage of 250V and 350V shown in Figure 5.7 (a), (b), and have the capability to charge or discharge the battery at a nominal battery voltage of 500V and 650V shown in Figure 5.7 (c), (d).

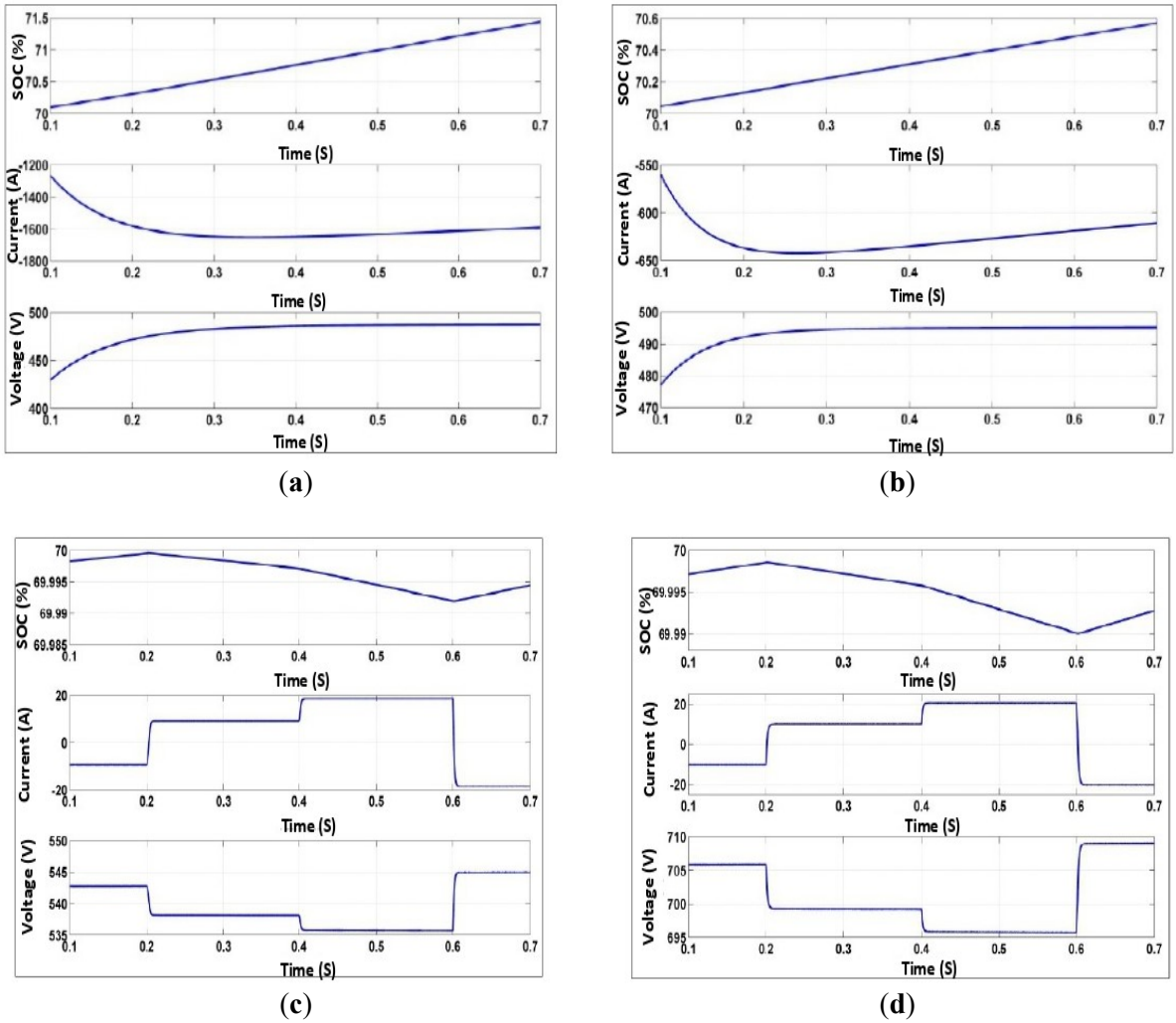

Figure 5.7. Battery states of charge with boost-buck converter for (a) 250 V, (b) 350 V (c) 500 V, and (d) 650 V

5.4.2 Simulation results using buck-boost converter

The simulation results show that the Buck-Boost converter can charge or discharge the battery at a nominal battery voltage of 250V and 350V shown in Figure 8 (a), (b), and cannot charge or discharge the battery at a nominal battery voltage of 500V and 650V shown in Figure 8 (c), (d).

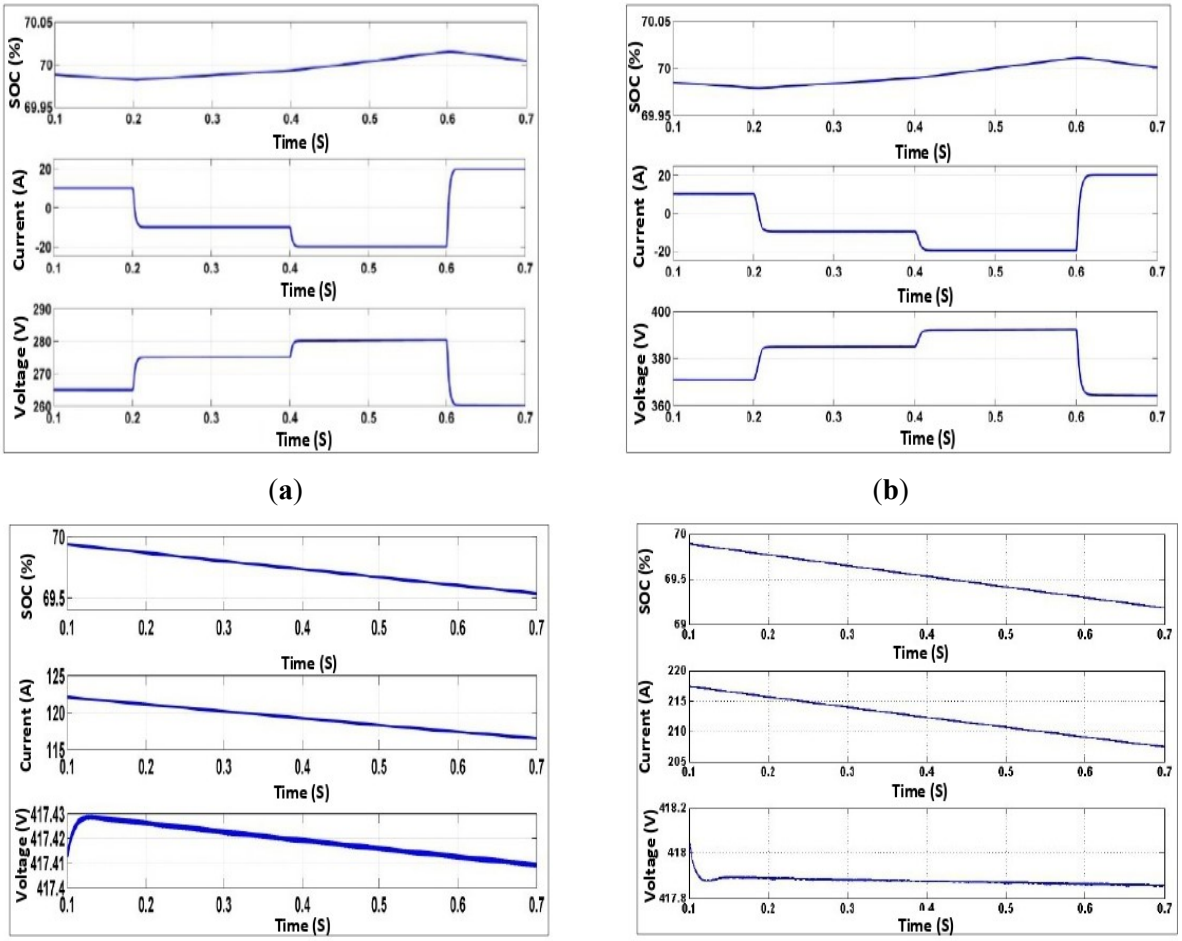

Figure 5.8 Battery states of charge with buck-boost converter for (a) 250 V, (b) 350 V (c) 500 V, and (d) 650 V

5.4.3 Simulation results using buck-boost converter with negative output voltage

The simulation results show that the Buck-Boost converter with negative output voltage has the capability to charge or discharge the battery at all the nominal battery voltages of 250V, 350V, 500V, and 650V shown in Figures 5.9 (a), (b), (c), and (d).

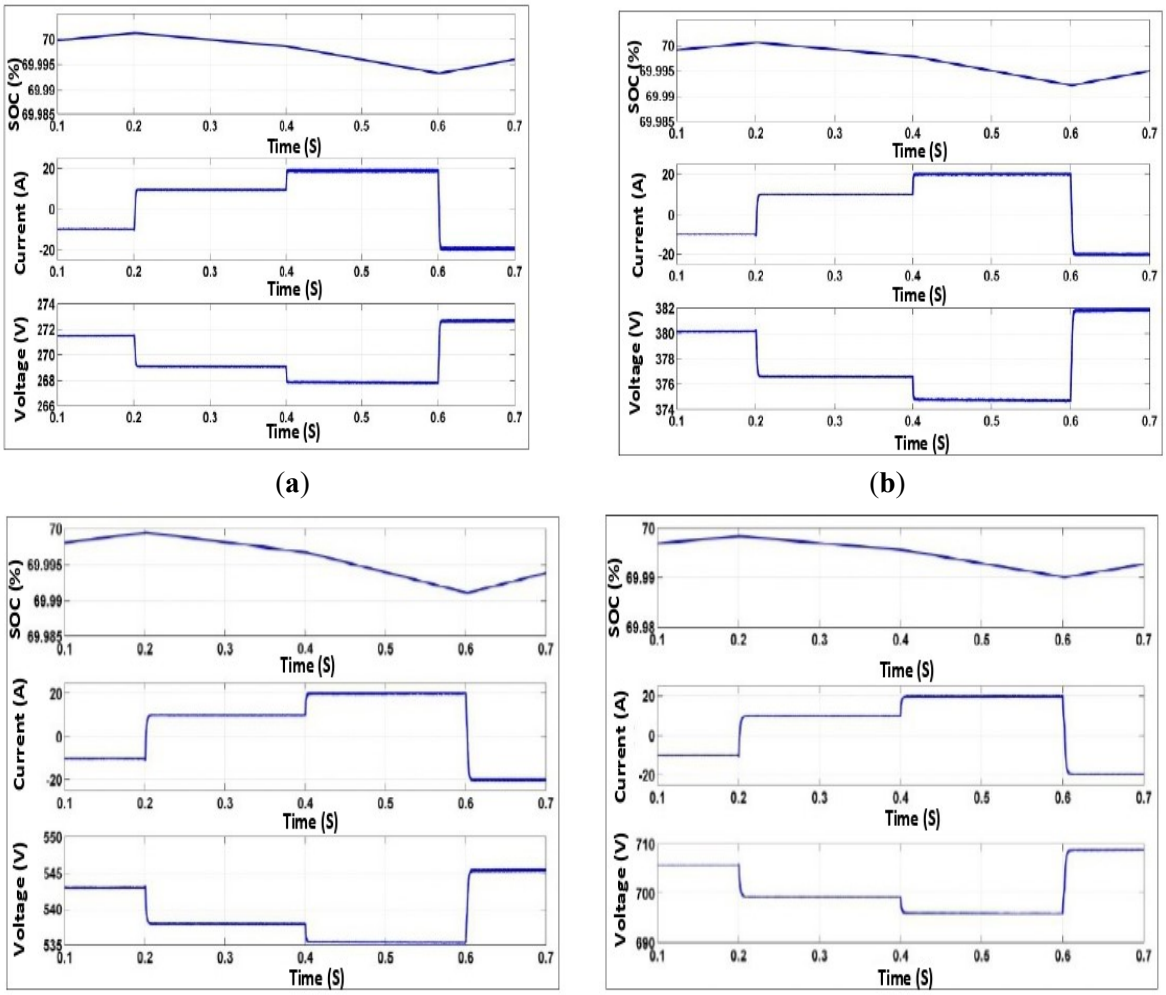

Figure 5.9 Battery states of charge with modified buck-boost converter for (a) 250 V, (b) 350 V (c) 500 V, and (d) 650 V

5.5 Resultant functional voltage of the converters

We summarize the converters used to know which voltage is functional for the energy storage system shown in Table 5.1.

Table 5.1 Summary of converters usable in an energy storage system

Converters	$\mathbf{V_{bat} > V_{in}}$	$\mathbf{V_{bat} = V_{in}}$	$\mathbf{V_{bat} < V_{in}}$	**Bidirectional**
Boost-Buck	Capable	Capable	Incapable	Capable
Buck-Boost	Incapable	Incapable	Capable	Capable
Buck-Boost ($-V_{out}$)	Capable	Capable	Capable	Capable

5.6 Conclusion

The study of the different types of existing converters and batteries are carried out to choose the most suitable in term of performance for the smart grid application system. We analyzed the different operating ranges of boost-buck, buck-boost, and buck-boost with negative output voltage using Matlab simulation. Then we studied the DC-DC converters capable of feeding the energy storage system. Each converter's control strategy is determined and chosen for the best topology. These converters help the batteries store a desired amount of energy and then return it to a grid at the desired speed. It is beneficial to store power from solar panels or wind turbines without wastage. The adaptability of a switched-mode power converter is appropriate for charging or discharging a battery. Also, the simplicity of the control techniques of converters gives significant efficiency. It seems efficient to use a bidirectional converter for the smart grid application to charge or discharge the battery without any constraints. Buck-Boost converter with negative output voltage can operate regardless of the value of the nominal battery voltage. For the future scope of this research, boost-buck, buck-boost, and buck-boost ($-V_{out}$) converters could be implemented in the smart grid application to charge and discharge the vehicle's storage (battery) system as it is capable of bidirectional power flow to supply or absorb the power from the electrical network. To achieve a power network devoid of disturbances, it is possible to create filters that are specifically designed to offset the reactive power and harmonic currents produced by the power electronics converter.

5.7 References

1. H. Ramírez-Murillo, C. Restrepo, J. Calvente, A. Romero and R. Giral, "Energy Management DC System Based on Current-Controlled Buck-Boost Modules," in *IEEE Transactions on Smart Grid*, vol. 5, no. 5, pp. 2644-2653, Sept. 2014, doi: 10.1109/TSG.2014.2330198.
2. J. W. Zapata, S. Kouro, G. Carrasco, H. Renaudineau and T. A. Meynard, "Analysis of Partial Power DC–DC Converters for Two-Stage Photovoltaic Systems," in *IEEE Journal of Emerging and Selected Topics in Power Electronics*, vol. 7, no. 1, pp. 591-603, March 2019, doi: 10.1109/JESTPE.2018.2842638.
3. Caio Meira Amaral da Luz, Enio Roberto Ribeiro, Fernando Lessa Tofoli, Analysis of the PV-to-PV architecture with a bidirectional Buck-Boost converter under shading conditions, *Solar Energy*, Volume 232, 2022, Pages 102-119, ISSN 0038-092X, doi:

10.1016/j.solener.2021.12.028.

4. Tao Chen, Peng Fu, Xiaojiao Chen, Sheng Dou, Liansheng Huang, Shiying He, Zhengshang Wang, An optimized bidirectional buck–boost converter for DC bus voltage stabilization in new generation poloidal field power supply, *Energy Reports*,Volume 8, Supplement 2, 2022, Pages 188-200, ISSN 2352-4847, doi: 10.1016/j.egyr.2021.11.016.
5. P.K. Gayen, P. Roy Chowdhury, P.K. Dhara, An improved dynamic performance of bidirectional SEPIC-Zeta converter based battery energy storage system using adaptive sliding mode control technique, Electric Power Systems Research, Volume 160, 2018, Pages 348-361, ISSN 0378-7796, https://doi.org/10.1016/j.epsr.2018.03.016.
6. M. J. Rahman, T. Tafticht and M. L. Doumbia, "Power Stability and Frequency Control Techniques of DG for a High Penetration Wind-Based Energy Storage System Using Integral–Derivative Controller," in *IEEE Canadian Journal of Electrical and Computer Engineering*, vol. 45, no. 3, pp. 232-241, Summer 2022, doi: 10.1109/ICJECE.2021.3103524.
7. Rahman, M.J.; Tafticht, T.; Doumbia, M.L.; Mutombo, N.M.-A. Dynamic Stability of Wind Power Flow and Network Frequency for a High Penetration Wind-Based Energy Storage System Using Fuzzy Logic Controller. *Energies* 2021, *14*, 4111. https://doi.org/10.3390/en14144111.
8. M.C. Mira, Z. Zhang, K. L. JΦrgensen and M. A. Andersen, "Fractional charging converter with high efficiency and low cost for electrochemical energy storage devices", *IEEE Transactions on Industry Applications*, vol. 55, no. 6, pp. 7461-7470, 2019.
9. M.J. Rahman, T. Tafticht and M. L. Doumbia, "Frequency Control for a High Penetration Wind-Based Energy Storage System in the Power Network," *2020 IEEE Electric Power and Energy Conference (EPEC)*, 2020, pp. 1-6, doi: 10.1109/EPEC48502.2020.9320083.
10. S. -i. Hamasaki, R. Mukai and M. Tsuji, "Control of power leveling unit with super capacitor using bidirectional buck/boost DC/DC converter," *2012 International Conference on Renewable Energy Research and Applications (ICRERA)*, 2012, pp. 1-6, doi: 10.1109/ICRERA.2012.6477316.
11. [Smolenski, R., 2012. *Conducted electromagnetic interface (EMI) in smart grid,* London : springer, pages: 162, ISSN: 1612-1287 https://doi.org/10.1007/978-1-4471-2960-8.
12. Karshenas, H. R. , Daneshpajooh, H., Safaee, A., Jain, P., & Bakhshai, A. (2011). Bidirectional DC - DC Converters for Energy Storage Systems. In (Ed.), Energy Storage in the Emerging Era of Smart Grids. IntechOpen. https://doi.org/10.5772/23494.
13. N. Hassanpour, A. Chub, A. Blinov and D. Vinnikov, "Comparison of Full Power and Partial Power Buck-Boost DC-DC Converters for Residential Battery Energy Storage Applications," *2022 IEEE 16th International Conference on Compatibility, Power Electronics, and Power Engineering (CPE-POWERENG)*, 2022, pp. 1-6, doi: 10.1109/CPE-POWERENG54966.2022.9880862.

14. Mohamed Kaouane, Akkila Boukhelifa, Ahmed Cheriti, Regulated output voltage double switch Buck-Boost converter for photovoltaic energy application, International Journal of Hydrogen Energy, Volume 41, Issue 45, 2016, Pages 20847-20857, ISSN 0360-3199, doi.10.1016/j.ijhydene.2016.06.140.

15. R. W. A. A. De Doncker, D. M. Divan and M. H. Kheraluwala, "A three-phase soft-switched high-power-density DC/DC converter for high-power applications," in *IEEE Transactions on Industry Applications*, vol. 27, no. 1, pp. 63-73, Jan.-Feb. 1991, doi: 10.1109/28.67533.

16. Soomro, A.M., Khahro, S.F., Talpur, S., Xiaozhong, L. &Manzoor, F. 2014. Input-current and load voltage sharing in input-parallel output-series connected boost Half briGDe DC-DC converter using stable control scheme. *TELKOMNIKA Indonesian Journal of Electrical Engineering*, 12(5), http://dx.doi.org/10.11591/telkomnika.v12i5.4188.

17. Kai Shi, Truong Bui, James Marco, Optimal control of bidirectional active clamp forward converter with synchronous rectifier based cell-to-external-storage active balancing system, Journal of Energy Storage, Volume 41, 2021, 102851, ISSN 2352-152X, https://doi.org/10.1016/j.est.2021.102851.

18. Tao, H., Kotsopoulos, A., Duarte, J.L. & Hendrix, M.A.M. 2006. Family of multiport bidirectional DC-DC converters. *IEE Proceedings - Electric Power Applications*, 153(3): 451, doi: 10.1049/ip-epa:20050362.

19. M. Parchomiuk, R. Strzelecki, K. Zymmer and A. Domino, "Modular power converter topologies for energy storage and electric power distribution systems," *2017 Progress in Applied Electrical Engineering (PAEE)*, 2017, pp. 1-6, doi: 10.1109/PAEE.2017.8009022.

20. J. R. R. Zientarski, M. L. d. S. Martins, J. R. Pinheiro and H. L. Hey, "Series-Connected Partial-Power Converters Applied to PV Systems: A Design Approach Based on Step-Up/Down Voltage Regulation Range," in *IEEE Transactions on Power Electronics*, vol. 33, no. 9, pp. 7622-7633, Sept. 2018, doi: 10.1109/TPEL.2017.2765928.

21. M. C. Mira, Z. Zhang, K. L. Jørgensen and M. A. E. Andersen, "Fractional Charging Converter With High Efficiency and Low Cost for Electrochemical Energy Storage Devices," in *IEEE Transactions on Industry Applications*, vol. 55, no. 6, pp. 7461-7470, Nov.-Dec. 2019, doi: 10.1109/TIA.2019.2921295.

22. M. C. Mira, Z. Zhang and A. E. Michael Andersen, "Analysis and Comparison of dc/dc Topologies in Partial Power Processing Configuration for Energy Storage Systems," *2018 International Power Electronics Conference (IPEC-Niigata 2018 - ECCE Asia)*, Niigata, Japan, 2018, pp. 1351-1357, doi: 10.23919/IPEC.2018.8507937.

23. Yahong Yang, Xiaobin He, Riming Shao, Shuang Xu, Liuchen Chang. Multi-Input Single-Phase Grid-Connected Inverter for Hybrid PV/Wind Power System. International Journal of Renewable and Sustainable Energy. Vol. 3, No. 2, 2014, pp. 35-42. doi: 10.11648/j.ijrse.20140302.11.

24. Tahar Tafticht, Mouctar Tchakala**,** Md Jahidur Rahman (2022)."GMPPT Approach for Photovoltaic Systems under Partial Shading Conditions Using Genetic Algorithm, "*International Journal of Power Electronics and Drive Systems (IJPEDS),* Vol 13, No 2, doi: 10.11591/ijpeds.v13.i2.pp1238-1245.

25. G. Canciello, A. Russo, B. Guida and A. Cavallo, "Supervisory Control for Energy Storage System Onboard Aircraft," *2018 IEEE International Conference on Environment and Electrical Engineering and 2018 IEEE Industrial and Commercial Power Systems Europe (EEEIC / I&CPS Europe)*, Palermo, Italy, 2018, pp. 1-6, doi: 10.1109/EEEIC.2018.8494347.

26. Khan, M.F.; Pervez, A.; Modibbo, U.M.; Chauhan, J.; Ali, I. Flexible Fuzzy Goal Programming Approach in Optimal Mix of Power Generation for Socio-Economic Sustainability: *A Case Study*. *Sustainability* **2021**, *13*, 8256. https://doi.org/10.3390/su13158256.

27. V. M. Iyer, S. Gulur, S. Bhattacharya and R. Ramabhadran, "A Partial Power Converter Interface for Battery Energy Storage Integration with a DC Microgrid," *2019 IEEE Energy Conversion Congress and Exposition (ECCE)*, 2019, pp. 5783-5790, doi: 10.1109/ECCE.2019.8912590.

28. K. E. L. Marcillo *et al*., "Interval Robust Controller to Minimize Oscillations Effects Caused by Constant Power Load in a DC Multi-Converter Buck-Buck System," in *IEEE Access*, vol. 7, pp. 26324-26342, 2019, doi: 10.1109/ACCESS.2019.2901441.

29. Y. Yao, F. Fassinou and T. Hu, "Stability and Robust Regulation of Battery-Driven Boost Converter With Simple Feedback," in *IEEE Transactions on Power Electronics*, vol. 26, no. 9, pp. 2614-2626, Sept. 2011, doi: 10.1109/TPEL.2011.2112781.

CONCLUSIONS

This doctorate thesis focuses on the environmental and economic benefits of distributed generation (DG) while highlighting the inherent challenges in managing fluctuating renewable energy sources (RESs). To maintain the dynamic stability of power flow and control the frequency in high-penetration wind-based energy storage systems, a logical algorithm was developed by designing a power-sharing method. The fluctuating behavior of Renewable Energy Sources (RESs) was identified. The control strategies of a converter/inverter were developed to maintain the proper power supply in the entire microgrid. Moreover, this thesis explored critical aspects of distributed generation (DG), renewable energy integration, and energy storage systems, focusing on enhancing power network efficiency while minimizing environmental air pollution. The main results of this thesis can be summarized by addressing each distinct challenge and proposing innovative solutions:

- A control algorithm for a high-penetration hybrid diesel-wind-based energy storage system, specifically designed to maintain dynamic stability in power flow and control network frequency. The key findings include the effective reduction of transient time in wind power flow and frequency fluctuations through the use of an integral-derivative (I-D) controller. Additionally, a storage system (battery) is employed to store excess wind energy efficiently, reducing wastage and supplying surplus wind power during high-load demand periods. The main advantage of this approach is the reduction of transient time of wind power flow and fluctuation behavior of frequency using an I–D controller. In addition, the algorithm provides a solution to regulate the network frequency using a storage system.
- A Fuzzy Logic (FL) control algorithm for a wind-based energy storage system is developed and compared the approaches to the traditional Proportional Integral Derivative (PID) controller. The study demonstrates substantial improvements in reducing transient time in wind power flow and frequency fluctuations. A storage system (battery) plays a crucial role in maintaining the network stability and minimizing energy losses. The

research's key contributions include: Designing a control scheme facilitating power sharing between networks; Efficient regulation of network frequency using a storage system; Reduction of transient time in wind power flow and frequency fluctuations through fuzzy logic control; Storing the surplus wind power and maintaining a high load demand by supplying it into the network; Comparison of the robustness of FL controller against PID controller.

- A simulation scheme has been developed utilizing a solar system instanced by Photovoltaic (PV) panels coupled to the grid, loads, and an energy storage device by designing a nonlinear controller. The study explored various nonlinear control techniques to address the challenges of managing power converters/inverters, compensating for reactive power, and mitigating harmonic currents. The research's key contributions include: Designing the control scheme for an inverter/rectifier to help the batteries store/supply a desired amount of energy at maximum speed; Designing DC/AC converters to maintain the unbalanced nonlinear load of the PV-based battery storage system; Modifying the adaptive notch filter to adequately compensate the input currents and perform an inverse transformation before injecting them at the output; and Reducing the (THD) rate of the converters/inverters using nonlinear controller without filter to enhance the efficiency of the power grid.
- A comprehensive survey of various DC-DC converters has been carried out to determine the most suitable energy storage device for smart grid applications. The study analyzed the efficiency and reliability of different converters and evaluated their performance in charging batteries. Operating ranges of boost-buck, buck-boost, and buck-boost ($-V_{out}$) converters are also analyzed to optimize energy storage. The key contributions include: Designing the control scheme for switched-mode converters to help the batteries store/supply the desired amount of energy; Analyzing the operating ranges of Boost-Buck, Buck-Boost, and Buck-Boost ($-V_{out}$) converters to enhance the efficiency of battery and renewable energy sources; and Comparing the DC converters to know the functional voltage for the energy storage system.

RECOMMENDATIONS

For future research endeavors, it is recommended to delve deeper into the integration of distributed generation (DG) and renewable energy sources (RESs) with an emphasis on hybrid systems that combine different RESs, such as wind and solar, to optimize energy production and storage. Investigating the development of advanced control algorithms, possibly leveraging artificial intelligence and machine learning techniques, can enhance the dynamic stability and efficiency of power flow control. Additionally, further exploration into the economic aspects, regulatory frameworks, and grid integration of DG and RESs will contribute to a comprehensive understanding of their real-world impact. Robustness and reliability should remain a focal point, particularly in unforeseen scenarios or adverse conditions, ensuring the resilience of distributed generation systems. Lastly, a focus on practical implementation and field testing will provide valuable insights and validation of theoretical findings, facilitating the transition from research to real-world application. These recommendations collectively aim to advance the state-of-the-art in sustainable energy systems, reducing environmental impact and promoting efficient power networks.

APPENDIX

- **Comparison of this thesis with prior research [7, 126-128]**

A model representing the High-Penetration, No Storage, Wind-Diesel (HPNSWD) system is outlined in [7, 126-128]. Originally developed by Hydro-Quebec, this technology aimed to lower electricity supply costs in remote northern communities [128]. The ideal wind penetration for this system relies on factors such as fuel delivery costs and available wind resources. The HPNSWD system described here features a 480 V, 300 kVA synchronous machine, a wind turbine linked to a 480 V, 275 kVA induction generator, a 50 kW customer load, and a variable secondary load (ranging from 0 to 446.25 kW). A secondary load bank, acting as a dump load, manages system frequency by absorbing excess wind power beyond consumer demand.

In [126], an example of dynamic simulation for Wind-Diesel Isolated Microgrids (WDIM) without storage is presented. This simulation, conducted using Matlab–Simulink, illustrates the WDIM operating in Wind-Diesel (WD) mode. It demonstrates how a Dump Load (DL) enhances WDIM stability and reliability by utilizing surplus power generated by the wind turbine.

In [127], a hybrid wind diesel system-based (HWDS) standalone system and micro-grid system are simulated to study the performance of the grid system. The complete HWDS is modeled with a secondary Dump Load (DL) and simulated in a MATLAB Simulink environment which, manages system frequency by absorbing excess wind power beyond consumer demand.

<u>Proposed power-saving option by installing Battery Based Energy Storage System (BESS)</u>

From the above research statements, they didn't propose any storage system in the power grid. According to their research works, when there is surplus power generated through wind turbines, a large amount of wind power needs to be dumped in a secondary/dump load bank to maintain the network frequency as well as total load demand which is not efficient for a renewable energy-based power system.

Therefore, without throwing a large amount of wind power in a secondary/dump load, we developed a storage system (battery) with a power-sharing method in this thesis to charge when power from the wind turbine is more than the load demand and discharge when wind power is less than the total load demand. Here, DL only consumed the surplus power that the battery could not store.

Therefore,

$$P_{S\_ref} = P_{ref} \text{ when } Pref \leq 0 \quad \text{A 1}$$

$$P_{S\_ref} = P_{S\_max} \text{ when } P_{ref} > 0 \quad \text{A 2}$$

In the DL,

$$P_{D\_ref} = P_{ref} - P_{S\text{-}max} \text{ when } P_{ref} > 0 \quad \text{A 3}$$

$$P_{D\_ref} = 0 \text{ when } P_{ref} \leq 0 \quad \text{A 4}$$

Where P_{S_ref} is battery reference power, P_{S_max} is maximum battery power, P_{D_ref} is dump load reference power. The battery and DL recognize the P_{ref} (reference power) simultaneously and maintain the accuracy at the time of operation. Thus, three types of control techniques are implemented.

Using the DL only when the BESS is completely charged,

$$P_{s\text{-}max} < P_T - P_L, P_S = 0; \quad \text{A 5}$$

By using the battery only,

$$(0 = P_D) \text{ if } |P_T - P_L| \leq P_{S\_nom}; \quad \text{A 6}$$

By using both battery and DL if,

$$(P_{ref} > 0)\ P_T - P_L > 0. \quad \text{A 7}$$

Where P_T is wind power, P_L is total load demand, P_{S_nom} is battery nominal power, and P_D is dump load power.

Proposed fuzzy logic controller to maintain the robustness of the power network

[126] proposed PID controller in WD mode, no storage with variable loads and wind speed. They have considered the Diesel Generator (DG) and Wind Turbine Generator (WTG) to produce 108 kW and 92 kW (for a wind speed of 8 m/s), respectively and the load and DL consume 200 kW and 0 kW, respectively.

In real-time conditions, DL can not be zero (if there is no storage system). To regulate the network dynamic system there should be more power generation compared to the total load demand (here DG+WTG can not be less than or equal to the PL) so that the DL or battery system can absorb some excess power to regulate the network voltage and frequency. Figures A 1, A 2, and A 3 represent the WDIM frequency (pu), WDIM voltage (pu), and Active power generation and consumption in the WDIM components respectively.

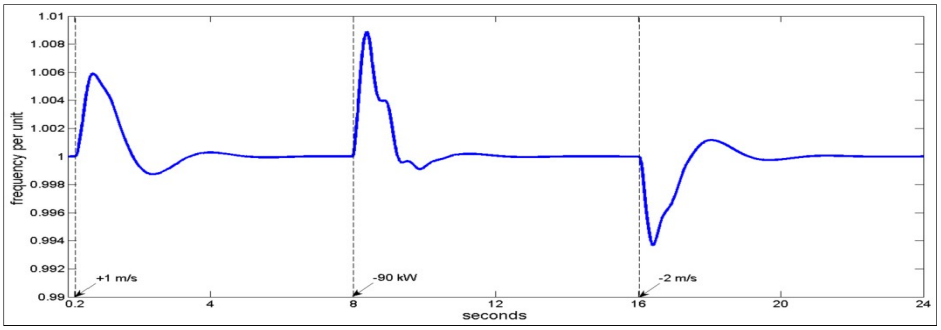

Figure A 1. WDIM frequency (pu) [126].

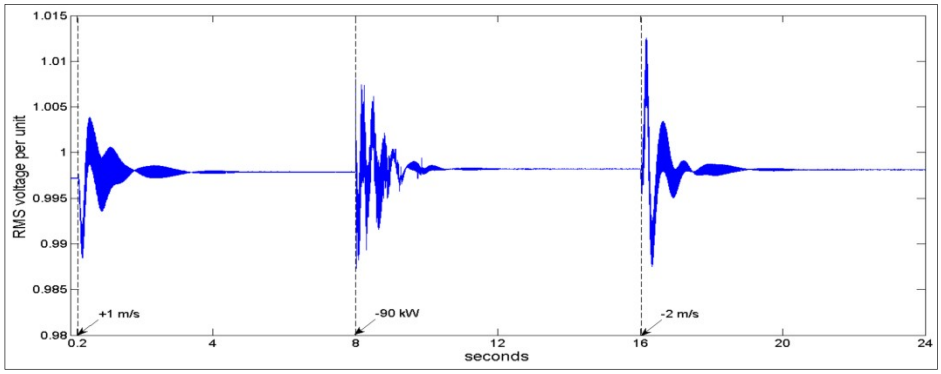

Figure A 2. WDIM voltage (pu) [126].

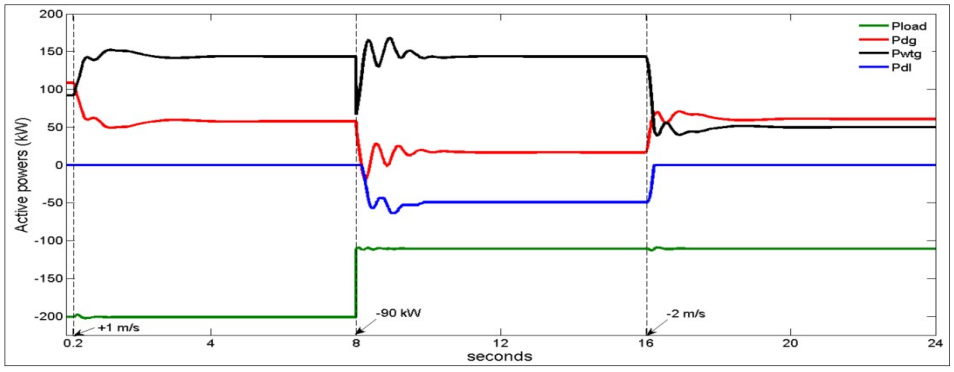

Figure A 3. Active power generation and consumption in the WDIM components [126].

Now if we compare to the [126] and its Figures (A 1, A 2, and A 3), then we will see in Figure 4 A (a) (b) (c) that the fluctuation behavior and transient time of network frequency, wind turbine speed, and wind power flow are significantly reduced using fuzzy logic controller over PID controller used in [126]. Figure 4 A (d) shows there is no voltage flicker observe compare to Figure A 2 [126].

In [7, 126-128], the excess power from RESs is thrown to the dump load to regulate the network frequency. Which is not efficient for future RESs-based power generation systems. Therefore, this thesis proposed and developed a power-sharing method with a battery and DL system to minimize the power losses for the future power grid.

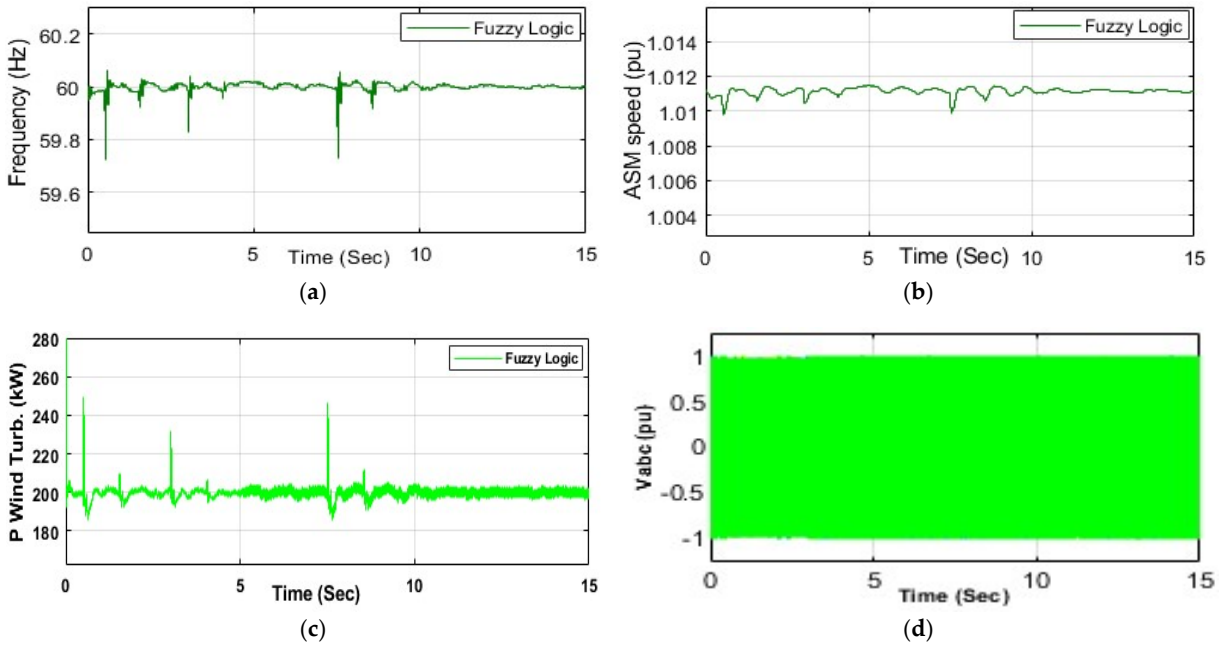

Figure A 4 (a) Network frequency conditions. (b) Speed generated by ASM generator. (c) The power produced by the wind turbine, and (d) Voltage at load bus.

BIBLIOGRAPHIE

[1] M. J. Rahman, T. Tafticht and M. L. Doumbia, "Power Stability and Frequency Control Techniques of DG for a High Penetration Wind-Based Energy Storage System Using Integral–Derivative Controller," in *IEEE Canadian Journal of Electrical and Computer Engineering*, vol. 45, no. 3, pp. 232-241, Summer 2022, doi: 10.1109/ICJECE.2021.3103524.

[2] Rahman, M.J.; Tafticht, T.; Doumbia, M.L.; Mutombo, N.M.-A. Dynamic Stability of Wind Power Flow and Network Frequency for a High Penetration Wind-Based Energy Storage System Using Fuzzy Logic Controller. *Energies* 2021, *14*, 4111. https://doi.org/10.3390/en14144111.

[3] M.J. Rahman, T. Tafticht, and M.L. Doumbia (2023). Power Converters Analyzed in Energy Storage Systems to Enhance the Performance of Smart Grid Applications. *International Journal of Power Electronics and Drive Systems*. ISSN: 2088-8694. (Accepted).

[4] Rahman, M.J.; Tafticht, T.; Doumbia, M.L.; Messaïf, I. Optimal Inverter Control Strategies for a PV Power Generation with Battery Storage System in Microgrid. *Energies* 2023, *16*, 4228. https://doi.org/10.3390/en16104228.

[5] M. H. Nazari, M. Ilić and J. P. Lopes, "Dynamic stability and control design of modern electric energy systems with large penetration of distributed generators, "*2010 IREP Symposium Bulk Power System Dynamics and Control - VIII (IREP)*, Rio de Janeiro, 2010, pp. 1-7, doi: 10.1109/IREP.2010.5563270.

[6] Sebastián, R. & Quesada, J., 2006. "Distributed control system for frequency control in a isolated wind system," *Renewable Energy, Elsevier,* vol. 31(3), pages 285-305.

[7] Mott, L., B. Saulnier. 2014. "Commercial Wind-Diesel Project, St. Paul Island, Alaska," *14th Prime Power Diesel Inter-Utility Conference*, May 28-June 2, Winnipeg, Manitoba, Canada.

[8] N. E. L. Yakine Kouba, M. Menaa, M. Hasni and M. Boudour, "Load Frequency Control in multi-area power system based on Fuzzy Logic-PID Controller," *2015 IEEE International Conference on Smart Energy Grid Engineering (SEGE)*, Oshawa, ON, 2015, pp. 1-6, doi: 10.1109/SEGE.2015.7324614.

[9] Salama, H.S., Aly, M.M., Abdel-Akher, M. *et al.* "Frequency and voltage control of microgrid with high WECS penetration during wind gusts using superconducting magnetic energy storage". *Electr Eng* 101**,** 771–786 (2019). https://doi.org/10.1007/s00202-019-00821-w.

[10] M. Parchomiuk, R. Strzelecki, K. Zymmer and A. Domino, "Modular power converter topologies for energy storage and electric power distribution systems," *2017 Progress in Applied Electrical Engineering (PAEE)*, 2017, pp. 1-6, doi: 10.1109/PAEE.2017.8009022.

[11] R. W. A. A. De Doncker, D. M. Divan and M. H. Kheraluwala, "A three-phase soft-switched high-power-density DC/DC converter for high-power applications," in *IEEE Transactions on Industry Applications*, vol. 27, no. 1, pp. 63-73, Jan.-Feb. 1991, doi: 10.1109/28.67533.

[12] Park, C.-Y.; Hong, S.-H.; Lim, S.-C.; Song, B.-S.; Park, S.-W.; Huh, J.-H.; Kim, J.-C. Inverter Efficiency Analysis Model Based on Solar Power Estimation Using Solar Radiation. *Processes* 2020, *8*, 1225.http://dx.doi.org/10.11591/telkomnika.v12i5.4188.

[13] Li, X.; Wang, L.; Yan, N.; Ma, R. Cooperative Dispatch of Distributed Energy Storage in Distribution Network With PV Generation Systems. *IEEE Trans. Appl. Supercond.* 2021, *31*, 0604304.

[14] Bineeta, M.; Das, D. Multi-objective dynamic and static reconfiguration with optimized allocation of PV-DG and battery energy storage system. *Renew. Sustain. Energy Rev.* 2020, *124*, 109777.

[15] Salem, R.; Mendalek, N.; Al-Haddad, K. Experimental design of a nonlinear control technique for three-phase shunt active power filter. *IEEE Trans. Ind. Electron.* 2010, *57*, 3364–3375.

[16] Gopiya Naik S, Khatod DK, Sharma MP. Optimal allocation of combined DG and capacitor for real power loss minimization in distribution networks. *Int J Electr Power Energy Syst* 2013;53:967–73. https://doi.org/10.1016/j. ijepes.2013.06.008.

[17] Liu Y, Cetenovi ´ ´c D, Li H, Gryazina E, Terzija V. An optimized multi-objective reactive power dispatch strategy based on improved genetic algorithm for wind power integrated systems. *Int J Electr Power Energy Syst* 2022;136:107764. https://doi.org/10.1016/j.ijepes.2021.107764.

[18] Mahmoud K, Yorino N, Ahmed A. Optimal distributed generation allocation in distribution systems for loss minimization. *IEEE Trans Power Syst* 2016;31(2): 960–9. https://doi.org/10.1109/TPWRS.2015.2418333.

[19] Doagou-Mojarrad H, Gharehpetian GB, Rastegar H, Olamaei J. Optimal placement and sizing of DG (distributed generation) units in distribution networks by novel hybrid evolutionary algorithm. *Energy* 2013;54:129–38. https://doi.org/10.1016/ j.energy.2013.01.043.

[20] Rathore A, Patidar NP. Optimal sizing and allocation of renewable based distribution generation with gravity energy storage considering stochastic nature using particle swarm optimization in radial distribution network. *J Energy Storage* 2020;35:2021. https://doi.org/10.1016/j.est.2021.102282.

[21] Driesen J, Belmans R. Distributed generation: challenges and possible solutions. In: 2006 *IEEE Power Eng. Soc. Gen. Meet*. PES; 2006. p. 1–8. doi: 10.1109/ pes.2006.1709099.

[22] Mirzaei M, Jasni J, Hizam H, Wahab NIA, Mohamed SEG. An analytical method for optimal sizing of different types of DG in a power distribution system. In: Conf.

Proceeding, *IEEE Int. Conf. Power Energy, PECon* 2014, no. March; 2014. p. 309–14. doi: 10.1109/PECON.2014.7062462.

[23] Huang D, Li H, Cai G, Huang N, Yu N, Huang Z. An efficient probabilistic approach based on area grey incidence decision making for optimal distributed generation planning. *IEEE Access* 2019;7:93175–86. https://doi.org/10.1109/ACCESS.2019.2927713.

[24] Hemeida MG, Ibrahim AA, Mohamed AAA, Alkhalaf S, El-Dine AMB. Optimal allocation of distributed generators DG based Manta Ray Foraging Optimization algorithm (MRFO). *Ain Shams Eng J* 2021;12(1):609–19. https://doi.org/10.1016/j.asej.2020.07.009.

[25] Ali A, Keerio MU, Laghari JA. Optimal site and size of distributed generation allocation in radial distribution network using multi-objective optimization. *J Mod Power Syst Clean Energy* 2021;9(2):404–15. https://doi.org/10.35833/MPCE.2019.000055.

[26] Al-Ammar EA, Farzana K, Waqar A, Aamir M, Saifullah, Ul Haq A, et al. ABC algorithm based optimal sizing and placement of DGs in distribution networks considering multiple objectives. *Ain Shams Eng J* 2021;12(1):697–708. https://doi.org/10.1016/j.asej.2020.05.002.

[27] Truong KH, Nallagownden P, Elamvazuthi I, Vo DN. A Quasi-Oppositional-Chaotic Symbiotic Organisms Search algorithm for optimal allocation of DG in radial distribution networks. *Appl Soft Comput J* 2020;88:106067. https://doi.org/10.1016/j.asoc.2020.106067.

[28] Eid A, Kamel S, Korashy A, Khurshaid T. An enhanced artificial ecosystem-based optimization for optimal allocation of multiple distributed generations. *IEEE Access* 2020;8:178493–513. https://doi.org/10.1109/ACCESS.2020.3027654.

[29] Almabsout EA, El-Sehiemy RA, An ONU, Bayat O. A hybrid local search-genetic algorithm for simultaneous placement of DG units and shunt capacitors in radial distribution systems. *IEEE Access* 2020;8:54465–81. https://doi.org/10.1109/ACCESS.2020.2981406.

[30] Moghaddam MJH, Kalam A, Shi J, Nowdeh SA, Gandoman FH, Ahmadi A. A new model for reconfiguration and distributed generation allocation in distribution network considering power quality indices and network losses. *IEEE Syst J* 2020;14 (3):3530–8. https://doi.org/10.1109/JSYST.2019.2963036.

[31] Ackermann T, Andersson G, Soder L. Distributed generation: a definition. *Electr Power Syst Res* 2001;57(3):195–204. https://doi.org/10.1016/S0378-7796(01) 00101-8.

[32] Saha S, Mukherjee V. Optimal placement and sizing of DGs in RDS using chaos embedded SOS algorithm. *IET Gener Transm Distrib* 2016;10(14):3671–80. https://doi.org/10.1049/iet-gtd.2016.0151.

[33] Quadri IA, Bhowmick S, Joshi D. A comprehensive technique for optimal allocation of distributed energy resources in radial distribution systems. Appl. *Energy* 2018; 211:1245–60. https://doi.org/10.1016/j.apenergy.2017.11.108.

[34] Prakash P, Khatod DK. An analytical approach for optimal sizing and placement of distributed generation in radial distribution systems. In: 1st IEEE Int. Conf. *Power Electron. Intell. Control Energy Syst. ICPEICES* 2016; 2017. p. 4–8. doi: 10.1109/ ICPEICES.2016.7853119.

[35] Prakash P, Khatod DK. An analytical approach for placement of distributed generation in radial distribution systems considering load variation. In: 2016 IEEE *7th Power India International Conference (PIICON)*, Nov; 2016. p. 1–6. https://doi. org/10.1109/POWERI.2016.8077210.

[36] Hung DQ, Mithulananthan N, Bansal RC. Analytical expressions for DG allocation in primary distribution networks. *IEEE Trans Energy Convers* 2010;25(3):814–20. https://doi.org/10.1109/TEC.2010.2044414.

[37] Mahmoud K, Lehtonen M. Simultaneous allocation of multi-type distributed generations and capacitors using generic analytical expressions. *IEEE Access* 2019; 7:182701–10. https://doi.org/10.1109/ACCESS.2019.2960152.

[38] Sa'ed JA, Amer M, Bodair A, Baransi A, Favuzza S, Zizzo G. A simplified analytical approach for optimal planning of distributed generation in electrical distribution networks. *Appl. Sci*. 2019;9(24). https://doi.org/10.3390/app9245446.

[39] Abdelkader MA, Elshahed MA, Osman ZH. An analytical formula for multiple DGs allocations to reduce distribution system losses. *Alexandria Eng J* 2019;58(4): 1265–80. https://doi.org/10.1016/j.aej.2019.10.009.

[40] Niveditha P, Sujatha MS. Optimal allocation and sizing of DG in radial distribution system-a review. *Int J Grid Distrib Comput* 2018;11(6):49–58. https://doi.org/ 10.14257/ijgdc.2018.11.6.05.

[41] Murty VVSN, Kumar A. Optimal placement of DG in radial distribution systems based on new voltage stability index under load growth. *Int J Electr Power Energy Syst* 2015;69:246–56. https://doi.org/10.1016/j.ijepes.2014.12.080.

[42] Sharma S, Bhattacharjee S, Bhattacharya A. Quasi-oppositional swine influenza model based optimization with quarantine for optimal allocation of DG in radial distribution network. *Int J Electr Power Energy Syst* 2016;74:348–73. https://doi. org/10.1016/j.ijepes.2015.07.034.

[43] Sultana S, Roy PK. Krill herd algorithm for optimal location of distributed generator in radial distribution system. *Appl Soft Comput J* 2016;40:391–404. https://doi.org/10.1016/j.asoc.2015.11.036.

[44] Martinez JA, Guerra G. A parallel Monte Carlo method for optimum allocation of distributed generation. *IEEE Trans Power Syst* 2014;29(6):2926–33. https://doi. org/10.1109/TPWRS.2014.2317285.

[45] M.E. Mondejar, et al., Digitalization to achieve sustainable development goals: steps towards a smart green planet, Sci. *Total Environ*, (June) (2021), https://doi.org/10.1016/j.scitotenv.2021.148539.

[46] N. T. Mbungu et al., "A dynamic energy management system using smart metering," *Appl. Energy*, vol. 280, p. 115990.

[47] M.S. Masaki, L. Zhang, X. Xia, A hierarchical predictive control for supercapacitor-retrofitted grid-connected hybrid renewable systems, *Appl. Energy* 242 (2019) 393–402. May, https://doi.org/10.1016/J.APENERGY.201 9.03.049. May.

[48] A.A. Ismail, N.T. Mbungu, A. Elnady, R.C. Bansal, A.K. Hamid, M. AlShabi, Impact of Electric Vehicles on Smart Grid and Future Predictions: *A Survey*, 2022, https://doi.org/10.1080/02286203.2022.2148180.

[49] Z. Shi, W. Wang, Y. Huang, P. Li, L. Dong, Simultaneous optimization of renewable energy and energy storage capacity with the hierarchical control, *CSEE J. Power Energy Syst*. 8 (1) (2022) 95–104. Jan. 10.17775/CSEEJPES.201 9.01470.

[50] R. De Castro, R.E. Araujo, J.V. Barreras, C. Pinto, Smart and Hybrid Battery Balancing For Electric Vehicles [Online]. Available: http://elib.dlr.de.Pleaseco nsulttheoriginalpublicationforcitation.

[51] R. Banos, ˜ F. Manzano-Agugliaro, F.G. Montoya, C. Gil, A. Alcayde, J. Gomez, ´ Optimization methods applied to renewable and sustainable energy: a review, *Renew. Sust. Energ. Rev*. 15 (4) (2011) 1753–1766. May, https://doi.org/10.10 16/j.rser.2010.12.008. May.

[52] L. Zhang, X. Ye, X. Xia, F. Barzegar, A real-time energy management and speed controller for an electric vehicle powered by a hybrid energy storage system, *IEEE Trans. Ind. Inform*. 16 (10) (2020) 6272–6280. Oct. https://doi.org/10.11 09/TII.2020.2964389. Oct.

[53] Wongdet, P., & Marungsri, B. (2018, March). Hybrid energy storage system in standalone DC microgrid with ramp rate limitation for extending the lifespan of battery. In *2018 International Electrical Engineering Congress (iEECON)* (pp. 1-4). IEEE.

[54] N.T. Mbungu, A.A. Ismail, M. AlShabi, R.C. Bansal, A. Elnady, A.K. Hamid, Control and estimation techniques applied to smart microgrids: a review, *Renew. Sust. Energ. Rev.* 179 (2023), 113251. Jun. https://doi.org/10.1016/J.RSER.20 23.113251. Jun.

[55] S. Hajiaghasi, A. Salemnia, M. Hamzeh, Hybrid energy storage system for microgrids applications: a review, *J. Energy Storage* 21 (2019) 543–570. Feb. 01, https://doi.org/10.1016/j.est.2018.12.017.

[56] A. Kargarian, G. Hug, J. Mohammadi, A multi-time scale co-optimization method for sizing of energy storage and fast-ramping generation*, IEEE Trans. Sustain. Energy* 7 (4) (2016) 1351–1361. Oct. https://doi.org/10.1109/TSTE.2016.2541.

[57] M.W. Siti, 'Optimal Energy Control of a Grid Connected Solar-wind Based Electric Power Plant', 2016.

[58] T. Madiba, R.C. Bansal, N.T. Mbungu, M. Bettayeb, R.M. Naidoo, M.W. Siti, Under-frequency load shedding of microgrid systems: a review, *Int. J. Model. Simul*. 42 (4) (2022) 653–679, https://doi.org/10.1080/ 02286203.2021.1964061.

[59] Y. Zhang, H. Liu, Z. Zhang, Y. Luo, Q. Guo, S. Liao, Cloud computing-based realtime global optimization of battery aging and energy consumption for plug-in hybrid electric vehicles, *J. Power Sources* 479 (2020), https://doi.org/10.1016/j. jpowsour.2020.229069. Dec.

[60] M.M. Rana, M. Uddin, M.R. Sarkar, G.M. Shafiullah, H. Mo, M. Atef, A review on hybrid photovoltaic – battery energy storage system: current status, challenges, and future directions, *J. Energy Storage* 51 (2022), https://doi.org/10.1016/j. est.2022.104597, Jul. 01.

[61] J. Kim, Y. Suharto, T.U. Daim, Evaluation of electrical energy storage (EES) technologies for renewable energy: a case from the US Pacific northwest, *J. Energy Storage* 11 (2017) 25–54. Jun. https://doi.org/10.1016/J.EST.201 7.01.003. Jun.

[62] J. Siecker, K. Kusakana, B.P. Numbi, A review of solar photovoltaic systems cooling technologies, Renew. *Sust. Energ. Rev*. 79 (2017) 192–203, https://doi. org/10.1016/j.rser.2017.05.053. Elsevier Ltd.

[63] Y.J. Zheng, S.Y. Chen, Y. Lin, W.L. Wang, Bio-inspired optimization of sustainable energy systems: a review, *Math. Probl. Eng*. 2013 (2013), https://doi.org/ 10.1155/2013/354523.

[64] Lakshminarayana, S., Xu, Y., Poor, H. V., & Quek, T. Q. (2016). Cooperation of storage operation in a power network with renewable generation. *IEEE Transactions on Smart Grid*, *7*(4), 2108-2122.

[65] Ross Jr, M. J. (2018). *Modeling and control of a microgrid using a hybrid energy storage system with supercapacitors* (Doctoral dissertation, Monterey, CA; Naval Postgraduate School).

[66] Munir, B. (2020). Hybrid energy-storage system for mobile RF energy harvesting wireless sensors.

[67] T.C. Chen, et al., Development of machine learning methods in hybrid energy storage systems in electric vehicles, *Math. Probl. Eng*. 2022 (2022), https://doi. org/10.1155/2022/3693263.

[68] Tu, C. H. (2016). *A Hybrid Energy Storage System Using Series-Parallel Reconfiguration Technique* (Doctoral dissertation).

[69] Yu, H., Castelli-Dezza, F., Cheli, F., Tang, X., Hu, X., & Lin, X. (2020). Dimensioning and power management of hybrid energy storage systems for electric vehicles with multiple optimization criteria. *IEEE Transactions on Power Electronics*, *36*(5), 5545-5556.

[70] A.K. Vincent, R. Nersisson, Particle swarm optimization based PID controller tuning for level control of two tank system, in: IOP Conference Series: *Materials Science and*

Engineering, Institute of Physics Publishing, 2017, https://doi.org/ 10.1088/1757-899X/263/5/052001. Dec.

[71] C. Capasso, D. Lauria, O. Veneri, Optimal control strategy of ultra-capacitors in hybrid energy storage system for electric vehicles, *Energy Procedia* (2017) 1914–1919, https://doi.org/10.1016/j.egypro.2017.12.390.

[72] Z. Belboul, et al., Multiobjective optimization of a hybrid PV/wind/battery/diesel generator system integrated in microgrid: a case study in Djelfa, Algeria, *Energies* (Basel) 15 (10) (2022), https://doi.org/10.3390/en15103579. May.

[73] D. Bhowmik and A. K. Sinha, "Cost-based allocation model for hybrid power system considering solar, wind and thermal generations separately," *IET Gener. Transm. Distrib*., vol. 11, no. 18, pp. 4576–4587, Dec. 2017, doi:https://doi. org/10.1049/iet-gtd.2017.0305.

[74] Tang, L. (2017). *Optimal energy management strategy for hybrid electric vehicles with consideration of battery life* (Doctoral dissertation, The Ohio State University).

[75] S.S. Thale, R.G. Wandhare, V. Agarwal, A novel reconfigurable microgrid architecture with renewable energy sources and storage, *IEEE Trans. Ind. Appl*. 51 (2) (2015) 1805–1816. Mar. https://doi.org/10.1109/TIA.2014.2350083. Mar.

[76] A. Neffati, A. Marzouki, Local energy management in hybrid electrical vehicle via fuzzy rules system, *AIMS Energy* 8 (3) (2020) 421–437, https://doi.org/10.3934/ energy.2020.3.421.

[77] Min Dai, Mohammad N. Marwali, Jin-Woo Jung, Ali Keyhani, Power Flow Control of a Single Distributed Generation Unit with Nonlinear Local Load, *IEEE PES Power Systems Conference and Exposition*, 2004, p. 398-403.

[78] Min Dai, Mohammad Nanda Marwali, Jin-Woo Jung, Ali Keyhani, Power Flow Control of a Single Distributed Generation Unit, IEEE Transactions on Power Electronics, vol. 23, no. 1, 2008, p. 343-352.

[79] M. Prodanovic, K. De Brabandere, J. Van den Keybus, T. Green, J. Driesen, Harmonic and reactive power compensation as ancillary services in inverter-based distributed generation, *Generation, Transmission & Distribution (IET),* vol. 1, no. 3, 2007, p. 432-438.

[80] Pedro M. S. Carvalho, Pedro F. Correia, Luís A. F. M. Ferreira, Distributed Reactive Power Generation Control for Voltage Rise Mitigation in Distribution Networks, *IEEE Transactions on Power Systems*, vol. 23, no. 2, 2008, 213 p. 766-772.

[81] Ferry A. Viawan, Daniel Karlsson, Coordinated Voltage and Reactive Power Control in the Presence of Distributed Generation, *IEEE Power and Energy Society General Meeting* - Conversion and Delivery of Electrical Energy in the 21st Century, 2008, p. 1-6.

[82] M.G. Molina, P.E. Mercado, Stabilization and control of tie-line power flow of microgrid including wind generation by distributed energy storage, *International Journal of Hydrogen Energy,* vol 35, no. 11, 2010, p. 5827- 225 5833.

[83] Maria Stefania Carmelia, Francesco Castelli-Dezza, Marco Mauri, Gabriele Marchegiani, Daniele Rosati, Control strategies and configurations of hybrid distributed generation systems, *Renewable Energy*, vol. , 2012, p. 228 294-305.

[84] Qiong Tao, Deshun Wang, Bo Yang, Huan Liu, Shengchi Yan, Voltage Control of Distribution Network with distributed generation based on Voltage Sensitivity Matrix, *IEEE International Conference on Energy Internet*, 2018, p. 298-302.

[85] Irvin J. Balaguer, Qin Lei, Shuitao Yang, Uthane Supatti, Fang Zheng Peng, Control for Grid-Connected and Intentional Islanding Operations of Distributed Power Generation, *IEEE Transactions on Industrial Electronics*, vol. 58, no. 1, 2011, p. 147-157.

[86] Hua Geng, Dewei (David) Xu, Bin Wu, Geng Yang, Active Islanding Detection for Inverter-Based Distributed Generation Systems With Power Control Interface, *IEEE Transactions on Energy Conversion,* vol. 26, no. 4, 243 2011, p. 1063-1072.

[87] Xiaolong Chen, Yongli Li, An Islanding Detection Algorithm for Inverter-Based Distributed Generation Based on Reactive Power Control, *IEEE Transactions On Power Electronics*, vol. 29, no. 9, 2014, p. 4672-4683.

[88] P. Hušek, "Pid controller design for hydraulic turbine based on sensitivity margin specifications," *Electrical Power and Energy Systems*, vol. 55, p. 460–466, 2014.

[89] G. Liang, W. Li, and Z. Li, "Control of superheated steam temperature in large-capacity generation units based on active disturbance rejection method and distributed control system*," Control Engineering Practice*, vol. 21, no. 3, p. 268–285, 2013.

[90] B. Malinga, J. E. Sneckenberger, and A. Feliachi, "Modeling and control of a wind turbine as a distributed resource," in Proceedings of the *35th Southeastern Symposium on System Theory*, p. 108–112, 2003.

[91] P. Li, L. Zhang, V. Wang, and Y.-B. Sheng, "Research on the control of the single-stage photovoltaic system in microgrid," in China *International Conference on Electricity Distribution (CICED),* p. 1–7, 2008.

[92] P. Dash, L. C. Saikia, and N. Sinha, "Automatic generation control of multi area thermal system using bat algorithm optimized pd-pid cascade controller," *Electrical Power and Energy Systems*, vol. 68, p. 364–372, 2015.

[93] S. Sondhi and Y. V. Hote, "Fractional order pid controller for load frequency control," *Energy Conversion and Management*, vol. 85, p. 343–353, 2014.

[94] K. Ashok Mohan Jadhav, "Performance verification of pid controller in an interconnected power system using particle swarm optimization," in Energy Procedia, *2nd International Conference on Advances in Energy 276 Engineering (ICAEE),* vol. 14, p. 2075–2080, 2012.

[95] C. S. Thelukuntla and M. Veerachary, "Resonant controller based single-phase z-source inverter with lcl filter," in *Joint International Conference on Power Electronics, Drives and Energy Systems (PEDES),* p. 1–6, 2010.

[96] E. d. S. J. J.M. Pacas, M.G. Molina, "Design of a robust and efficient power electronic interface for the grid integration of solar photovoltaic generation systems," *International Journal of hydrogen energy*, vol. 37, p. 10076–10082, 2012.

[97] S. Sinan and A. Elnady, "Optimized pid controller based voltage oriented control of the 7-level diode clamped inverter for distributed generation system," in *International Conference on Electrical and Computing Technologies and Applications (ICECTA),* p. 1–5, 2017.

[98] F. Habibi, A. H. Naghshbandy, and H. Bevrani, "Robust voltage controller design for an isolated microgrid using kharitonov's theorem and d-stability concept," *Electrical Power and Energy Systems*, vol. 44, p. 656–665, 2013.

[99] M. Shiroei, M. R. Toulabi, and A. M. Ranjbar, "Robust multivariable predictive based load frequency control considering generation rate constraint," *Electrical Power and Energy Systems, vol*. 46, p. 405–413, 2013.

[100] M. M. Rezaei and J. Soltani, "A robust control strategy for a grid-connected multi-bus microgrid under unbalanced load conditions," *Electrical Power and Energy Systems*, vol. 71, p. 68–76, 2015.

[101] V. P. Singh, S. R. Mohanty, N. Kishor, and P. K. Ray, "Robust h-infinity load frequency control in hybrid distributed generation system," *Electrical Power and Energy Systems,* vol. 46, p. 294–305, 2013.

[102] S. R. Mohanty, N. Kishor, and P. K. Ray, "Robust h-infinite loop shaping controller based on hybrid pso and harmonic search for frequency regulation in hybrid distributed generation system," *Electrical Power and Energy Systems*, vol. 60, p. 302–316, 2014.

[103] De Pascali, L., Biral, F., & Onori, S. (2020). Aging-aware optimal energy management control for a parallel hybrid vehicle based on electrochemical-degradation dynamics. *IEEE Transactions on Vehicular Technology*, *69*(10), 10868-10878.

[104] Y. A.-R. I. Mohamed, H. H. Zeineldin, M. Salama, and R. Seethapathy, "Seamless formation and robust con trol of distributed generation microgrids via direct voltage control and optimized dynamic power sharing," *IEEE Transactions on Power Electronics*, vol. 27, no. 3, p. 1283–1294, 2012.

[105] M. Mehrasa, E. Pouresmaeil, and J. P. Catalão, "Direct lyapunov control technique for the stable operation of multilevel converter-based distributed generation in power grid," *IEEE Journal of Emerging and SelectedTopics in Power Electronics*, vol. 2, no. 4, p. 931–941, 2014.

[106] Y.-T. Weng and Y.-Y. Hsu, "Sliding mode regulator for maximum power tracking and copper loss minimi sation of a doubly fed induction generator," *IET Renewable Power Generation,* vol. 9, no. 4, pp. 297–305, 2015.

[107] J. Chai and R. G. Sanfelice, "A robust hybrid control algorithm for a single-phase dc/ac inverter with variable input voltage," *American Control Conference (ACC),* p. 1420–1425, 2014.

[108] M. Shiroei and A. Ranjbar, "Supervisory predictive control of power system load frequency control," *Electrical Power and Energy Systems*, vol. 61, p. 70–80, 2014.

[109] M. Ma, H. Chen, X. Liu, and F. Allgöwer, "Distributed model predictive load frequency control of multi area interconnected power system*," Electrical Power and Energy Systems,* vol. 62, p. 289–298, 2014.

[110] G. Bruni, S. Cordiner, V. Mulone, V. Rocco, and F. Spagnolo, "A study on the energy management in domes336 tic micro-grids based on model predictive control strategies," in Energy Procedia, *International Conference on Applied Energy (ICAE),* vol. 61, p. 1012–1016, 2014.

[111] P. Kou, F. Gao, and X. Guan, "Stochastic predictive control of battery energy storage for wind farm dis patching: Using probabilistic wind power forecasts," *Renewable Energy*, vol. 80, p. 286–300, 2015.

[112] Guo, Z., Jiang, H., Zheng, Y., & Li, S. (2017, October). Distributed model predictive control for efficient operation of islanded microgrid. In *2017 Chinese Automation Congress (CAC)* (pp. 6253-6258). IEEE.

[113] H. Yousef, "Adaptive fuzzy logic load frequency control of multi-area power system," *Electrical Power and Energy Systems*, vol. 68, p. 384–395, 2015.

[114] H. Weiss and J. Xiao, "Fuzzy system control for combined wind and solar power distributed generation unit," *IEEE International Conference on Industrial Technology*, vol. 2, p. 1160–1165, 2003.

[115] T. Kumar, N. Subrahmanyam, and M. Sydulu, "Control strategies of a fuzzy controlled solid oxide fuel cell/battery distributed generation system for power quality enhancement," in *International Conference on Circuit, Power and Computing Technologies (ICCPCT),* p. 64–69, 2014.

[116] T. Kumar, Y. Chandrashekar, N. Subrahmanyam, and M. Sydulu, "Control strategies of a fuzzy controlled grid connected hybrid pv/pemfc/battery distributed generation system," in *IEEE Power and Energy Con ference at Illinois (PECI),* 2015.

[117] I. Pan, Saptarshi Das, Fractional order fuzzy control of hybrid power system with renewable generation usingchaotic PSO. ISATransactions, 2015.

[118] T. V. Mukherjee, "A novel quasi-oppositional harmony search algorithm and fuzzy logic controller for frequency stabilization of an isolated hybrid power system," *Electrical Power and Energy Systems*, vol. 66, 389 p. 247–261, 2015.

[119] I. Mado, A. Soeprijanto, and Suhartono, "Design of robust-fuzzy controller for smib based on power-load cluster model with time series analysis, electrical power, electronics," in Communications, Controls and Informatics Seminar (EECCIS), p. 8–15, 2014.

[120] S. Seyedalipour, H. A. Aalami, and A. Barzegar, "A lyapunov function-based adaptive fuzzy control for integration of distributed generation resources to electrical networks," in *5th Iranian Joint Congress on Fuzzy and Intelligent Systems (CFIS)*, p. 184–189, 2017.

[121] A. Hajizadeh and M. A. Golkar, “Intelligent power management strategy of hybrid distributed generation system,” *Electrical Power and Energy Systems*, vol. 29, p. 783–795, 2007.

[122] A. Hajizadeh and M. Golkar, “Fuzzy neural control of a hybrid fuel cell/battery distributed power gener ation system,” *IET Renewable Power Generation*, vol. 3, no. 4, p. 402–414, 2009.

[123] S. K. Nayak, D. Gaonkar, and R. Shivarudraswamy, “Fuzzy logic controlled microturbine generation system for distributed generation,” in 2nd International Conference on Advances in Energy Engineering (ICAEE2011), *Energy Procedia*, vol. 14, p. 1213–1219, 2011.

[124] A. R. Sakhare, A. Davan, and A. Feliachi, “Control of stand alone solid oxide fuel cell using fuzzy logic,” in Proceedings of the *35th Southeastern Symposium on System Theory,* p. 473–476, 2003.

[125] D. Pan and F. Wang, “Modeling and simulation of fuzzy control system for dual stator winding induction generator,” in Proceeding of *International Conference on Electrical Machines and Systems*, 2007.

[126] Sebastián R. Review on Dynamic Simulation of Wind Diesel Isolated Microgrids. *Energies*. 2021; 14(7):1812. https://doi.org/10.3390/en14071812

[127] Rajasekaran, V. (2013). *Modeling, simulation and development of supervision control system for hybrid wind diesel system*. Masters Theses, Saint Mary's University, Halifax, NS, Canada.

[128] R. Gagnon, B. Saulnier, G. Sybille, P. Giroux; "Modeling of a Generic High-Penetration No-Storage Wind-Diesel System Using MATLAB®/Power System Blockset" *2002 Global Windpower Conference, April 2002*, Paris, France